https://ntrs.nasa.gov/search.jsp?R=19800007611 2020-03-21T19:33:39+00:00Z

N O T I C E

THIS DOCUMENT HAS BEEN REPRODUCED FROM MICROFICHE. ALTHOUGH IT IS RECOGNIZED THAT CERTAIN PORTIONS ARE ILLEGIBLE, IT IS BEING RELEASED IN THE INTEREST OF MAKING AVAILABLE AS MUCH INFORMATION AS POSSIBLE

JOINT INSTITUTE FOR AERONAUTICS AND ACOUSTICS

STANFORD UNIVERSITY

AMES RESEARCH CENTER

JIAA TR-2

(NASA-CR-162464) AN EXPERIMENTAL STUDY OF THE STRUCTURE AND ACOUSTIC FIELD OF A JET IN A CROSS STREAM (Stanford Univ.) 134 p HC A07/MF A01 CSCL 20A G3/71 Unclas 44853 N80-15871

AN EXPERIMENTAL STUDY OF THE STRUCTURE AND ACOUSTIC FIELD OF A JET IN A CROSS STREAM

Ivan Camelier and K. Karamcheti

STANFORD UNIVERSITY
Department of Aeronautics and Astronautics
Stanford, California 94305

January 1976

RECEIVED
NASA STI FACILITY
ACCESS DEPT.

JIAA TR - 2

AN EXPERIMENTAL STUDY OF THE STRUCTURE AND ACOUSTIC FIELD OF A JET IN A CROSS STREAM

IVAN CAMELIER AND K. KARAMCHETI

JANUARY 1976

The work here presented has been supported by the National Aeronautics and Space Administration under Grants NGR 05-020-526 and NSG 2007.

ABSTRACT

In order to understand the noise generated and radiated by a high speed circular jet issuing normally into an otherwise uniform stream, such as in the case of V/STOL aircraft, experimental studies have been carried out in the 7 x 10 foot wind tunnel at NASA Ames Research Center. The jet is 1.5 inches in diameter and is operated at a fixed Mach number equal to .58. The tunnel velocity is changed to vary the ratio of the speed of the jet to that of the uniform stream in the range from 3.7 to 9.4. Measurements for zero crossflow have also been included.

A survey of the plane of symmetry of the jet has been performed to measure the mean and turbulent velocity fields by using constant temperature hot wire anemometry. The intensity of the noise radiated from the jet has been determined in the tunnel test section by utilizing the cross-corrlation at a particular time delay between the signals of two microphones suitably located along a given direction. Such a technique gives the intensity radiated directly by the source without the effects due to the tunnel environment.

Experimental results indicate that the turbulent intensity inside the crossflow jet increase by a factor of $\left(1 + \frac{1}{r}\right)$ as compared to the turbulent intensity of the same jet under free conditions, with r indicating the ratio of the jet velocity by the cross stream velocity. The peak observed in the turbulence spectra obtained inside the potential core of the jet has a frequency that increases by the same factor

$\left(1 + \frac{1}{r}\right)$ with respect to the corresponding frequency measured in the case of the free jet. The acoustic intensity of the free jet measured by the two microphone cross-correlation technique inside the test section of the wind tunnel shows a very good agreement with results obtained by a previous worker inside an anechoic chamber. The noise radiated by the jet becomes more intense as the crossflow velocity increases. The measured acoustic intensity of the crossflow jet is higher than the value which would be expected from the increase of the turbulent intensity only. This fact together with the observation that the noise radiated by the crossflow jet, even for small values of cross stream velocity is more than 8 dB higher than the noise intensity of the same jet under free conditions suggests the existence of flow features and noise generating mechanisms not explored in the present study.

ACKNOWLEDGEMENT

We wish to express our gratitude to Mr. David Hickey of NASA Ames Research Center and Professor I-Dee Chang for reading the manuscript and for many helpful suggestions. Special thanks go to Mr. Brent K. Hodder of NASA for fruitful discussions and for his invaluable assistance during the experimental part of this study.

The help of Mr. Vadim Matte and of Mr. Ray Schmoranc is gratefully acknowledged.

The typing of the manuscript was ably handled by Miss Patricia Ortiz and by Miss Phyllis Cain. The figures were prepared by Miss Marianne Rudolph. Our sincere thanks to them.

The research was sponsored by NASA Ames Research Center under Grants 05-020-526 and NSF 2007.

TABLE OF CONTENTS

LIST OF FIGURES

LIST OF FIGURES (CONT.)

LIST OF SYMBOLS

a_e	sound speed at jet exit
a_o	sound speed in the plenum chamber
D	diameter of jet orifice
f	frequency
f_p	peak frequency in jet spectrum
$\underline{I}$	intensity vector
I	sound intensity
$\underline{M}$	Mach number vector ($\underline{U}/a$)
M_e	Mach number at jet exit (U_j/a_e)
M_2	Crossflow Mach number
p	local static pressure
p_e	static pressure at jet exit
p_o	local total pressure
p_{oe}	total pressure at jet exit
p_∞	undisturbed crossflow static pressure
p_∞^*	control room ambient pressure
p'	acoustic pressure perturbation caused by the jet (without effects of reflections)
p_r'	acoustic pressure perturbation due to reflections
p_m'	measured acoustic pressure ($p'+p_r'$)
q_∞	undisturbed crossflow dynamic pressure
r	velocity ratio (U_j/U_∞)
R	$R = \dfrac{[(1-M_2^2)\,\lvert\underline{x}-\underline{y}\rvert^2+M_2^2(x_2-y_2)^2]^{1/2} - M_2(x_2-y_2)}{1-M_2^2}$
R_e	Reynolds number

$R_{v_x^2 v_x^2}(\underline{y},\underline{z};\tau)$ cross correlation $[\overline{v_x^2(\underline{y},t)\, v_x^2(\underline{z},t+\tau)}]$

$R_{pp}(\underline{x};\tau)$ acoustic pressure auto correlation $[\overline{p'(\underline{x},t)p'(\underline{x},t+\tau)}]$

s	coordinate along jet axis
s_c	length of potential core
St	Strouhal number
t	time
T	absolute temperature
T_e	absolute temperature at jet exit
T_o	absolute temperature in the plenum chamber
T_∞	absolute temperature of the ambient medium
T_{ij}	Lighthill stress tensor (after Eq. 3.4)
u_i	general velocity component in i^{th} direction (i=1,2,3)
u_x	velocity component in the direction of observer
u'	root mean square of turbulent velocity
u_i'	velocity perturbation in i^{th} direction (i=1,2,3)
U	local jet velocity (mean)
U_j	mean velocity at jet exit
U_∞	undisturbed crossflow velocity
v_x	compounded jet velocity ($u_x - M_2 u_2$)
V_{CTA}	constant temperature anemometer output voltage
V_{LIN}	linearizer output voltage
$\underline{x}$	position vector
x_i	Cartesian coordinates (i=1,2,3)
$\underline{y}$	position vector
$\underline{z}$	position vector
δ_{ij}	Kronecker delta

Δ_p	pressure measured by differential manometer $(p-p_\infty^*)$
γ	ratio of specific heats of air
ρ	local density
ρ_e	density at jet exit
ρ_o	undisturbed density or density of air inside plenum chamber
ρ_∞	undisturbed crossflow density
ρ'	density perturbation
ξ	stretched coordinate along jet axis $[s\frac{s_c(r=\infty)}{s_c(r)}]$
τ	time delay
τ_{ij}	viscous stress tensor
θ	angle formed by position vector and coordinate axis x_1
[2(3)]	microphone number 2 in disposition number 3

I INTRODUCTION

The prospective use of V/STOL (vertical/short take off and landing) airplanes presents a series of advantages, comforts, and conveniences for most of the people using air transportation. Due to their capability for taking off and landing in very small areas these airplanes will be operating in airports located much closer to the center of our communities than the airports presently in use. Therefore they constitute a potential source of strong acoustic annoyance for a large part of the population living and working in the neighborhood of those future airfields. This has been the motivation recently for an increasing interest on the problem of noise produced by a jet in a crossflow, a situation that is created whenever a V/STOL aircraft is landing or taking off with the lifting jet producing a vertical thrust while the airplane is moving with a small horizontal velocity. The need for understanding and subsequently reducing the noise caused by the interaction of the cross stream, due to the aircraft forward motion, with the lifting jet makes necessary a detailed investigation of the internal structure and acoustic field of the modified jet flow.

Most of the work done so far in the field of jet noise has been related particularly to the case of a free circular jet, that is, a jet issuing into a medium at rest. Led by the classical studies of Lighthill (1952, 1954), a large number of theoretical and experimental investigators have contributed for

a reasonably good understanding of the turbulent free jet as a source of sound. However, even considering that there usually exists a good qualitative agreement of the experimental measurements with the theory, the whole picture is not yet clear or precise enough to simply extend the results of the free jet for an accurate prediction of the noise produced by a jet in a crossflow. The cross stream interacts with the jet changing the basic structure of the turbulence inside the jet flow. This causes a modification of the noise generation mechanisms with a consequent variation of the acoustic far field characteristics. An analytical approach to the problem has already been done in some extent by Cole (1972, 1974). Experimental studies by Kirk, Hall, and Hodder (1971) and also by Stimpert and Fogg (1973), to determine the effect of crossflow velocity on the jet noise generation of lift fans have shown that the jet noise increases with the increase of the cross stream velocity.

In the present study a methodical measurement of simple turbulent quantities within the jet and of noise intensity in the acoustic far field has been performed to evaluate the effects of the interaction of the jet with the crossflow upon the noise problem. Different values of crossflow provide various degrees of jet deformation necessary for the investigation. The experiment requires the use of a wind tunnel for obtaining the crossflow. The measurement of noise in wind tunnels, as previously discussed by Hickey, Soderman, and Kelly (1969), is a long, complex, and difficult task due primarily to the reverberant

effects of the tunnel walls. In this report a new method for measuring acoustic intensity in a reverberant environment has been proposed. It consists essentially of a measurement of the cross-correlation function of the signals from two microphones conveniently located in the radiation field, at an appropriate time delay. The result of this measurement gives the noise directly radiated from the source, practically free from any effect of reflections.*

In the next chapter the reader will find a background of previous works related to jet noise and also to the general problem of a crossflow jet. Chapter III has a brief introduction of the equation governing the noise radiated from a jet in a cross stream as derived by Cole (1972). This equation is then simplified to a form similar to Proudman's equation of the free jet noise and used afterwards to show how the method of cross-correlation can be applied for obtaining the noise intensity in a reverberant acoustic field when the noise source is a jet. Chapter IV contains the description of the experimental apparatus and instrumentation used for the testing. The test procedure including calibration of the measuring instruments is also included. Chapter V has all the test results. Interpretations and discussions are presented together with the experimental data and are directed towards understanding the effects of changes of crossflow velocity on the experimental observations.

---

*At the completion of this report we learned through personal communication from Mr. Warren F. Ahtye at NASA-Ames Research Center that he had recently used the two microphone cross correlation method to measure the noise radiated from a single source located in a room with no acoustic treatment and that he obtained good results with both wide and narrow band two microphone cross correlations.

Chapter VI is the conclusion of the report with a summary of the principal results. In Appendix A some considerations about the interpretation of measurements by a linearized hot wire anemometer in compressible flows are discussed. Finally in Appendix B a simple dimensional analysis is performed to show how the acoustic intensity of a jet should be expected to increase when a cross stream is present.

II BACKGROUND

As already mentioned in the previous chapter, the noise problem related to a jet in a cross stream is very recent. Most of the literature pertaining to jet noise has been concerned with the case of a jet under free conditions. Therefore, an initial presentation of some previous works related to the noise produced by a free jet seems to be appropriate. The general problem of a crossflow jet is discussed afterwards.

2.1 Free Jet Noise

Theoretical Notions

The general theory discussing the problem of noise produced by the turbulent flow of a jet has been introduced by Lighthill (1952, 1954) and complemented by Proudman (1952), Lilley (1958), Powell (1959), Ffowcs Williams (1963), Ribner (1964), and several others. In a few words and in a very simplified way it says that the noise is produced inside the jet by a large number of uncorrelated, time varying, turbulent eddies which are convected in the same direction as the jet flow and radiate sound independently as acoustic quadrupoles. The convection of the eddies together with the refraction of the sound waves caused by the gradients of different properties across the jet are responsible for the directivity pattern experimentally observed in the acoustic far field. The intrinsic complexity of the turbulent jet as a source of sound has motivated a large number of experimental investigations.

Experimental Studies

a) Noise Producing Region (within the jet). Laurence (1956) was one of the first workers to make measurements concerned with Lighthill's theory, within a circular free jet. With a constant temperature hot wire he investigated the effect of varying the exit velocity upon the intensity, scale and spectrum of the turbulence at several points inside the jet. He used a 3.5 in. diameter jet with a range of exit Mach numbers from 0.2 to 0.7.

Davies, Fisher, and Barratt (1963) complemented the measurements previously obtained by Laurence (1956) and obtained for the first time important characteristics of the turbulence with respect to a frame of reference being convected with the turbulent eddies, a point which had already been discussed in theory by Lighthill (1952, 1954) and Ffowcs Williams (1963). The range of Mach numbers in this experiment was from 0.2 to 0.55 and the jet was 1 in. in diameter.

Davies, Ko, and Bose (1968), later complemented by Ko and Davies (1971), have determined the existence of a near pressure field within the potential core of a free circular jet. They also made microphone measurements in the near field outside the jet. Some characteristics of these two near fields, inside the core and outside the jet, showed discrepancies which were explained by the authors as being an indication of the Dopler effect of moving sources, moving medium, and refraction of sound waves in the noise producing region.

Later, using hot wire techniques, Wooten, Wooldridge, and

Amaro (1972) studied a 1.5 in. diameter jet at exit Mach numbers of 0.3, 0.5, and 0.7. They investigated the mixing region, the potential core and the transition region. Particular attention was given to spectral peaks and to the convection velocity of turbulent eddies. They also suggested swirling of the jet as a way to reduce the noise production.

b) Radiation Field. Other workers have investigated the characteristics of the noise in the radiation field. Among them Lassiter and Hubbard (1952) used jets of several sizes to study the effect of varying jet velocity, density, turbulence level, and jet size upon the intensity, directivity, and spectrum of the noise produced by the jet. Their results, obtained at approximately the same time that Lighthill published his first work, showed good agreement with some of Lighthill's results obtained from dimensional analysis.

In a recent work Lush (1971) studied the noise radiated from a 25 mm. diameter jet at several subsonic exit speeds and compared his data with Lighthill's theory of convected quadrupoles. His results include total intensity corrected for the effects of convection as a function of both the jet velocity and the angular position with respect to the jet. It is interesting to note that at 90^{o}, where the effect of source convection does not exist, the experimental data show the overall intensity as a function of U_j^8. However, for smaller angles the theory overpredicts the results for high frequencies, while for angles larger than 90^{o} (i.e., at the rear part of the

jet) the theory is clearly below the obtained experimental results. The latter result is found in Fisher, Lush, and Bourne (1973). The authors spectulated that this effect is caused by a lack of convective amplification whenever the wavelength of the generated sound is several times greater than the space the sound waves have to travel before emerging from the jet.

c) Causality Cross-Correlations. A more recent experimental technique has been now in use to identify the individual characteristics of the sound sources within the jet with the noise produced by them. It can be essentially described as a measurement of a cross-correlation between a certain property inside the jet (the cause) and the sound pressure in the radiation field (the effect). The cross-correlation is measured at a time delay corresponding to the amount of time that an acoustic perturbation takes to go from the sound source to the measuring point in the radiation field. The measurable property within the jet can be either the fluctuating pressure or the turbulent velocity, the former based on the theory of simple source dilatation, [see Ribner (1964)], and the latter on Lighthill's quadrupole theory. A complete discussion about this method with a vast list of references can be found in Siddon (1974).

2.2 Jet in a Cross Stream

Theoretical Notions

Only recently has the effect of a crossflow been considered in the equations of jet noise. Cole (1972) studied the case

where the jet, representing the source of noise, and the observer are both at rest and the acoustic medium is at uniform motion. This situation happens during a testing inside a wind tunnel where the jet and the microphone (representing the observer) are fixed and the acoustic medium, provided by the wind tunnel uniform stream, is moving. In his studies Cole derived the equation for the acoustic intensity starting from the basic equations of Fluid Mechanics. Part of his work will be shown in the next chapter to introduce the equation relating the sound field to the turbulent fluctuations inside the jet. In a latter publication Cole (1974) discussed the case of a crossflow jet moving through a stationary acoustic medium (also briefly presented in the Appendix of the 1972 report). The acoustic intensity of the crossflow jet is greater upstream of the jet than at an equal distance downstream. Even though this characteristic is more accentuated in the case of a crossflow jet in a moving medium, the analytical comparison presented by Cole (1972) with the two acoustic media (moving, and at rest) shows that the difference between the two cases is practically negligible for crossflows at small subsonic velocities.

Kirk, Hall, and Hodder (1971), have made aerodynamic and acoustic investigations of a large scale lift fan model in the NASA-Ames 40 x 80 foot wind tunnel. Sound pressure levels were observed to increase when the jet was under the influence of a crossflow.

Later, Stimpert and Fogg (1973) performed an analytical study and an examination of experimental data to determine the

ct of crossflow velocity on the jet noise generation of lift fans. The noise measurements were taken in the NASA-Ames 40 x 80 foot wind tunnel with a complete lift fan V/STOL transport aircraft model. It was also found that the jet noise increases when the velocity of the cross stream increases.

Several other experimental studies have been related to the aerodynamic aspects of the crossflow jet, particularly the shape of the jet plume and the distribution of mean velocity and pressure across the jet. Some of these investigations will be mentioned below as we discuss the characteristics of a jet in a crossflow.

A circular jet exhausting perpendicularly into a crossflow is deformed and altered in shape, bending into the direction of the stream. A complete physical description of the interaction of the two flows is given by Keffer (1969) who divides the jet into three arbitrary regions (see Figure 1). The first region is denominated by Keffer (1969) as the source flow region*. It contains both the potential core and the turbulent mixing zone that surrounds the potential core. As in the case of the free jet, inside the potential core the turbulence is very low and the mean velocity has practically the same value as the jet velocity at the exit. On the other hand, within the mixing zone both the turbulence and the radial variation of mean velocity are very large. Jordinson (1956) noticed that the jet has a circular

*The source flow region should not be mistaken by the noise producing region of the jet. As will be discussed later in the report, the source flow region contributes with a large part of the total noise produced by the jet but it is only a part of the noise producing region.

contour at the exit but at the end of the source flow region this contour has already changed to a kidney shape, due to the lateral deformation of the jet by the crosswind. The source flow region extends from the jet exit up to the end of the potential core. Its length, as observed by Keffer and Baines (1963) and also by Pratte and Baines (1967), depends on the value of the ratio r of the jet velocity to the cross stream velocity. The next region of the jet starts at the end of the potential core and is called the curvilinear or the transition region. Within the transition region the turbulent mixing zone occupies the whole cross section of the jet. This region is also characterized by a constant change of direction of the jet flow which describes a curvilinear trajectory. Keffer and Baines (1963), and more recently Chassaing, et.al. (1974) have found some similarity laws for the jet trajectory and for the distribution of mean velocity inside the transition region. The last region of the jet is the far region where the jet has approximately the same direction as the crossflow and the mixing between the two flows is almost completely accomplished. The jet mean velocity is equal to the crossflow velocity and the only characteristic of the jet which makes possible to distinguish it from the crossflow is now a pair of counter rotating vortices which are believed to have been started at the beginning of the transition region. As pointed out by Pratte and Baines (1967), no end has been observed yet for this far region. There is also the wake, a not very well known region behind the jet, where the mean velocity is much smaller than in either the jet or the

crossflow. For small values of crossflow Pratte and Baines (1967) have observed two attached vortices in the wake just behind the jet, similarly to the attached vortices found behind a cylinder at small Reynolds number. When the crossflow velocity increases however, those vortices shed, as has been experimentally observed by McMahon, Hester, and Palfery (1971).

Other workers had interests in the distribution of pressure on the surface around the jet exit. These investigations are related to the change of a pitching moment which a V/STOL aircraft experiences during the transition flight due to the movement of the center of pressure. Mosher (1970) and Mikolowsky (1972) studied the pressures on the surface around the jet orifice located on a flat plate and on an airplane wing respectively.

2.3 The Present Investigation

The experimental works mentioned in the previous section, besides many others on the same subject, have contributed for a clear understanding of the physical aspects of a circular jet in a crossflow. For instance, the ratio r of the jet velocity by the cross stream velocity is considered to be the governing parameter influencing the jet trajectory and the entrainment process. The crossflow velocity, or more precisely, the Reynolds number of the crossflow (based on the jet diameter), is evidently the important parameter influencing vortex shedding behind the jet. The maximum free stream Reynolds number of the tests reported by Pratte and Baines (1967) was about 500. The vortices were not shed in that experiment. On the other hand,

vortex shedding has been observed in the experiments of McMahon, Hester, and Palfery (1971), where the Reynolds number of the free stream (in the case of the circular jet) was about 52000. These works have established the aerodynamic peculiarities of the crossflow jet without going into the details of the jet noise mechanisms. In his analysis of noise radiated from a jet in a crossflow, Cole (1972) was forced to use experimental data from the free jet due to the absolute lack of information concerning the turbulent characteristics of a jet in a cross stream.

The objective of this study is therefore, to gain insight into some aspects of the basic modifications occurring within the noise producing region and also in the acoustic far field of a turbulent jet under the influence of different crossflows. The noise producing region, from which most of the noise produced by a subsonic jet radiates, is mainly composed by the source flow region and by the beginning of the transition region (see Figure 1).

Preliminary measurements were obtained at Stanford University (Department of Aeronautics and Astronautics). The experiment was greatly useful for a first acquaintance with the problem, experimental instrumentation, and acoustic measuring techniques.

This report is related to the results of the experimental testing of a jet in a cross stream at NASA-Ames Research Center. The test description is fully discussed in Chapter IV.

III THEORETICAL CONSIDERATIONS

This chapter is concerned with a brief discussion of the governing equations for the noise radiated from a jet in the presence of a crossflow. It introduces the equation relating the sound field with the turbulent fluctuations inside the jet as derived by Cole (1972). This equation is then simplified to a form similar to the equation first presented by Proudman (1952) in the case of the free jet, and used afterwards to discuss the noise intensity in the radiation field. It is further shown how the intensity of the noise produced by the jet may be obtained when the radiation field is a reverberant environment, as usually occurs inside the test section of a wind tunnel.

The system of coordinates to be used is shown in Figure 1. The vector $\underline{x}$ defines the position of a point outside the jet flow, while $\underline{y}$ is the position vector of a point inside the noise producing region of the jet.

3.1 Equation of Sound Generation in a Uniformly Moving Medium

In light of the proposed investigation of some aspects of the noise generation of a jet in a cross stream, it is appropriate to set up the basic equation for the sound generation for such a case in a form analogous to that of sound propagation in an initially uniformly moving medium owing to a distribution of acoustic sources.

In a fluid medium the equation for conservation of mass is written as:

$$\frac{\partial \rho}{\partial t} + \frac{\partial \rho u_i}{\partial x_i} = 0 \qquad (3.1)$$

and the equation for conservation of momentum, in the absence of external forces acting on the fluid, is expressed by:

$$\frac{\partial \rho u_i}{\partial t} + \frac{\partial \rho u_i u_j}{\partial x_j} = - \frac{\partial p}{\partial x_i} + \frac{\partial \tau_{ij}}{\partial x_j} \qquad (3.2)$$

In these equations, ρ is the density of the fluid, u_i is the component of fluid velocity in the i direction, p is the fluid pressure which is associated with other fluid variables through thermodynamic relations, and τ_{ij} is the viscous stress tensor. Equations 3.1 and 3.2 can be combined to give:

$$\frac{\partial^2 \rho}{\partial t^2} - a_0^2 \frac{\partial^2 \rho}{\partial x_i^2} = \frac{\partial^2}{\partial x_i \partial x_j} [\rho u_i u_j + (p - a_o^2 \rho) \delta_{ij} - \tau_{ij}] \qquad (3.3)$$

where δ_{ij} is the Kronecker delta. Observe that equation 3.3 is an exact equation of fluid motion. It is valid, without restrictions, in any region of the flow. In the particular case of a finite turbulent airflow surrounded by an infinite fluid medium moving uniformly with a constant velocity U_∞ in the positive x_2 direction (see Fig. 1), equation 3.3 can be rewritten, as shown by Cole (1972), in the following approximate

form:

$$\frac{\partial^2 \rho}{\partial t^2} - a_0^2 \frac{\partial^2 \rho}{\partial x_i^2} + 2U_\infty \frac{\partial^2 \rho}{\partial x_2 \partial t} + U_\infty^2 \frac{\partial^2 \rho}{\partial x_2^2} = \frac{\partial^2 T_{ij}}{\partial x_i \partial x_j} \qquad (3.4)$$

where a_o is the sound speed of the acoustic moving medium outside the turbulent region, and $T_{ij}=\rho u_i u_j+(p-a_o^2\rho)\delta_{ij}-\tau_{ij}$ is the well known Lighthill stress tensor. The left hand side of equation 3.4, due to acoustic linearizations made in its derivation, is valid only in the unformly moving medium outside the turbulent airflow. The two terms $U_\infty \frac{\partial^2 \rho}{\partial x_2 \partial t}$ and $U_\infty^2 \frac{\partial^2 \rho}{\partial x_2^2}$ are the only part of $\frac{\partial^2 T_{ij}}{\partial x_i \partial x_j}$ which is non-negligible in the moving medium. Inside the turbulent airflow, however, the term $\frac{\partial^2 T_{ij}}{\partial x_i \partial x_j}$ which is shown in the right-hand side of equation 3.4 remains intact, without linearizations, and represents the distribution of acoustic sources. The mentioned equation shows that outside the turbulent airflow the density satisfies the equation of sound propagation for a uniformly moving medium:

$$\frac{\partial^2 \rho}{\partial t^2} - a_o^2 \frac{\partial^2 \rho}{\partial x_i^2} + 2U_\infty \frac{\partial^2 \rho}{\partial x_2 \partial t} + U_\infty^2 \frac{\partial^2 \rho}{\partial x_2^2} = 0$$

and the density disturbances, which were produced by the forcing term $\frac{\partial^2 T_{ij}}{\partial x_i \partial x_j}$ within the turbulent airflow, are propagated acoustically.

Formal Representation of the Solution. The solution of equation 3.4 is fully discussed by Cole (1972). The density disturbance

in the uniformly moving medium outside the turbulent airflow is given by:

$$\rho'(\underline{x},t) = \frac{1}{4\pi a_o^2} \frac{\partial^2}{\partial x_i \partial x_j} \iint_{V_y \infty} \frac{T_{ij}(\underline{y},t')}{[(1-M_2^2)\,|\underline{x}-\underline{y}\,|^2+M_2^2(x_2-y_2)^2]^{1/2}}$$

$$\delta(t'-t+\frac{R}{a_o})\; dt\; d^3y \qquad (3.5)$$

where V_y is the volume of the turbulent airflow, the jet flow in the particular case of this report, $M_2 = \frac{U_\infty}{a_o}$ is the Mach number of the crossflow, and $\frac{R}{a_o}$ is the time the radiated sound takes to go from each point within the jet to a position $\underline{x}$ in the surrounding medium. $\frac{R}{a_o}$ is a delayed time in the sense that a particular perturbation arriving at $\underline{x}$ at time t was produced inside the jet at an earlier time $t-\frac{R}{a_o}$. Cole (1972) also shows that the value of R is given by:

$$R = \frac{[(1-M_2^2)\,|\underline{x}-\underline{y}| + M_2(x_2-y_2)^2]^{1/2} - M_2(x_2-y_2)}{(1-M_2^2)} \qquad (3.6)$$

Equation 3.5 is the formal solution for the acoustic perturbations produced by a turbulent jet flow issuing into an infinite, unbounded, uniformly moving medium.

Approximate Forms. In jet noise problems the radiation field is usually defined by $|\underline{x}|$ being much larger than the dimensions of the jet and also larger than $(2\pi)^{-1}$ times a typical acoustic wave length. If the Mach number of the moving medium is small $(M_2 \ll 1)$, the value of $\rho'(\underline{x},t)$ in the radiation

field is given by Cole (1972) in the following approximate form:

$$\rho'(\underline{x},t) \simeq \frac{1}{4\pi a_o^4 |\underline{x}|} \int_{V_y} \int_{\infty} \left[\frac{x_i x_j}{|\underline{x}|^2} - \frac{M_2}{|\underline{x}|} x_i \delta_{j2} - \frac{M_2}{|\underline{x}|} x_j \delta_{i2} + M_2^2 \delta_{i2}\delta_{j2}\right]$$

$$\frac{\partial^2 T_{ij}(\underline{y},t')}{\partial t^2} \delta(t'-t+\frac{R}{a_o})\, dt' d^3\underline{y} \qquad (3.7)$$

In turbulent cold jets at low Mach numbers where heating or cooling is caused only by friction or by rapid acceleration, and if it is assumed that viscosity effects can be neglected, Lighthill (1952) shows that the stress tensor can be approximated in the following form:

$$T_{ij} \simeq \rho_o u_i u_j \qquad (3.8)$$

where ρ_o is the undisturbed density of the surrounding medium. With this approximation for T_{ij} equation 3.7 may be rewritten as:

$$\rho'(\underline{x},t) \simeq \frac{\rho_o}{4\pi a_o^4 |\underline{x}|} \int_{V_y} \int_{\infty} \left[\frac{x_i x_j}{|\underline{x}|^2} - \frac{M_2}{|\underline{x}|} x_i \delta_{j2} - \frac{M_2}{|\underline{x}|} x_j \delta_{i2} + M_2^2 \delta_{i2}\delta_{j2}\right]$$

$$\frac{\partial^2 u_i u_j(\underline{y},t')}{\partial t^2} \delta(t'-t+\frac{R}{a_o})\, dt' d^3\underline{y} \qquad (3.9)$$

For a free jet, where $M_2=0$, the only term which survives inside the integral is $\frac{x_i x_j}{|\underline{x}|^2} \frac{\partial^2 u_i u_j}{\partial t^2}$. Proudman (1952) was the first one to notice that this term can be simplified in

the following way:

$$\frac{x_i x_j}{|\underline{x}|^2} \frac{\partial^2 u_i u_j}{\partial t^2} = \frac{\partial^2}{\partial t^2}\left[\frac{x_i x_j}{|\underline{x}|^2} u_i u_j\right] = \frac{\partial^2 u_x^2}{\partial t^2}$$

where u_x is the component of the instantaneous velocity within the jet in the direction of the observer located at the point defined by the position vector $\underline{x}$. The same procedure followed by Proudman (1952) can be applied to the three other terms in equation 3.9 to give:

$$\frac{M_2}{|\underline{x}|} x_i \delta_{j2} \frac{\partial^2}{\partial t^2} u_i u_j = \frac{\partial^2}{\partial t^2} M_2 u_x u_2$$

$$\frac{M_2}{|x|} x_j \delta_{i2} \frac{\partial^2}{\partial t^2} u_i u_j = \frac{\partial^2}{\partial t^2} M_2 u_2 u_x$$

and,

$$M_2^2 \delta_{i2}\delta_{j2} \frac{\partial^2}{\partial t^2} u_i u_j = \frac{\partial^2}{\partial t^2} M_2^2 u_2^2$$

where u_2 is the component of the instantaneous velocity within the jet in the positive x_2 direction, that is, parallel to the crossflow. From the simplifications just obtained, the four terms inside the integral of equation 3.9 can be rewritten as:

$$\left[\frac{x_i x_j}{|\underline{x}|^2} - \frac{M_2}{|\underline{x}|} x_i \delta_{j2} - \frac{M_2}{|\underline{x}|} x_j \delta_{i2} + M_2 \delta_{i2}\delta_{j2}\right] \frac{\partial^2}{\partial t^2} u_i u_j =$$

$$= \frac{\partial^2}{\partial t^2} \left[u_x^2 - 2M_2 u_2 u_x + M_2^2 u_2^2 \right] = \frac{\partial^2}{\partial t^2} \left[(u_x - M_2 u_2)^2 \right] \qquad (3.10)$$

If a velocity v_x is defined as

$$v_x \equiv u_x - M_2 u_2 \qquad (3.11)$$

equation 3.9 can be expressed in a more compact form by:

$$\rho'(\underline{x},t) \simeq \frac{\rho_o}{4\pi a_o^4 |\underline{x}|} \int_{V_y} \int_{\infty} \frac{\partial^2}{\partial t^2} v_x^2 (\underline{y},t') \delta(t'-t+\frac{R}{a_o}) \, dt' d^3y \qquad (3.12)$$

Acoustic Pressure and Intensity. In the radiation field the sound waves can be taken locally as plane waves and the relation $p'=a_o^2\rho'$ applied. The equation for the acoustic pressure perturbations is then obtained from equation 3.12 and written as:

$$p'(\underline{x},t) \simeq \frac{\rho_o}{4\pi a_o^2 |\underline{x}|} \int_{V_y} \int_{\infty} \frac{\partial^2}{\partial t^2} v_x^2(\underline{y},t') \delta(t'-t+\frac{R}{a_o}) dt' d^3\underline{y} \qquad (3.13)$$

Equation 3.13 shows that the sound pressure at $\underline{x}$ in the radiation field at a time t is given by the integral over the jet volume of the second time derivative of the quantity v_x^2, calculated at the earlier time $t-\frac{R}{a_o}$. The velocity v_x, defined by equation 3.11, is called hereafter the instantaneous compounded velocity of the jet in the direction of the observer. It is composed of the product of the crossflow Mach number M_2 by the instantaneous jet velocity in the x_2 direction subtracted from the instantaneous velocity of the jet in the direction of the observer. The sound pressure as given by

equation 3.13 is in a form which is very similar to the equation derived by Proudman (1952) in the case of a free jet, and it actually reduces to Proudman's equation when the Mach number of the crossflow is zero.

One useful quantity often measured in the radiation field is the sound intensity which is defined as the flux of acoustic energy per unit area normal to the direction of propagation. In a moving medium the acoustic intensity vector is defined by the following equation:

$$\underline{I}\ (x) = \frac{\overline{[p'(\underline{x},t)]^2}}{\rho_o a_o}\ (\underline{M} + \underline{n}) \tag{3.14}$$

where $\underline{M}$ is the Mach number vector of the moving medium, $\underline{n}$ is a unit vector perpendicular to the acoustic wave front, and $\overline{[p'(\underline{x},t)]^2}$ is the mean square value of the acoustic pressure, with the overbar indicating time average. If the Mach number of the moving medium is small enough, the value of $\underline{M}$ in equation 3.14 can be neglected and the sound intensity may be expressed by the following approximate form:

$$I(\underline{x}) \simeq \frac{\overline{[p'(\underline{x},t)]^2}}{\rho_o a_o} \tag{3.15}$$

The value of the acoustic pressure given by equation 3.13 substituted in equation 3.15 gives

$$I(\underline{x}) \simeq \frac{\rho_o}{16\pi^2 a_o^5 |\underline{x}|^2} \int_{V_y}\int_{V_z}\int_{\infty}\int_{\infty} \overline{\frac{\partial^2 v_x^2}{\partial t_1^2}(\underline{y},t_1)\ \frac{\partial^2 v_x^2}{\partial t_2^2}(\underline{z},t_2)}\ \delta\left(t_1 - t + \frac{Ry}{a_o}\right)\delta\left(t_2 - t + \frac{Rz}{a_o}\right)$$

$$dt_1 dt_2 d^3\underline{z} d^3\underline{y} \tag{3.16}$$

where $\underline{y}$ and $\underline{z}$ are position vectors inside the turbulent flow, R_y is given by equation 3.6, and R_z is obtained from equation 3.6 by substituting $\underline{z}$ and z_2 respectively for $\underline{y}$ and y_2.

Ffowcs Williams (1963) shows that if the turbulence is a stationary function of time, the averaged value in the integrand can be written as

$$\overline{\frac{\partial^2 v_x^2}{\partial t_1^2}(\underline{y},t_1)\,\frac{\partial^2 v_x^2}{\partial t_2^2}(\underline{z},t_2)} = \frac{\partial^4}{\partial \tau^4} R_{v_x^2 v_x^2}(\underline{y},\underline{z};\tau)$$

where, the cross correlation function of the velocity is given by

$$R_{v_x^2 v_x^2}(\underline{y},\underline{z};\tau) = \overline{v_x^2(\underline{y},t_1)\,v_x^2(\underline{z},t_1+\tau)} = \overline{v_x^2(\underline{y},0)\;v_x^2(\underline{z},\tau)}$$

the second equality applying for stationary processes. Equation 3.16 can then be rewritten as

$$I(\underline{x}) = \frac{\rho_o}{16\pi^2 a_o^5 |\underline{x}|^2} \int_{V_y}\int_{V_z}\int_{\infty}\int_{\infty} \frac{\partial^4}{\partial \tau^4} R_{v_x^2 v_x^2}(\underline{y},\underline{z};\tau)\;\delta\left(t_1 - t + \frac{R_y}{a_o}\right)\delta\left(t_1+\tau-t+\frac{R_z}{a_o}\right) dt,\, d\tau\, d^3\underline{z}\, d^3\underline{y}$$

which gives after integration with respect to t_1

$$I(\underline{x}) \simeq \frac{\rho_o}{16\pi^2 a_o^5 |\underline{x}|^2} \int_{V_y}\int_{V_z}\int_{\infty} \frac{\partial^4}{\partial \tau^4} R_{v_x^2 v_x^2}(\underline{y},\underline{z};\tau)\;\delta(\tau-\tau^*)\, d\tau\, d^3\underline{z}\, d^3\underline{y} \qquad (3.17)$$

where

$$\tau^* = \frac{R_y - R_z}{a_o}$$

The acoustic intensity in the radiation field depends on the fourth derivative with respect to time of the cross correlation function $R_{v_x^2 v_x^2}(\underline{y},\underline{z};\tau)$ at the time $\tau^* = \frac{R_y - R_z}{a_o}$. Equation 3.17 gives the value of the acoustic intensity in the radiation field as a function of measurable quantities within the jet. The cross correlation $Rv_x^2 v_x^2$ have a higher degree of complexity than the corresponding cross-correlation $R_{u_x^2 u_x^2}$ of the free jet because v_x, as defined by equation 3.11, is the combination of two velocities $u_x - M_2 u_2$.

3.2 Measurement of Acoustic Intensity in a Reverberant Environment

The most common way to obtain the sound intensity in the radiation field is by using a microphone located at the point of interest. The response of the microphone to the pressure fluctuations can be read through a meter which gives the mean square value of the acoustic pressure detected by the microphone, and the intensity is then calculated by using equation 3.15.

In the absence of reflections or other sources of sound besides the jet itself, as usually happens inside an anechoic chamber, the total acoustic pressure measured by the microphone, $p'_m(\underline{x},t)$, will be the same as the acoustic pressure produced by the jet and radiated directly to the point $\underline{x}$, $p'(\underline{x},t)$. In this case, the following equality can be written:

$$R_{p_m p_m}(\underline{x};0) = R_{pp}(\underline{x};0) \qquad (3.18)$$

where $R_{pp}(\underline{x};0) = \overline{p'(\underline{x},t)\ p'(\underline{x},t+0)}$ is the mean square value,

or the autocorrelation with zero time delay, of the acoustic pressure produced by the jet and radiated directly to $\underline{x}$, and

$R_{p_m p_m}(\underline{x},0) = \overline{p'_m(\underline{x},t)\ p'_m(\underline{x},t+0)}$ is the measured mean square value of the acoustic pressure detected by the microphone.

In the presence of reflections, as inside a reverberant room where the noise radiated from the jet is reflected by the walls, the total acoustic pressure detected by a microphone at $\underline{x}$ is given by the following expression:

$$p'_m(\underline{x},t) = p'(\underline{x},t) + p'_r(\underline{x},t) \tag{3.19}$$

where $p'(\underline{x},t)$ is still the acoustic pressure produced by the jet and radiated directly to the point $\underline{x}$. $p'_r(\underline{x},t)$ is the acoustic pressure at $\underline{x}$ caused by the jet noise reflected from the walls, and $p'_m(\underline{x},t)$ is the total acoustic pressure measured at $\underline{x}$. The mean square value of equation 3.19 can be written as:

$$R_{p_m p_m}(\underline{x};0) = R_{pp}(\underline{x};0) + R_{p_r p_r}(\underline{x};0) \tag{3.20}$$

where $R_{p_r p_r}(\underline{x};0) = \overline{p'_r(\underline{x},t)\ p'_r(\underline{x};t+0)}$ is the mean square value of the acoustic pressure due to the reflections; R_{pp} and $R_{p_m p_m}$ have been already defined after equation 3.18.

The cross cor elation $R_{pp_r}(\underline{x},\underline{x};0) = \overline{p'(\underline{x},t)\ p'_r(\underline{x},t+0)}$, which should also appear in equation 3.20, is actually equal to zero because $p'(\underline{x},t)$ is uncorrelated with any reflection

at zero time delay; R_{pp_r} may have a value different from zero at some time delay τ, $\tau > 0$, corresponding to the time the acoustic wave takes to go from $\underline{x}$ to a reflecting surface and come back to $\underline{x}$ again.

In equation 3.20, the term $R_{p_r p_r}(\underline{x};0)$ represents a substantial contribution to the mean square of the measured acoustic pressure, and because it is unknown, the mean square of the acoustic pressure produced by the jet and radiated directly to a point $\underline{x}$, $R_{pp}(\underline{x};0)$, cannot be determined. Hence, the acoustic intensity of the directly radiated jet noise (without the effect of reflections) cannot be obtained in a reverberant room by the conventional method of using one microphone for the measurement.*

Acoustic Intensity by Two Microphone Cross Correlations. The mean square value of the acoustic pressure produced by a jet and radiated directly to a point in the radiation field inside a reverberant environment can be obtained, with a good approximation, by cross-correlating the response from two microphones. This is a new method related to jet noise measurements which will be discussed with the equations of the jet in the cross-flow for more generality, but that is also valid for the case of the free jet as well.

---

*When other sources of sound are present in the room, the right-hand side of equation 3.20 does have another term, $R_{p_s p_s}$, representing the mean square of the pressure disturbances caused by the other sources. However, $R_{p_s p_s}$, is not a part of the problem since its value can be easily determined by measuring the background noise, i.e., the noise with the jet turned off.

Take two microphones at two different points, in the radiation field, defined by the position vectors $\underline{x}_1$ and $\underline{x}_2$. The vectors $\underline{x}_1$ and $\underline{x}_2$ have the same direction and $|\underline{x}_2|>|\underline{x}_1|$. Also define a particular time τ' equal to the time which a wave front, coming directly from the jet, takes to go from $\underline{x}_1$ to $\underline{x}_2$.

The instantaneous response of the two microphones to the total acoustic pressure at $\underline{x}_1$ and at $\underline{x}_2$ is obtained from equation 3.19 and given by:

$$p'_m(\underline{x}_1,t) = p'(\underline{x}_1,t) + p'_r(\underline{x}_1,t) \quad \text{at } \underline{x}_1$$

and

$$p'_m(\underline{x}_2,t) = p'(\underline{x}_2,t) + p'_r(\underline{x}_2,t) \quad \text{at } \underline{x}_2.$$

The cross correlation of these two pressures with the time delay τ' previously defined can be written in the following form:

$$R_{p_m p_m}(\underline{x}_1,\underline{x}_2;\tau') = R_{pp}(\underline{x}_1,\underline{x}_2;\tau') + R_{p_r p_r}(\underline{x}_1,\underline{x}_2;\tau') \qquad (3.21)$$

The cross correlations $R_{pp_r}(\underline{x}_1,\underline{x}_2;\tau')$ and $R_{p_r p}(\underline{x}_1,\underline{x}_2;\tau')$ which should also appear in equation 3.21 are both zero at the particular value of the time delay τ' under consideration. The only part of p'_r which contributes to the cross correlations R_{pp_r} and $R_{p_r p}$ is the reflection of the acoustic pressure produced by the jet and radiated in the direction of $\underline{x}_1$. In the case of $R_{pp_r}(\underline{x}_1,\underline{x}_2;\tau)$ it is zero because $p'(\underline{x}_1,t)$ is well

correlated with its own reflection at $\underline{x}_2$ only at a time delay τ, different from τ', corresponding to the time the acoustic wave front takes to go from $\underline{x}_1$ to a reflecting surface and return to $\underline{x}_2$. The other correlation $R_{p_r p}(\underline{x}_1, \underline{x}_2; \tau)$ is actually zero for any positive value of the time delay τ because the sound perturbations emitted from the jet in the direction $\underline{x}_1$, always arrives at $\underline{x}_2$ before any reflection of this same sound arrives at $\underline{x}_1$.

The first term in the right-hand side of equation 3.21, the cross-correlation $R_{pp}(\underline{x}_1, \underline{x}_2; \tau')$, can be written as

$$R_{pp}(\underline{x}_1, \underline{x}_2; \tau') = \overline{p'(\underline{x}_1, t)\, p'(\underline{x}_2, t + \tau')} \tag{3.22}$$

The pressure perturbations $p'(\underline{x}_1, t)$ and $p'(\underline{x}_2, t + \tau')$ are both obtained from equation 3.13 and expressed in the following form:

$$p'(\underline{x}_1, t) \simeq \frac{\rho_0}{4\pi a_0^2 |\underline{x}_1|} \int_{V_y} \int_{\infty} \frac{\partial^2 v_{x_1}^2}{\partial t^2} (\underline{y}, t') \, \delta\left(t' - t + \frac{R_1}{a_0}\right) dt' d^3\underline{y} \tag{3.23}$$

and

$$p'(\underline{x}_2, t+\tau') \simeq \frac{\rho_0}{4\pi a_0^2 |\underline{x}_2|} \int_{V_y} \int_{\infty} \frac{\partial^2 v_{x_2}^2}{\partial t^2} (\underline{y}, t') \, \delta\left(t' - t - \tau' + \frac{R_2}{a_0}\right) dt' d^3\underline{y} \tag{3.24}$$

The combination of equations 3.22, 3.23, and 3.24 gives

$$R_{pp}(\underline{x}_1, \underline{x}_2; \tau') \simeq \frac{\rho_0^2}{16\pi^2 a_0^4 |\underline{x}_1| |\underline{x}_2|} \int_{V_y} \int_{V_z} \int_{\infty} \int_{\infty} \overline{\frac{\partial^2 v_{x_1}^2}{\partial t_1^2} (\underline{y}, t_1) \frac{\partial^2 v_{x_2}^2}{\partial t_2^2} (\underline{z}, t_2)}$$

$$\delta\left(t_1 - t + \frac{R_{1y}}{a_0}\right) \delta\left(t_2 - t - \tau' + \frac{R_{2z}}{a_0}\right) dt_1 dt_2 d^3\underline{z} d^3\underline{y} \tag{3.25}$$

The same steps already used for the derivation of equation 3.17 from equation 3.16 can be repeated to show how equation 3.25 is transformed to give:

$$R_{pp}(\underline{x}_1,\underline{x}_2;\tau') \simeq \frac{\rho_0^2}{16\pi^2 a_0^4 |\underline{x}_1||\underline{x}_2|} \int_{V_y}\int_{V_z}\int_{\infty} \frac{\partial^4}{\partial\tau^4} R_{v_{x_1}^2 v_{x_2}^2}(\underline{y},\underline{z};\tau)$$

$$\delta\left(\tau - \frac{R_{1y}}{a_0} + \frac{R_{2z}}{a_0} - \tau'\right) d\tau d^3\underline{z} d^3\underline{y} \qquad (3.26)$$

In this equation, $\underline{x}_1$ and $\underline{x}_2$ have been previously defined as being in the same direction and representing the position vectors of two points in the radiation field such that $|\underline{x}_1| \gg |z|$ and $|\underline{x}_2| \gg |z|$. The time τ' has also been characterized as the particular time in which a same sound disturbance travels from position $\underline{x}_1$ to position $\underline{x}_2$ in the direction of $\underline{x}_1$ to $\underline{x}_2$. In light of these definitions the cross-correlation $R_{v_{x_1}^2 v_{x_2}^2}$ in the integrand of equation 3.26 may be rewritten as $R_{v_{x_1}^2 v_{x_1}^2}$, and the retarded time $\frac{R_{2z}}{a_0} - \tau'$ in the delta function of the same equation may be approximated, for all practical applications, by $\frac{R_{1z}}{a_0}$. The discussed modifications in the appropriate places in equation 3.26 give:

$$R_{pp}(\underline{x}_1,\underline{x}_2;\tau') \simeq \frac{\rho_0^2}{16\pi^2 a_0^4 |\underline{x}_1||\underline{x}_2|} \int_{V_y}\int_{V_z}\int_{\infty} \frac{\partial^4}{\partial\tau^4} R_{v_{x_1}^2 v_{x_1}^2}(\underline{y},\underline{z};\tau)$$

$$\delta\left(\tau - \frac{R_{1y}}{a_0} + \frac{R_{1z}}{a_0}\right) d\tau d^3\underline{z} d^3\underline{y} \qquad (3.27)$$

The expression for the mean square value of the acoustic pressure

at $\underline{x}_1$ can be obtained from equations 3.15 and 3.17 and expressed as:

$$R_{pp}(\underline{x}_1;0) \simeq \frac{\rho_0^2}{16\pi^2 a_0^4 |\underline{x}_1|^2} \int_{V_y}\int_{V_z}\int_{\infty} \frac{\partial^4}{\partial\tau^4} R_{v_{x_1}^2 v_{x_1}^2}(\underline{y},\underline{z};\tau)$$

$$\delta\left(\tau - \frac{R_{1y}}{a_0} + \frac{R_{1z}}{a_0}\right) d\tau d^3\underline{z}\, d^3\underline{y} \qquad (3.28)$$

Equation (3.27) can now be compared to equation (3.28) to give:

$$R_{pp}(\underline{x}_1,\underline{x}_2;\tau') = \frac{|\underline{x}_1|}{|\underline{x}_2|} R_{pp}(\underline{x}_1;0)$$

which substituted back in equation 3.21 provides the following expression to be written:

$$R_{p_m p_m}(\underline{x}_1,\underline{x}_2;\tau') = \frac{|\underline{x}_1|}{|\underline{x}_2|} R_{pp}(\underline{x}_1;0) + R_{p\,p}(\underline{x}_1,\underline{x}_2;\tau') \qquad (3.29)$$

In this last equation, the cross-correlation $R_{p_r p_r}(\underline{x}_1,\underline{x}_2;\tau')$ represents a very small fraction of the total reflected noise. Observe that in a reverberant environment the reflected waves propagate in all directions without preference. The pressure perturbations of the reflected noise, $p_r'(\underline{x}_1,t)$ and $p_r'(\underline{x}_2,t)$, are such that the mean square values $R_{p_r p_r}(\underline{x}_1;0)$ and $R_{p_r p_r}(\underline{x}_2;0)$ are very important in a reverberant environment because each one of them is the representation of the total reflected noise at each point $\underline{x}_1$ and $\underline{x}_2$. However, in the cross-correlation $R_{p_r p_r}(\underline{x}_1,\underline{x}_2;\tau')$, the only part of $p_r'(\underline{x}_2,t)$ that correlates with $p_r'(\underline{x}_1,t)$ is the fraction of $p_r'(\underline{x}_1,t)$ which propagates

from $\underline{x}_1$ to $\underline{x}_2$ in the direction of $\underline{x}_1$ to $\underline{x}_2$. Therefore it is not unreasonable to assume that $R_{p_r p_r}(\underline{x}_1, \underline{x}_2; \tau')$ is negligible in comparison to $R_{pp}(\underline{x}_1; 0)$. In view of this assumption, equation 3.29 may be rewritten in the following approximate form:

$$R_{pp}(\underline{x}_1; 0) \simeq \frac{|\underline{x}_2|}{|\underline{x}_1|} R_{p_m p_m}(\underline{x}_1, \underline{x}_2; \tau') \tag{3.30}$$

This equation shows how to obtain the mean square value of the acoustic pressure (and consequently the acoustic intensity) produced by the jet and radiated to the far field, by measuring the total acoustic pressure with microphones conveniently located at two different points $\underline{x}_1$ and $\underline{x}_2$ and then cross-correlating the response of these two microphones with a particular value for the time delay τ'. Experimental results, later shown in this report, seem to confirm that the term $R_{p_r p_r}(\underline{x}_1, \underline{x}_2; \tau')$ neglected in equation 3.30 by some intuitive arguments is actually very small*.

---

* In the presence of other sources of sound it can be shown that the right-hand side of equation 3.29 does have another term, $R_{p_s p_s}(\underline{x}_1, \underline{x}_2; \tau')$, representing the cross-correlation of the pressure perturbations caused by the other sources. The value of $R_{p_s p_s}$ will usually be negligible, unless some of the sources are located on the same line that passes through $\underline{x}_1$ and $\underline{x}_2$, emitting sound which propagates into the direction of $\underline{x}_1$ to $\underline{x}_2$. However, in any case, $R_{p_s p_s}$ is not considered as part of the problem since its value can easily be determined by measuring the cross-correlation with the jet turned off.

IV EXPERIMENTAL APPARATUS, INSTRUMENTATION AND PROCEDURES

4.1 Preliminary Considerations

To have the appropriate conditions for the investigation, a subsonic jet is exhausted from a circular orifice located on the surface of a symmetric airfoil into a perpendicular cross stream inside the test section of a wind tunnel. A general view of the test section is presented in Figure 2. The jet is 1.5 inches in diameter and has a fixed velocity at the exit corresponding to a Mach number of .58 and a Reynolds number equal to 520,000. The crossflow velocity provided by the uniform stream of the wind tunnel is varied to change the value of the parameter r representing the ratio of the jet velocity by the cross stream velocity. Five different values of r have been used during the test: $r = \infty$ (free jet), 9.4, 7.5, 5.6, and 3.7 . The range of Reynolds numbers of the cross stream is from 55.000 to 141.000, based on the jet diameter. The turbulent measurements have been performed inside the plane of symmetry of the jet by using a linearized constant temperature hot wire anemometer, while the acoustic measurements have been obtained five feet away from the jet orifice with microphones equipped with nose cones. The experiment is divided in two parts, each one corresponding to a different period of testing. In the first part of the experiment the jet has been surveyed for distributions of mean and turbulent velocities. In the second part, the turbulent component of the velocity has been frequency analyzed at different points inside the jet and the acoustic intensity in the

radiation field has been measured.

A comparison of the flow parameters for some experimental STOL research aircraft with the parameters which have been used in the present investigation is shown in Table 4.1. The data and a detailed description of each wing type mentioned in that Table have been presented by Galen Hu, Flügge-Lotz, and Karamcheti (1971).

Wing Type	Jet Angle	Vel. Ratio	Jet Speed fps	Aircraft Model
Augmentor	20^{o} to 90^{o}	3.3 to 1.4	320	DHC-5
Lift-fan	45^{o} to 90^{o}	10.0 to 1.4	300 to 520	Ryan XV-5
Adam	30^{o} to 90^{o}	10.0 to 2.5	520	Proposed research aircraft
Present Investigation	90^{o}	9.4 to 3.7	620	Present Investi-gation

Table 4.1 Summary of Flow Parameters for Some Experimental STOL Aircrafts and Present Investigation.

4.2 Test Apparatus

The experimental apparatus consisted of a circular jet issuing perpendicularly from the upper surface of a symmetrical airfoil located inside the test section of a wind tunnel.

Wind Tunnel. The wind tunnel is a closed circuit tunnel located at NASA-Ames Research Center in Moffett Field, California, and

operated by the Large Scale Aerodynamics Group of that Organization. The tunnel velocity in the test section can be continuously varied from 0 to approximately 290 ft/sec. During the test the velocity was always kept below 180 ft/sec. The test section is 7 ft. high by 10 ft. wide by 14 ft. long.

Air Jet System. The jet system is shown in Figure 3. It consists essentially of a manual valve, an electrical valve, a muffler, a plenum chamber, and a convergent nozzle. The electrical valve is remotely controlled to adjust the desired velocity of the jet. The plenum chamber is connected to the nozzle through a circular pipe with a diameter of 4.125 inches. The nozzle is 12 inches long, 4.125 inches in diameter at the beginning of the convergent part, and 1.5 inches in diameter at the exit orifice; it is the only part of the air jet system that stays inside the test section. The air is supplied by a line connected to a central system that also provides high pressure air for other facilities at Ames.

Airfoil. Figure 4 shows the airfoil inside the test section. It is made of aluminum with dimensions as shown in Figure 5. The jet exit is fitted with a circular orifice at the center of the airfoil in a section where the surface is flat. This provides the end of the jet nozzle to be flush with the airfoil upper surface. The distance from the airfoil lower surface to the wind tunnel floor is 10-7/8 inches. A circular cylinder, involving the jet nozzle, supports the airfoil. This support is not seen in Figure 4 because it is surrounded by an aerodynamically shaped surface for less

disturbance of the wind tunnel flow.

In the first part of the test, when mean velocity and turbulent intensity profiles in the central plane of the jet were obtained, a different airfoil was used. It was made of wood instead of aluminum with a chord length of 12 inches. The dimension in the spanwise direction was 24 inches, the same as in the aluminum airfoil. The wood airfoil also had a flat central section with no discontinuities between its upper surface and the end of the jet nozzle.

4.3 Instrumentation

A schematic diagram of the instrumentation used for the data acquisition and for the data processing is shown in Figures 6a and 6b respectively.

Hot Wire Equipment. The hot wire anemometer used for the experiment was a DISA 55D01 Constant Temperature Anemometer together with a DISA 55D10 Linearizer. The output voltage of the Linearizer consists of a fluctuating component superposed to a mean component. The fluctuating component was measured by a DISA 55D35 True RMS Meter, and the mean component was measured by a DISA 55D30 DC Voltmeter. In the second part of the experiment the fluctuating component was measured by a Hewlett Packard 3400A True RMS Meter.

A hot wire probe DISA 55A22 Straight General-Purpose Probe together with a DISA 55A27 Right-Angle Adapter were connected to a DISA 55A20 Probe Support. The Probe Support was attached to a DISA 55H01 Traversing Mechanism which was driven by a DISA 51C01 Stepper Motor. This motor was controlled by a DISA 52B01 Sweep Drive Unit

located outside the tunnel test section. The DISA traversing mechanism allows the hot wire to be remotely moved and positioned in the x_2 direction (see Figure 1 for coordinate system). A strong metallic structure connected the DISA traversing mechanism to the wind tunnel airfoil shaped traversing mechanism, which was also remotely controlled permitting the whole assemblage of hot wire probes and supports to be moved and positioned in the x_1 and x_2 directions. See Figures 2, 4, and 7 for position and connections pertaining to the hot wire probe and traversing mechanisms.

Microphone System. Four microphones placed at different positions in the radiation field were used for measuring the instantaneous acoustic pressure. The microphones were B & K Type 4133 1/2 inch Condenser Microphone with Nose Cone UA 0052 and B & K Type 2615 Cathode Follower. The power supply for the microphones was provided by a Mic Box B & K Model 321. The calibration of the microphones was performed with a B & K 4220 Pistonphone.

The four microphones were arranged in three different dispositions. In disposition number 1 the four microphones were all located in the plane formed by the coordinate axis x_1 and x_2. The position of each microphone in this first arrangement is shown in Figure 8. In disposition number 2 the four microphones were placed around the jet as defined by Figure 9. The distance from the jet exit to each microphone was approximately five feet. The four microphones were numbered

from 2 to 5 for a better identification of each microphone with the corresponding channel of the tape recorder. In disposition number 3, only two microphones were used. The microphone number 2 remained in the same location already shown by Figure 9 while the microphone number 3 was changed to a new point, approximately six feet away from the jet exit, defined in Figure 10.

Related Instrumentation. The instantaneous responses of the hot wire system, with the mean component removed, and of the four microphones were simultaneously recorded in an Ampex FR 1300 Tape Recorder. The recording was in FM with a speed of 60 inches per second, Extended Mode, which gives a frequency response in the range of 0 to 20 kHz The hot wore signal was always recorded in channel number 1, while the four microphone signals were recorded in channels 2 to 5, each channel corresponding to the microphone labeled with the same number.

The DC component of the hot wire system was removed prior to the recording by a KROHN-HITE model 3322 High Pass Filter with the low cut off frequency adjusted to 1 Hz.

The recording was constantly monitored through a Tektronix type 502 Dual Beam Oscilloscope.

During the data processing phase of the experiment the tapes were reproduced part by an Ampex FR 1300 Tape Recorder and part by a Honeywell 5600 Tape Recorder.

Third-octave-band frequency analysis of the hot wire and microphones signals were obtained with a B & K 2113 Audio Frequency Spectrometer. The analyses were recorded automatically on frequency

calibrated paper by a B & K 2305 Level Recorder connected to the Frequency Spectrometer.

A Hewlett-Packard Model 3721A Correlator was used for measuring cross-correlations. This correlator is essentially a digital instrument that simultaneously computes and displays 100 points of either probability, an auto-correlation, or a cross-correlation function. When computing correlation functions, the total time delay interval of the correlator can be adjusted up to 100 sec.

4.4 Test Procedure

This section is concerned with the adjustment of the jet and tunnel velocities, the calibration of the measuring instruments, and the techniques related to the acquisition and processing of experimental data.

The Air Jet. The local Mach number of the jet can be determined from the following isentropic expressions:

$$M_e = \sqrt{\frac{2}{\gamma-1}\left[\left(\frac{p_{0e}}{p_e}\right)^{\frac{\gamma-1}{\gamma}} - 1\right]} \qquad (4.1)$$

where γ is the ratio of specific heats ($\gamma = 1.4$ for air), p_0 is the total pressure, p is the static pressure, M_e is the local Mach number, and the subscript e stands for the jet exit. Since the total pressure at the jet exit would not be measured during the experiment, a few tests were initially performed to determine the correspondence of this pressure with the pressure measured at the plenum chamber. The jet was run at different Mach numbers under

free conditions. The pressure p_{0e} was measured by a total pressure probe located at the jet exit. The result of this measurement was read by a differential manometer which gives the excess of the total pressure with respect to the atmospheric pressure, or

$$\Delta p_{0e} = p_{0e} - p_{\infty}^{*} \tag{4.2}$$

In equation 4.2, p_{∞}^{*} represents the ambient pressure at the place where the manometer is located (the control room). The plenum pressure was measured by a pressure tap located in the plenum chamber wall. The value of this measurement, also read by a differential manometer, may be represented by the following expression:

$$\Delta p_c = p_c - p_{\infty}^{*} \tag{4.3}$$

where p_c is the pressure in the plenum chamber. The values of Δp_{0e} and Δp_c corresponding to the different jet velocities were then plotted in a curve as shown in Figure 11. In equation 4.1, the static pressure p_e is assumed to be equal to the ambient pressure, p_{∞}, of the medium surrounding the jet (usually $p_{\infty} = p_{\infty}^{*}$). Since the values of M_e obtained from equation 4.1 with p_{0e} differ by less than 1% from the values of M_e obtained with p_c, the plenum pressure has been used afterwards for the calculation of the jet Mach number. Equation 4.1 can then be rewritten in the following form:

$$M_e = \sqrt{\frac{2}{\gamma-1}\left[\left(\frac{p_{\infty}^{*} + \Delta p_c}{p_{\infty}}\right)^{\frac{\gamma-1}{\gamma}} - 1\right]} \tag{4.4}$$

Equation 4.4 was also used to calculate the value of Δp_c necessary

for running the jet at a pre-determined Mach number. The jet velocity can be obtained from this last equation by noticing that

$$U_j = M_e a_e = M_e a_0 \frac{a_e}{a_0} \tag{4.5}$$

where a_e and a_0 are the sound speeds at the jet exit and at the plenum chamber, respectively. The isentropic expression for $\frac{a_e}{a_0}$ is substituted in equation 4.5 to give

$$U_j = M_e a_0 \left[1 + \frac{\gamma-1}{2} M_e^2\right]^{-1/2} \tag{4.6}$$

Equations 4.4 and 4.6 were used to calculate the velocity of the free jet, with a_0 being equal to its standard value at sea level (1116 fps).

Hot Wire. The role of the linearizer in the hot wire system is briefly explained in Appendix A. For the case of a hot wire probe located at the exit of a subsonic cold jet, the output voltage of the linearizer may be expressed by either of the following equations:

$$V_{LIN} = K_1 \rho_\infty U_j \left[1 + \frac{\gamma-1}{2} M_e^2\right] \tag{4.7}$$

or

$$V_{LIN} = K_1 \rho_\infty a_0 M_e \left[1 + \frac{\gamma-1}{2} M_e^2\right]^{1/2} \tag{4.8}$$

The hot wire system was calibrated with the wire located inside the potential core of the free jet close to the jet exit. The jet was run at different velocities (up to a velocity corresponding to $M_e = .6$), while the controls of the linearizer were adjusted for the best fit of a straight line representing an approximation of equation 4.7 given by the following form:

$$V_{LIN} \simeq K_1 \rho_\infty U_j \tag{4.9}$$

In the second part of the experiment, when the hot wire signal was used for frequency analysis, the hot wire system was calibrated for the best fit of a straight line representing

$$V_{LIN} \simeq K_1 \rho_\infty a_0 M_e \tag{4.10}$$

This last equation is an approximate form of equation 4.8. The adjustment of the linearizer controls seems to be easier to obtain when V_{LIN} is plotted as a linear function of M_e instead of U_j. This can be explained by noticing that the output voltage of the linearizer is better approximated by equation 4.10 than by equation 4.9.

The calibration of the hot wire system was briefly checked before and after each run. A complete calibration was always done whenever a sensor was replaced due to failure.

In all measurements involving hot wire, the sensor was located in the plane of symmetry of the jet (plane defined by the coordinate axis x_1 and x_2) with its axis parallel to the direction defined by the coordinate axis x_3. It has been assumed that in the plane of symmetry the mean velocity of the jet in the direction x_3 is always zero. Therefore, the DC component of the hot wire corresponds to the mean speed in the plane x_1x_2 independent of its direction, while the fluctuating part of the hot wire signal corresponds to the component of turbulence in the direction of the mean velocity.

The Wind Tunnel Flow and its Effect on the Jet Velocity. The dynamic pressure q_∞ of the wind tunnel flow is measured by a pitot static probe located inside the test section in a region not

disturbed by the jet. The tunnel velocity U_∞ can be calculated from the equation relating the dynamic pressure with the velocity,

$$q_\infty = \frac{1}{2} \rho_\infty U_\infty^2 \quad ,$$

by assuming the density to be equal to its standard value at sea level (2.377×10^{-3} lb sec^2/ft^4). The tunnel was run at four different values of q_∞ (5.3, 8.4, 14.8, and 33.4 lb/ft^2) while the jet Mach number was kept constant at $M_e = .58$ during the tests involving the jet in the crossflow.

A certain amount of blockage of the jet flow caused by the cross stream seems to exist. This effect is noticed by the decrease of the output voltage of the hot wire system, with the sensor located at the center of the jet orifice, whenever the tunnel is turned on. In order to return the reading of the hot wire to the same value indicated before, when the jet was in free conditions, it is necessary to increase the pressure in the plenum chamber by a substantial amount. A reverse effect is observed when the tunnel is turned off. A pre-test was performed to verify the influence of the different values of q_∞ on other parameters related to the flow. In this pre-test the hot wire sensor was placed at the center of the jet orifice and the following sequence was executed:

a - Turn jet on. Adjust Δp_c to desired value of M_e .

b - Check the voltage of the hot wire system with calibration curve.

c - Turn tunnel on to the desired value of q_∞ .

d - Increase Δp_c until the hot wire voltage goes back to the same value shown after step b .

The result of this pre-test is presented below in Table 4.2.

q_∞ (lb/ft^2)	q_∞ (in. Hg)	Δp_c (in. Hg)	p_∞^* (in. Hg)	M_e (By Hot Wire)	$r = \frac{U_j}{U_\infty}$
0	0	7.6	30.02	.58	
5.3	.075	7.6	29.95	.53	
5.3	.075	9.3	—	.58	9.4
8.4	.119	7.6	29.92	.53	
8.4	.119	9.5	—	.58	7.5
14.8	.209	7.6	29.84	.53	
14.8	.209	9.6	—	.58	5.6
33.4	.472	7.6	29.63	.53	
33.4	.472	9.7	—	.58	3.7

Table 4.2 Effect of q_∞ on Other Parameters Related to the Jet Flow.

Since the hot wire system had been carefully calibrated, it was decided to rely on the hot wire reading for the adjustment of the jet Mach number whenever the jet was in the presence of a crossflow. Therefore, before each run, the hot wire sensor was located at the center of the jet orifice and the pre-test sequence was followed to adjust the plenum pressure. After this procedure the hot wire probe was then remotely moved to the required position for that particular run. In the acoustic measurements, where the hot wire probe was not present, the plenum pressure was adjusted for the values of Δp_c given by Table 4.2.

Microphones. The microphones were individually calibrated with a pistonphone. The sound pressure level of the pistonphone is

124 dB (ref. 2×10^{-4} μbar). During the calibration the electrical output of each microphone was adjusted to indicate a RMS value of .5V (or 14dB ref. .1V). The calibration was repeated before each day of testing. The calibration signal of each microphone was recorded in magnetic tape for reference during the data processing phase of the experiment.

Data Acquisition. In the first part of the experiment, when the jet was surveyed for distribution of mean velocity and turbulent intensity, no tape recording was made. The data acquisition was performed by a direct reading of the DC and RMS components of the hot wire system corresponding to each different position occupied by the hot wire sensor inside the jet. In the second part of the experiment, both the hot wire and the microphones signals were tape recorded for posterior processing. Before each recording, which was labeled with an identifying number, the RMS value of the fluctuating component of the hot wire signal and the gain of each one of the microphones were read and registered in the experiment log book.

Some vibrations of the hot wire probe were observed during the experiment. Though they could be reduced by shortening the length of the metallic structure which connects the hot wire supports to the wind tunnel traversing mechanism, they could not be avoided as a whole. When observed in the oscilloscope those vibrations were apparently at frequencies much lower than the frequencies associated with the velocity fluctuations inside the jet.

Data Processing. During the data processing phase of the experiment the output voltage of each channel of the tape recorder was checked with reference values obtained during the data acquisition. The RMS voltage of the channel corresponding to the hot wire signal was compared with the RMS value of the fluctuating component of the hot wire system registered in the experiment log book, and the output of each channel corresponding to one microphone was compared with the signal that had been recorded during the calibration of that microphone with the pistonphone. The output voltage of each channel was connected directly to the Frequency Spectrometer in those cases where frequency analyses were desired. The signals from channels 2 and 3 of the tape recorder were fed directly to the two inputs of the correlator for the calculation of the cross-correlation functions.

V RESULTS AND DISCUSSION

This chapter is divided into three sections, each being concerned with a particular group of experimental measurements. The first section presents the results obtained with hot wire anemometry mainly in the source flow region of the jet. The second section deals with conventional sound measurements in the radiation field, while the last section is concerned with the measurement of sound intensity by the technique of two microphone cross-correlations in the radiation field. Interpretations and discussions are presented together with the data and are directed towards assessing the effects of crossflow velocity.

5.1 Features of the Flow Inside the Jet

The experimental investigation with hot wire is limited to the plane of symmetry of the jet (plane x_1x_2) in the source flow region and in the very beginning of the transition region (see Figure 1b). The ratio r, of the jet and crossflow velocities, used during the tests assumes five different values. In all of them the jet velocity is kept constant while the crossflow velocity is changed whenever the value of r is to be modified.

Magnitude of the Mean Velocity. The hot wire was placed at a fixed vertical distance from the jet exit and then traversed in the direction of the coordinate x_2 to measure the horizontal profile of the mean

velocity* across the jet. Several of these profiles were obtained at different vertical distances x_1/D for all values of the ratio r . Figure 12 shows these three typical horizontal distributions of mean velocity normalized by the jet velocity at the exit. The velocity is low at the sides and increases toward a maximum at the center of the jet. In the transition region, the maximum of the velocity curve occurs at just one point which then defines the center line of the jet. Closer to the jet exit, in the source flow region, the maximum of the mean velocity profile occurs at various adjacent points x_2 simultaneously, giving a flat shape to the central part of the curve. That flat shaped section characterizes the interior of the potential core where the mean velocity is practically constant with a complete absence of shear in the radial direction. When the jet is under free conditions ($r=\infty$) , the velocity profiles are symmetrical with respect to the axis x_1 and the jet centerline coincides with that coordinate axis. Due to the crossflow, the jet is pushed back into a curved trajectory with different velocity distributions in the front and in the back part of the cross section. Inside the potential core, the flat section of the mean velocity profile is slightly inclined, with smaller velocities in the front part which is closer to the region

---

* As previously discussed in Chapter IV, the hot wire sensor was positioned to measure the magnitude of the mean velocity of the jet independent of its direction. Because it seems to be a common practice in the literature, the term mean velocity is also largely used in this report with the actual meaning of mean speed.

of impact of the crossflow with the jet. According to Abramovich (1963), this small radial variation of velocity inside the potential core is to be expected since the static pressure in the front part of the jet is higher than in the back part due to the deceleration of the crossflow. A schematic view of the mean velocity mapping in the central plane of the jet is shown in Figures 13a to 13e, each one representing a different value of r .

Mapping of the Jet - External Boundaries and Potential Core. The external limits of the jet are obtained from the mean velocity profiles by the use of Keffer and Baines (1967) criterion which defines the edge of the jet as the locus of points "where the velocity excess above the external undisturbed flow $(U-U_\infty)$, is 10% of the maximum excess $(U_m - U_\infty)$, at a given cross section." The boundaries of the jet are represented by the external dashed lines in Figures 13a to 13e. As observed by previous workers the jet cross section is circular at the orifice and then evolves to a horseshoe shape a few jet diameters away from the exit due to the interaction with the cross stream. As the cross stream changes its shape, more jet mass spreads to the sides, out of the central plane, therefore reducing the dimensions of the jet in the plane of symmetry This behavior is observed in Figures 13b to 13e by the gradual approximation of the front and aft limits of the jet as the axial distance from the exit increases.

The potential core is characterized by a flat distribution of the mean velocity, its magnitude in the core being maximum at any given cross section of the jet. The boundaries of the core are taken as the loci of points where the mean velocity is 2% less than the maximum velocity in the flat region. The limits of the potential core are shown by the internal dashed lines in Figures 13a to 13e. The source flow region, even in the case of higher crossflow velocities, remains very close to a vertical position as can be observed by the small distances between the tip of the potential core and the coordinate axis x_1. In a crossflow jet the length of the potential region, is a function of the velocity ratio r. As shown in Figure 14, the length of the potential core normalized by the jet diameter decreases with an increase of the cross stream velocity. The length of the potential core of the free jet was also determined and is presented in the same figure to show the limit of the curve when the velocity ratio approaches ∞. Also plotted in this figure is one of the curves obtained by Pratte and Baines (1967). Some differences between the two curves are clearly seen. First, the value of s_c/D in Pratte and Baines curve is higher than the corresponding value of s_c/D in our curve. This is due to the difference of jet diameters used in the two experiments. Pratte and Baines (1967) have measured the length of the potential core for different jet sizes and they have found that s_c/D slightly increases when the jet diameter

decreases. They also found that the shape of the curves describing s_c/D as a function of r was similar for all jet diameters used in their investigation. In figure 14, the slope of our curve is stronger than that of Pratte and Baines curve. The reason for this can be speculated as due to the following causes: a) the jet velocity used in Pratte and Baines experiment was of the order of 30 fps and lower and, b) in Pratte and Baines experiment the crossflow velocity was kept constant at a value of 3 fps while the jet velocity was changed to vary the value of r . The reader will recall that in the present experiment the jet velocity is kept constant at about 620 fps while the cross stream velocity is changed to vary the value of r . More investigation is needed to determine how the jet velocity and the way of varying the ratio r may affect the length of the potential core of the jet.

Turbulent Intensity. During the measurements of the magnitude of the jet mean velocity the root mean square (RMS) component of the hot wire system was also measured. The fluctuating component of the hot wire corresponds approximately to the turbulent component of the flow velocity in the direction of the mean velocity vector [see Davies, Fisher and Barratt (1963)]. The RMS value of the measured signal normalized by the jet velocity at the exit gives the turbulent intensity which is discussed in this section.

Three typical turbulent intensity profiles are shown in Figure 15. These profiles were obtained in the source flow region and in the very beginning of the transition region and they are characterized

by the presence of sharp peaks in the front and in the back mixing zones, with regions of low turbulence at the sides of the jet and also at the jet centerline. The turbulent peaks are usually located at points where the shear is very high. The turbulent intensity is particularly low inside the potential core close to the jet exit. A complete distribution of turbulent intensity in the central plane of the jet for different values of the velocity ratio r is shown in Figures 16a to 16e. Unlike the free jet where the turbulence is symmetrical with respect to the central axis of the jet, the jet in the crossflow has different turbulent intensity distributions in the front and in the back mixing regions.

Axial Distribution of Mean Velocity and Turbulent Intensity. It is interesting to compare for the same jet the axial distributions of the magnitude of the mean velocity and of the turbulent intensity for different crossflow velocities. For this purpose the coordinate s along the jet axis is stretched by the ratio of the length of the potential core of the free jet to that of the jet under consideration, such that the source flow region has the same length independent of the value of the crossflow velocity. The coordinate ξ obtained from s as explained above is further normalized by the jet diameter D. Figure 17 shows the axial distribution of mean velocity along the jet centerline. The use of the stretched coordinate ξ permits one to notice that the behavior of the jet mean velocity along the centerline in the source flow region and in the beginning of the transition region is similar for all values of r including $r=\infty$

which corresponds to the case of the free jet.

The axial distribution of turbulent intensity along the jet centerline and along the line connecting the points where the peaks of turbulent intensity are located both in the front and in the back mixing region is shown in Figure 18*. When carefully observed one can notice that the turbulent intensity becomes regularly higher as the crossflow velocity increases. It can also be observed that, except for those points corresponding to $r = 3.7$, the turbulent intensity in the front mixing region is approximately equal to or slightly higher than the turbulent intensity in the back mixing region. For $r = 3.7$, the experimental case where the crossflow velocity is stronger, the turbulent intensity is higher in the back mixing region. This is probably caused by the changing of the characteristics of the turbulence in the back mixing region due to the interaction of vortices shed from the jet with the entrainment process. Further consideration of this point will be given in discussing the frequency spectra inside the jet.

In light of the increase of the turbulent intensity with increasing crossflow, as is observed in Figure 18, an attempt was

---

* It may be of interest to mention that in the first part of the experiment some very high values of turbulent intensity were obtained for $r = 5.6$. Measurements repeated for this same value of r in the second part did not show those unexpected high values. It is possible that vibrations of the metallic structure connecting the hot wire probe to the wind tunnel traversing mechanism used in the first part of the experiment (which was different from the one used in the second part) have caused the mentioned discrepancy. Those unexpected high values of turbulent intensity are not shown in Figure 18.

made to find instead of U_j a more suitable characteristic velocity so as to bring the experimental results more into a single curve. It is found that this can be achieved by introducing $U_j + U_\infty = U_j \left(1 + \frac{1}{r}\right)$ as the characteristic velocity. As is shown in Figure 19, where the variation of $\frac{u'}{U_j \left(1 + \frac{1}{r}\right)}$ with $\bar{z}/D$ is plotted, all the experimental points seem to fit in just one curve representing the average of the maximum of the turbulent intensity in the two mixing zones, and another curve representing the turbulent intensity on the jet centerline.

The physical significance of this parameter $\left(1 + \frac{1}{r}\right)$ on theoretical grounds remains to be clarified. The present experimental results seem to indicate, however, that in the range of the values of r investigated, the jet in the presence of a crossflow has turbulent characteristics in the plane of symmetry inside the source flow region and in the beginning of the curvilinear region, similar to those of a free jet with an exit velocity increased by the factor $\left(1 + \frac{1}{r}\right)$. We note and emphasize that as $r \to 0$ this observation will not be valid.

Frequency Analysis of the Turbulence. In the second part of the experimental work, the hot wire sensor was located at different positions inside the jet and the RMS component of the hot wire system was recorded for posterior studies of frequency distribution of the signals. Most of the frequency analyses were limited to the jet centerline and to the mixing region at those points where the turbulence levels are the largest.

Initially some complete spectra (20 Hz to 20 kHz) obtained at the jet exit for different values of the velocity ratio r are shown in Figure 20 to explain some features caused by reasons not directly related to the flow perturbations. All the spectra were obtained in 1/3 octave band. In those spectra, the bump at lower frequencies is associated with the observed vibrations of the metallic structure connecting the hot wire probe and supports to the wind tunnel traversing mechanisms. The sharp peak at about 13 kHz is apparently not related to the fluctuations of the flow itself. This high frequency peak is observed in the potential core and at some places in the mixing region and its frequency does not change with the position inside the jet, neither does it change with the variation of the crossflow velocity. The hot wire data of Ko and Davies (1971) have a similar peak at about the same frequency. The same peak was also observed, in the mentioned reference, in the spectra obtained with microphone measurements in the near field outside the j . Ko and Davies (1971), associated this high frequency peak of the near field spectra with valve noise. This association is ruled out in the present experiment for the two following reasons: the high frequency peak has not been observed in the radiation field with microphone measurements, and neither has it been observed in the spectra obtained from pressure measurements inside the potential core of the same jet.* Due to the high velocity of the jet used in the

* Personal communication with Mr. Brent Hodder at NASA-Ames Research Center.

present test the wire is subjected to aerodynamic forces which can cause deformations of both the wire and prongs [see Widell (1965)]. These deformations are variable in time and produce the so-called "strain gage effect" discussed by Morkovin (1956). As a result, a high frequency "noise" appears in the output of the wire. Morkovin (1956) shows some results obtained at supersonic Mach numbers where the frequency of the peak due to this strain gage effect is a function of the jet Mach number. An extrapolation of these results to the subsonic side would give at $M_e = .58$ a frequency that is close to the frequency observed in Figure 20. Thus, it is reasonable to assume that the high frequency peaks in the hot wire spectra measured in this experiment are caused by prong and wire vibrations due to aerodynamic forces acting on the wire.

The spectra in the front mixing region of the jet are characterized by the predominance of wide band signal which is a peculiarity of the strong turbulence prevailing at those points. The spectral content is very similar for all values of the velocity ratio r. Typical spectra on this region of the jet are shown in Figure 21. The spectra content is generally flat up to a certain frequency and then decreases with a rate of the order of 6 dB/octave (3 dB/octave from the curve plus 3 dB/octave for correction of the 1/3 octave band filters), a figure which is in agreement with the experimental findings of Ko and Davies (1971).

In the back mixing region the spectra are more subjected to

changes in the crossflow velocity. For the smaller values of the crossflow velocity, ($r = 9.4$ and 7.5), the spectral behavior is very similar to that in the front mixing region. Some typical spectra obtained in the back mixing region for $r = 9.4$ are shown in Figure 22. For r equal to 5.6, the spectra still show some resemblance with those in the front mixing region but the appearance of a small bump is observed around the 200 Hz frequency, as can be seen in Figure 23. When the crossflow velocity is such that the value of r is equal to 3.7, the low frequency bump first observed at $r = 5.6$ is transformed to a peak dominating the spectrum close to the 300 Hz frequency (see Figure 24). This peak at 300 Hz is probably the cause for the higher values of the turbulent intensity observed in the back mixing region of the jet when the ratio r is equal to 3.7. Vortex shedding from a circular jet in a high Reynolds number crossflow has been previously detected by McMahon, Hester, and Palfery (1971), who used a two-inch circular jet exhausting perpendicularly into a crossflow with a fixed velocity of 50 ft/sec. The non-dimensional frequency associated with the vortex shedding, represented by the Strouhal number $S = \frac{fD}{U_\infty}$ (where D is the jet diameter), was observed to be slightly dependent on the ratio r, assuming the values of .083 and .093 for r equal to 12 and 8 respectively. The Reynolds number of the crossflow (based on the jet diameter) in that experiment was 52000. In the present test the range of the cross stream Reynolds number is from 55,000 to 141,000, corresponding to the values of the parameter r from

9.4 to 3.7 . Based on the observations of McMahon, Hester, and Palfery (1971) it is probable that vortices are being shed from the jet for all values of r in the present experiments. These vortices would probably be detected by a hot wire located in the wake of the jet. If the hot wire were placed at the sides of the wake, it would sense the frequency of the vortex shedding. On the other hand, if the hot wire were located at the center of the wake it would sense a frequency equal to twice the vortex shedding frequency. That would be so because vortices shed from both sides of the jet would influence the hot wire probe. It is interesting at this point to note that the frequencies of 200 Hz for r equal to 5.6 and 300 Hz for r equal to 3.7 obtained in the turbulent spectra inside the back mixing region, with the hot wire located in the plane of symmetry of the jet in the present tests, correspond to a Strouhal number which is approximately equal to twice the value of the Strouhal number associated with the vortex shedding reported by McMahon, et.al.(1971). But why would the frequency of the vortex shedding be felt inside the jet? A reasonable answer is that the vortices, after being shed, would push air from the wake into the back mixing region therefore contributing to the entrainment process of external fluid into the rear part of the jet. Why was the same phenomenon not observed for the cases of r equal to 7.5 and 9.4? At this point there is no answer for this question. More investigation is necessary to clarify the whole extent of this suspected interaction of the vortices shed from the jet with the entrainment process.

The most interesting features of the frequency analysis occur with the signals inside the potential core of the jet. Davies, Ko, and Bose (1968), later complemented by Ko and Davies (1971), have shown that inside the potential core of a free jet there exists a near pressure field caused by the strong fluctuations of the velocity in the surrounding mixing region. Due to the low velocity fluctuations inside the core, this pressure field gives rise to consequent density variations which are felt by the hot wire sensors. The frequency analysis of the hot wire signal shows a peak due to the near field pressure fluctuations and a flat part due to the turbulence itself. In the mixing region the turbulence signals are so high that they completely mask the part corresponding to the pressure fluctuations in the output of a hot wire sensor located in that region. For the case of the crossflow jet of this investigation it is also possible to observe the outgrowth of a peak (not necessarily sharp) at frequencies close to 3000 Hz. This peak does not exist close to the jet exit but it begins to form at an axial distance of approximately one jet diameter varying with the value of r. A typical development of this peak is shown in Figure 25 for $r = 7.5$. The peak shifts to lower frequencies and also becomes wider as the axial distance from the jet exit increases. As the measuring point approaches the end of the potential core, the spectral content becomes similar to that obtained in the mixing region. In the case of the free jet, the peak frequency of the spectra has a Strouhal number dependence on the axial distance, as shown by Ko and

Davies (1971). This Strouhal number is usually defined by the nondimensional parameter $\frac{f_p D}{U_j}$ where f_p is the frequency of the peak of the spectrum. For the case of a jet in the crossflow a similar dependence is obtained if a modified Strouhal number defined by $\frac{f_p D}{U_j\left(1 + \frac{1}{r}\right)}$ is plotted as a function of the stretched axial distance ξ as shown in Figure 26, for all values of r used in this experiment. Also plotted in Figure 26 in dashed lines is the envelope of points obtained by Ko and Davies (1971), in the case of the free jet. The limits of this envelope were presented by Wooten, Wooldridge and Amaro (1972). Observe that almost all the points fall inside the dashed envelope. It should be noticed, however, that the Strouhal number defined by our points (even for our free jet) decreases with the axial distance at a faster rate than that suggested by the dashed envelope. Ko and Davies (1971). results were obtained with a jet operating at a Mach number of .218 in contrast with the present experiment where the Mach number at the jet exit was equal to .58. This confirms one observation made by Wooten et. al. (1972), that the Strouhal number inside the potential core is also a function of the jet Mach number.

We note that in accounting for the variation of the peak Strouhal number in the core with distance along the jet axis, the suitable characteristic velocity turns out to be again $U_j\left(1 + \frac{1}{r}\right)$ instead of U_j. One may argue that this may be expected for, following Ko and Davies (1971), the origin of the peak frequencies in the core are due to the near pressure field which in itself is

caused by the turbulence in the mixing region, and as we have seen the variation of the turbulence intensity in the mixing zone with axial distance can be represented by almost a single curve if such intensity is normalized by the characteristic velocity $U_j \left(1 + \frac{1}{r}\right)$.

5.2 Microphone Measurements in the Radiation Field

The noise produced by the jet was measured by four microphones in the radiation field, arranged in two different dispositions as shown in Figures 8 and 9. The results of these measurements are presented in 1/3 octave spectra (SPL in dB ref $2X10^{-4}$ μbar) . The plots are already corrected for the background noise of the tunnel which is defined as the noise measured with the jet turned off and with the tunnel operating at a velocity appropriate to the desired value of the ratio r . Figure 27 shows one typical plot containing both the total noise and the background noise curves. The difference between the sound level with the jet operating and the background level determines the correccion to be used. The amount of this correction is given by Peterson and Gross (1972). The curve obtained after the correction represents the noise produced by the jet. This noise contains both the noise radiated directly from the jet to the point where the microphone is located plus another contribution due to the noise radiated from the jet and reflected from the walls of the wind tunnel. The interaction of the crossflow with the jet flow increases the noise produced by the jet as can be seen in Figure 28. This figure is for a particular position of one microphone in the

radiation field, but due to the effect of reverberation of the wind tunnel test section, it is also a valid representation for the results obtained with all the other microphones. This observation confirms the reverberation characteristics of the test section and the impracticability of obtaining any directivity effect of the noise produced by the jet when the measurement is performed in a reverberant environment by the traditional technique of using just one microphone. The lower frequencies do not appear in Figure 28 because at those frequencies the difference between the total measured noise and the background noise is less than 3 dB and therefore the noise produced by the jet cannot be accurately determined [see Peterson and Gross (1972)]. The spectra are, in general, very broad with most of the energy concentrated in the range of frequencies from 1 to 10 kHz. The curves presented in Figure 28 suggest a small shift of the maximum point of the spectra to higher frequencies as the crossflow velocity increases. Due to the broadness of the spectra though, this frequency shift in only clearly observed for the velocity ratio r equal to 3.7. The broadband linear weighted sound pressure level for each value of r is shown at the right side of Figure 28. The variation of the broadband sound intensity with the velocity ratio r is presented in the next section for comparative purposes with the intensity measured by the technique of two microphone cross-correlations.

5.3 Sound Intensity Measurements by Two Microphone Cross-Correlations

As has been shown in Chapter III, the noise radiated directly

from the jet cannot be obtained inside a reverberant room by the conventional method of measurement with just one microphone. What the microphone is actually measuring is a combination of the direct noise, i.e., noise coming directly from the jet to the measuring point, plus the reflected noise, i.e., noise radiated by the jet in all directions and reflected by the walls back to the point of measurement. The background noise is not being considered since it is always possible to correct its effect similarly to what has been done in the previous section 5.2. The direct noise, as defined above, can be obtained inside a reverberant room with a good approximation by the technique proposed in this report which consists in measuring the cross-correlation of the signals from two microphones conveniently located in the far field, at the appropriate time delay (see Chapter III). In order to make some experimental verification of the formulation shown in Chapter III, two microphones were located in the radiation field in the position shown by Figure 10. As can be seen in that figure, the position vectors $\underline{x}_2$ and $\underline{x}_3$, corresponding to microphones 2 and 3 respectively, are in the same direction which is one of the requirements for this type of measurement when the source of noise is a jet. The mean square value of the sound pressure directly radiated from the jet to the point $\underline{x}_2$ where microphone 2 is located was derived in Chapter III and is rewritten as:

$$R_{pp}(\underline{x}_2;0) \simeq \frac{|\underline{x}_3|}{|\underline{x}_2|} R_{p_m p_m}(\underline{x}_2, \underline{x}_3; \tau') \tag{5.1}$$

The appropriate time delay τ' is obtained from equation 3.6 and expressed by

$$\tau' = \frac{\left[\left(1-M_2^2\right)|\underline{x}_3-\underline{x}_2|^2 + M_2\left(x_{32}-x_{22}\right)\right]^{\frac{1}{2}} - M_2\left(x_{32}-x_{22}\right)}{a_0\left(1-M_2^2\right)} \tag{5.2}$$

where the coordinates corresponding to the vectors $\underline{x}_2$ and $\underline{x}_3$ are given in Figure 10.

To check the practical reliability of this measuring technique the jet was run at different Mach numbers such that the noise intensity obtained by the method of the two microphone cross-correlations could be compared with results measured by previous workers in an anechoic room. The time delay τ' in the case of the free jet is estimated from equation 5.2 to be 9.3×10^{-4} sec (with a_0 equal to 1116 fps). The total time delay of the correlator was adjusted to 1×10^{-3}sec which gives a sampling rate of 100,000 samples per second (the correlator has 100 calculating points). Since the highest frequency of the signals being investigated is 20kHz the sampling rate for the highest frequency component is equal to five samples per cycle, therefore complying with the sampling theorem [see Bendat and Piersol (1971)]. A typical cross-correlation curve is shown in Figure 29. This curve was obtained with the free jet operating at $U_j/a_0 = .56$. It was observed that all the correlation curves for various values of U_j have definite peaks at a certain value of the time delay, namely 9×10^{-4}sec , and have

essentially zero correlation level over most of the range of the time delay.

Incidentally, using the measured value of 9×10^{-4} sec for τ' in equation 5.2 and setting M_2 equal to zero, we find a_0 to be 1148 fps. This corresponds to the conditions in the tunnel room.

The value of the measured correlation at 9×10^{-4} sec applied in equation 5.1 and the result substituted in equation 3.15 relating the acoustic intensity to the mean square of the pressure perturbations, gives the sound intensity at the point $\underline{x_2}$. The results of the complete test with the free jet is shown in Figure 30 together with the results measured by just one microphone [Mic 2(3)] and also with the measurements of Lush* (1971) in an anechoic chamber. Lush's points as presented in Figure 30 have been adjusted for the three following effects: a) change in the reference level of the sound intensity (Lush used dB ref. 10^{-12} Watts/m^2); b) geometrical attenuation (Lush measurements were taken at three meters from the jet); c) jet dimension (Lush's jet was 25 mm in diameter). It is gratifying to observe that the present data obtained by the two microphone cross-correlation technique agree strikingly closely with those obtained by Lush (1971) inside an anechoic room. Actually, our data was obtained at 50° (Lush's were at 45°) and they should be slightly below Lush's results, according to the general trend of his Figure 3. The difference however is so

---

* See Figure 3, 45° data in the mentioned reference.

small that it can be neglected for all practical purposes. We have thus confirmed that the use of equation 5.1 above on the basis of the two microphone cross-correlation technique leads to a reliable value of the noise radiated directly from the jet.

Also observe in Figure 30 that the sound intensity obtained with one microphone (corrected for the background noise) is of the order of 6 dB higher than the sound intensity obtained by the two microphone cross-correlation. The effect of the reflections is then to increase the noise by a factor of 4 at that particular point where the measurements were obtained.

Now we consider the determination of the intensity of the acoustic radiation from the jet in the crossflow. Due to the position of the microphones, the appropriate time delay for the cross-correlations becomes smaller as the cross stream velocity increases. The appropriate time delay for $r = 3.7$ for example is 8.7×10^{-4} sec , with a_0 equal to 1148 fps (assuming the temperature of the uniform stream in the test section is the same as the control room temperature; recall that $M_2 \ll 1$) . The characteristics of the cross-correlation curves do not change very much when a crossflow is present. Figure 31 shows a cross-correlation curve for a value of the velocity ratio equal to 9.4 . The time delay appropriate for the correlation is now 8.9×10^{-4} sec . The most important feature of the correlation curve for our particular investigation, the peak at the appropriate value of the time delay, is definitely characterized in the curve. Some differences

from the free jet case shown in Figure 29 are noticed at other time delays but they are of no interest in our considerations.

Figure 32 is a cross-correlation obtained with $r = 3.7$ and with the total time delay interval of the correlator re-adjusted to 3.3×10^{-3} sec , which gives a rate of 30,000 samples per second. This representation was not used to calculate the noise intensity since it does not comply with the sampling theorem for frequencies higher than 15,000 Hz It was photographed to show how some reflections may affect the cross-correlation. The first peak occurs at the appropriate value of the time delay for a sound wave, coming from the jet, to travel from microphone 2 to microphone 3 in the direction of $\underline{x_2}$ to $\underline{x_3}$. Two other smaller peaks occur at a later time delay representing some reflections from the tunnel walls.

The noise intensity directly radiated from the jet to the point where microphone 2 is located is plotted in Figure 33 as a function of the velocity ratio r . Also shown in that figure is the noise intensity measured at the same point with just one microphone. The difference between the two measurements is still approximately 6 dB showing that even for louder noises the amplification factor of the tunnel is 4 , the same value observed for the case of the free jet. This amplification seems to be a characteristic of the reverberation room corresponding to that particular point of measurement. The dashed horizontal lines in the figure represent the noise intensity of the free jet, when $r \to \infty$.

As expected, the noise directly radiated from the jet increases with the cross stream velocity. It is interesting to notice that the noise intensity, even for the smaller values of the crossflow, is always much higher than the noise intensity of the free jet. In the range of r from 9.4 to 3.7 the noise intensity increases with the crossflow. The variation of the intensities with r, for r lower than 3.7 needs to be examined.

VI CONCLUSION

The present study has been primarily concerned with the modifications which occur in the internal structure and in the acoustic field of a high velocity jet when it is deformed by the pressence of a crossflow perpendicular to the direction of the undisturbed jet.

The use of the coordinate ξ, which stretches the jet in such a way that the length of the potential core becomes the same for any value of the cross stream velocity, has enabled the comparison of the internal flow characteristics of the jet under the influence of different crossflows. The experimental data have shown that the turbulent intensity inside the noise producing region of a crossflow jet increases by a factor of $\left(1 + \frac{1}{r}\right)$ as compared to the turbulent intensity of the same jet under free conditions. The parameter $\left(1 + \frac{1}{r}\right)$ has also been observed in the frequency analyses of the turbulence. The peak observed in the hot wire spectra obtained inside the potential core has a frequency that changes with the cross stream and, similar to the case of the turbulent intensity, increases by a factor of $\left(1 + \frac{1}{r}\right)$ with respect to the corresponding frequency measured in the free jet.

The two microphone cross-correlation technique, for acoustic measurements in a medium where sound directly radiated from a source co-exists with all kinds of reflected noise, has proved to be a very efficient tool for filtering the unwanted noise off of the measurement. The agreement of the acoustic intensity radiated from a free jet

measured by the two microphone cross-correlation technique in the present experiment, with the results obtained by Lush (1971) inside an anechoic chamber confirms the capability of the method.

The intensity of the noise radiated from a jet with a constant exit velocity becomes higher when the velocity of the cross stream increases. The variation of the acoustic intensity of a crossflow jet as compared to the acoustic intensity of the same jet under free conditions is shown in Figure 34 as a function of the velocity ratio r. Also plotted in that figure is the curve

$$\frac{I_r}{I_{r=\infty}} = \left(1 + \frac{1}{r}\right)^8 \tag{6.1}$$

representing the ratio of the acoustic intensity of the crossflow jet to the acoustic intensity of the free jet, and obtained by a simple dimensional analysis (see Appendix B). Observe from Figure 34 that for those values of r which are less than 6, the experimental curve shows a tendency to level off while the curve representing equation 6.1 keeps increasing as the value of r decreases. The behavior of the experimental curve for those small values of r suggests that the decrease of the noise producing region of the jet has some effect on the reduction of the acoustic intensity. This is not observed in the curve obtained from the dimensional analysis because we have not considered the decrease of the noise producing region with the increase of the crossflow velocity in the derivation of equation 6.1. For those values of r between 6 and 10 the

two curves have a very similar shape showing that the increase of the turbulent level of the jet contributes to the acoustic intensity as expected from the analytical expression used for the dimensional analysis. The size of the noise producing region seems to have a small effect, if any, in the noise output for those values of r under consideration. The experimental curve however, shows a higher level of acoustic intensity. Since the hot wire measurements were performed only in the plane of symmetry of the jet, it is not unreasonable to speculate about the lateral sides of the jet as a region of strong noise production due to the deformation caused by the cross stream.

The measurement of simple turbulent quantities outside the central plane of the jet, the verification of the parameter $\left(1 + \frac{1}{r}\right)$ for other values of jet velocity and jet diameter, and the investigation of possible effects of vortex shedding on the entrainment process are some of the features that need further study. The measurement of noise at several points in the radiation field, by the two microphone cross-correlation method needs to be undertaken for determining how the noise directivity is affected when the jet is under the influence of a crossflow. The two microphone cross-correlation technique promises to be a useful method for applications in other problems directly related to the exciting field of Aerodynamic Noise and should be further explored.

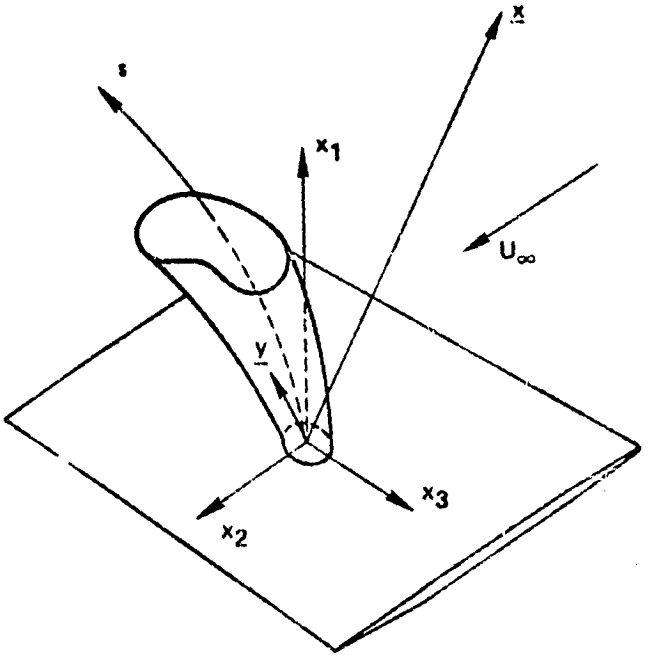

Figure 1a Coordinate System

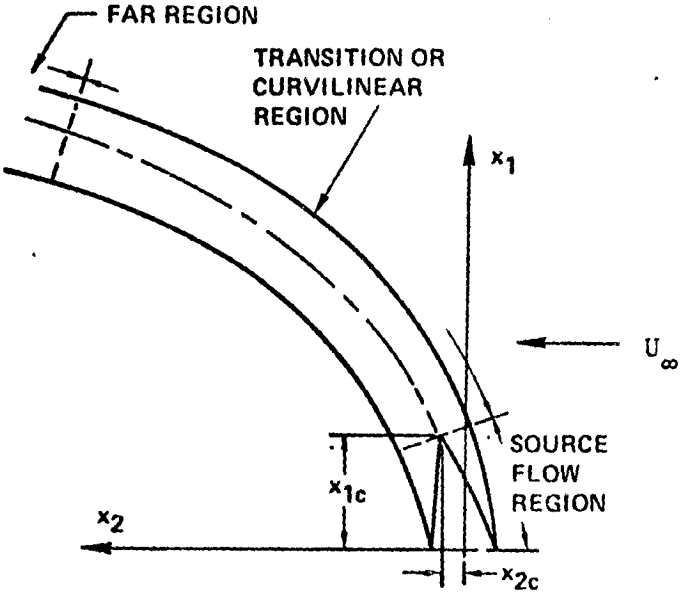

Figure 1b Schematic View of the Plane of Symmetry

ORIGINAL PAGE IS
OF POOR QUALITY

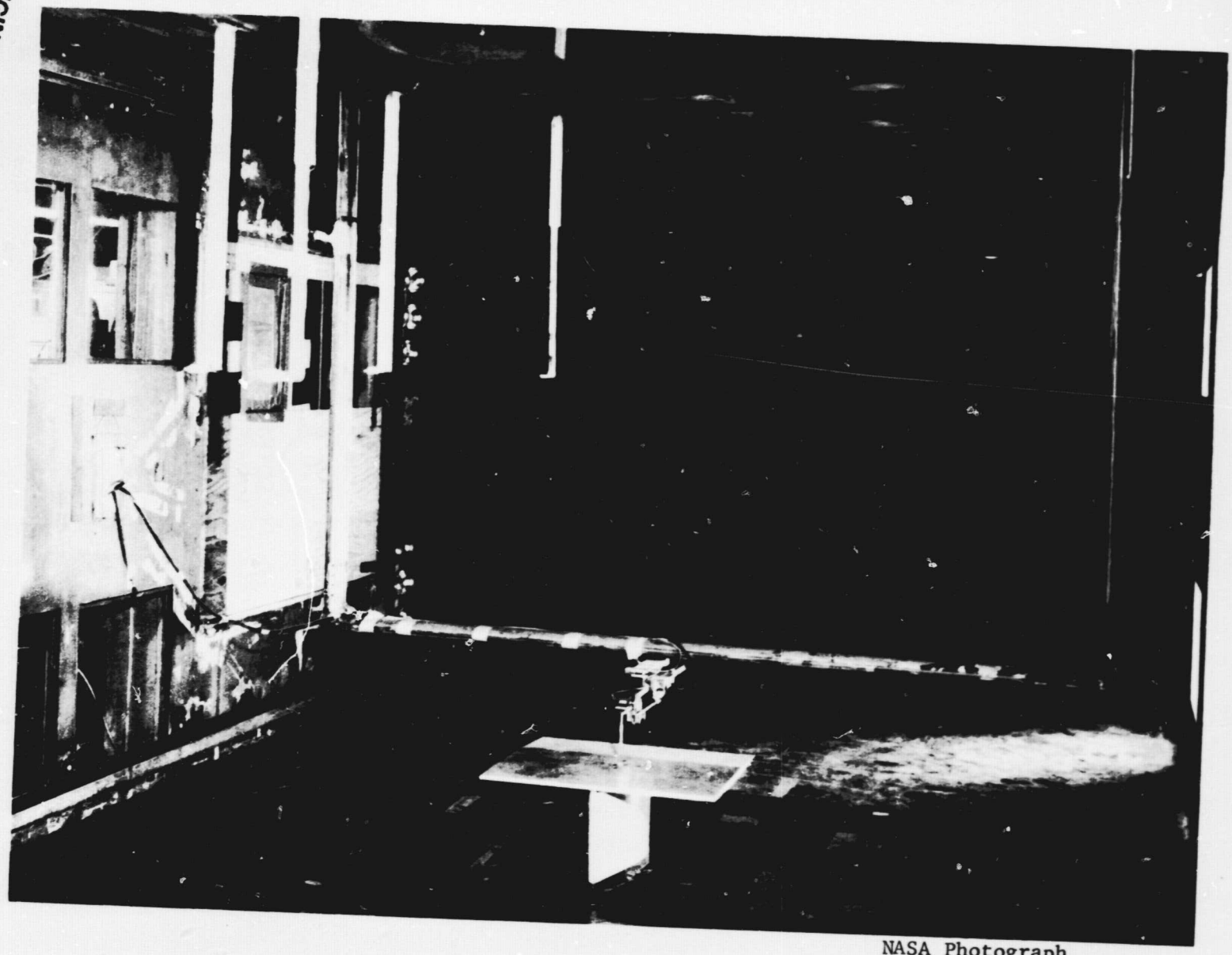

NASA Photograph

Figure 2 General View of the Test Section

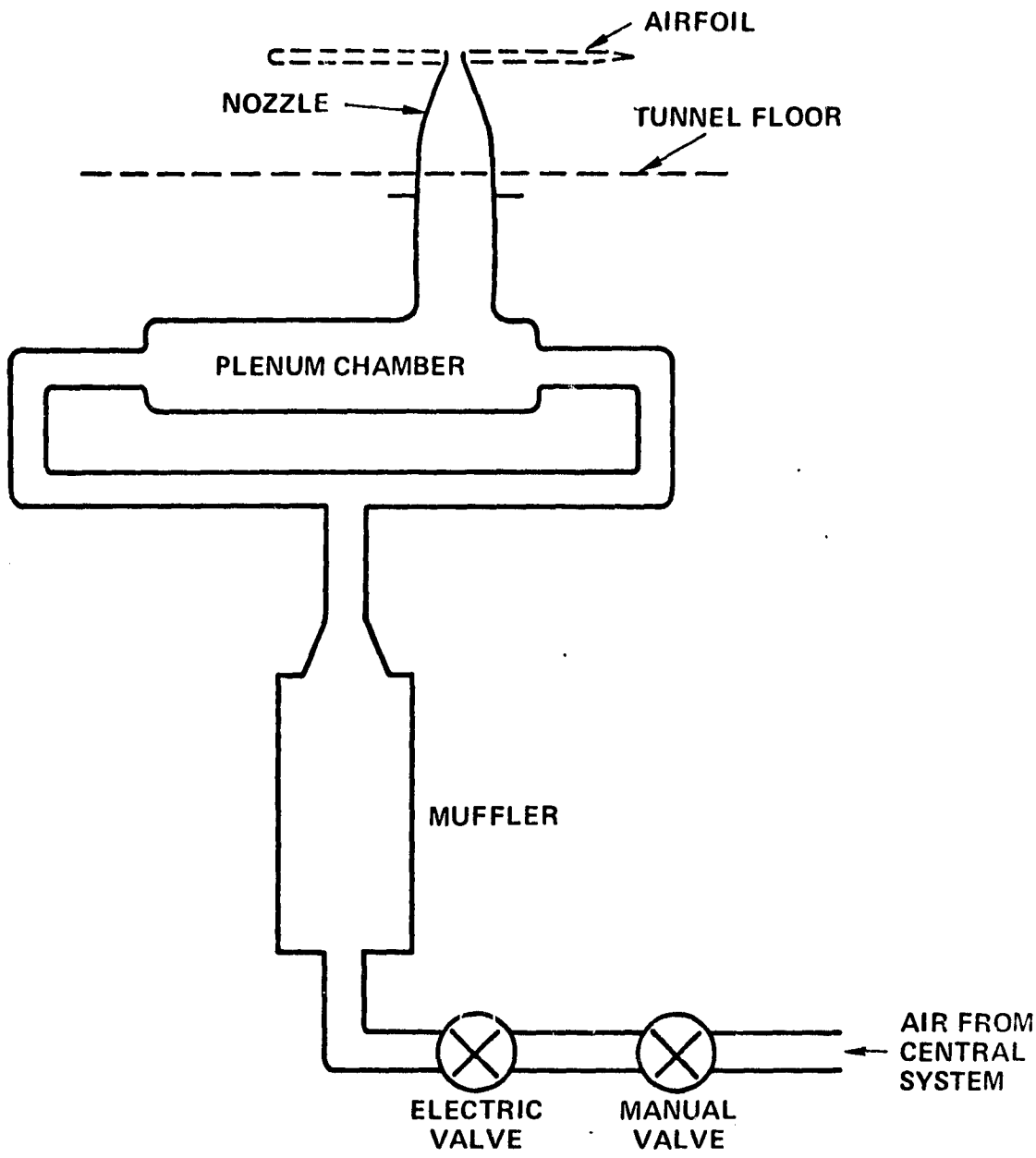

Figure 3 Schematic Diagram of the Jet System

ORIGINAL PAGE IS
OF POOR QUALITY

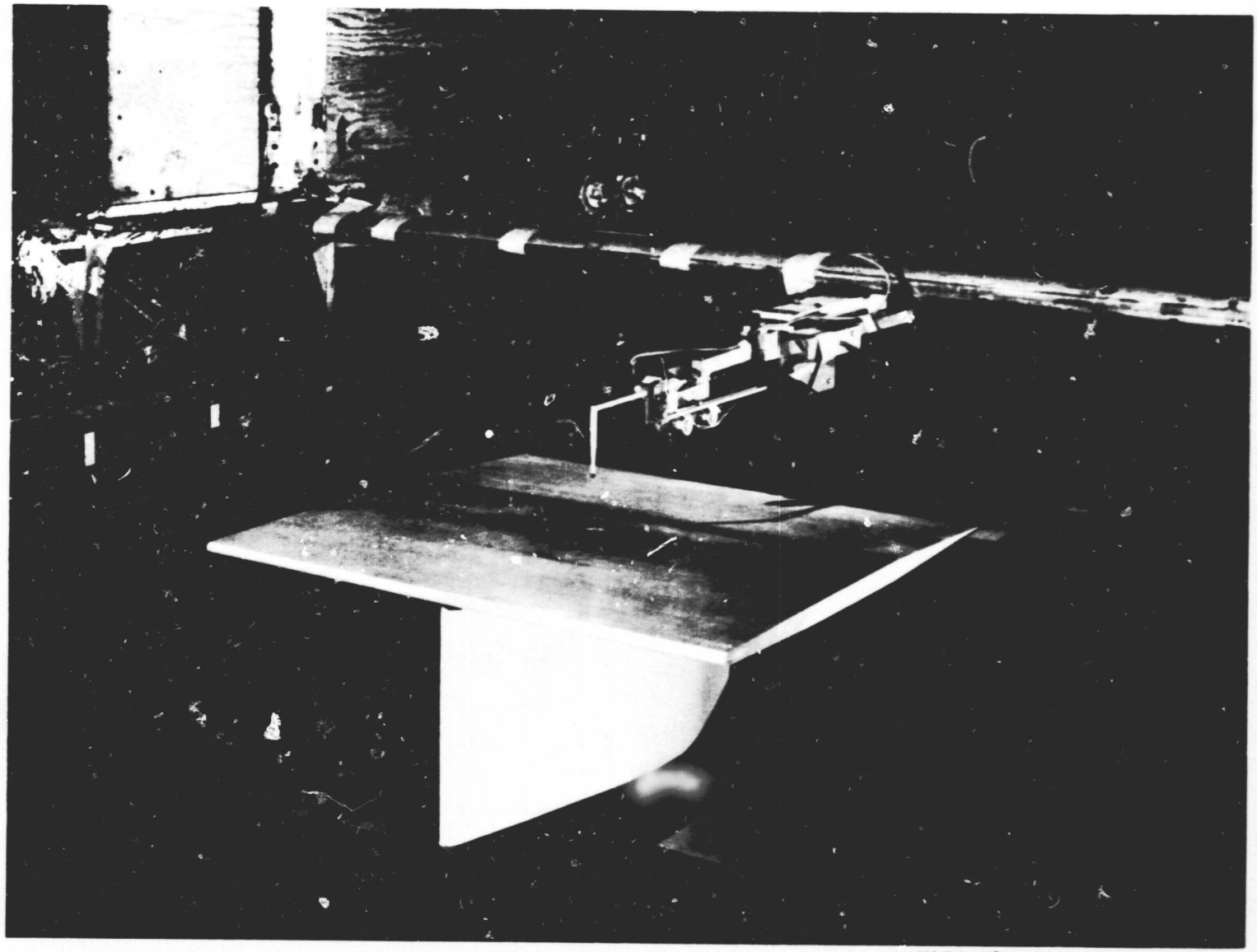

NASA Photograph

Figure 4 Airfoil in the Test Section

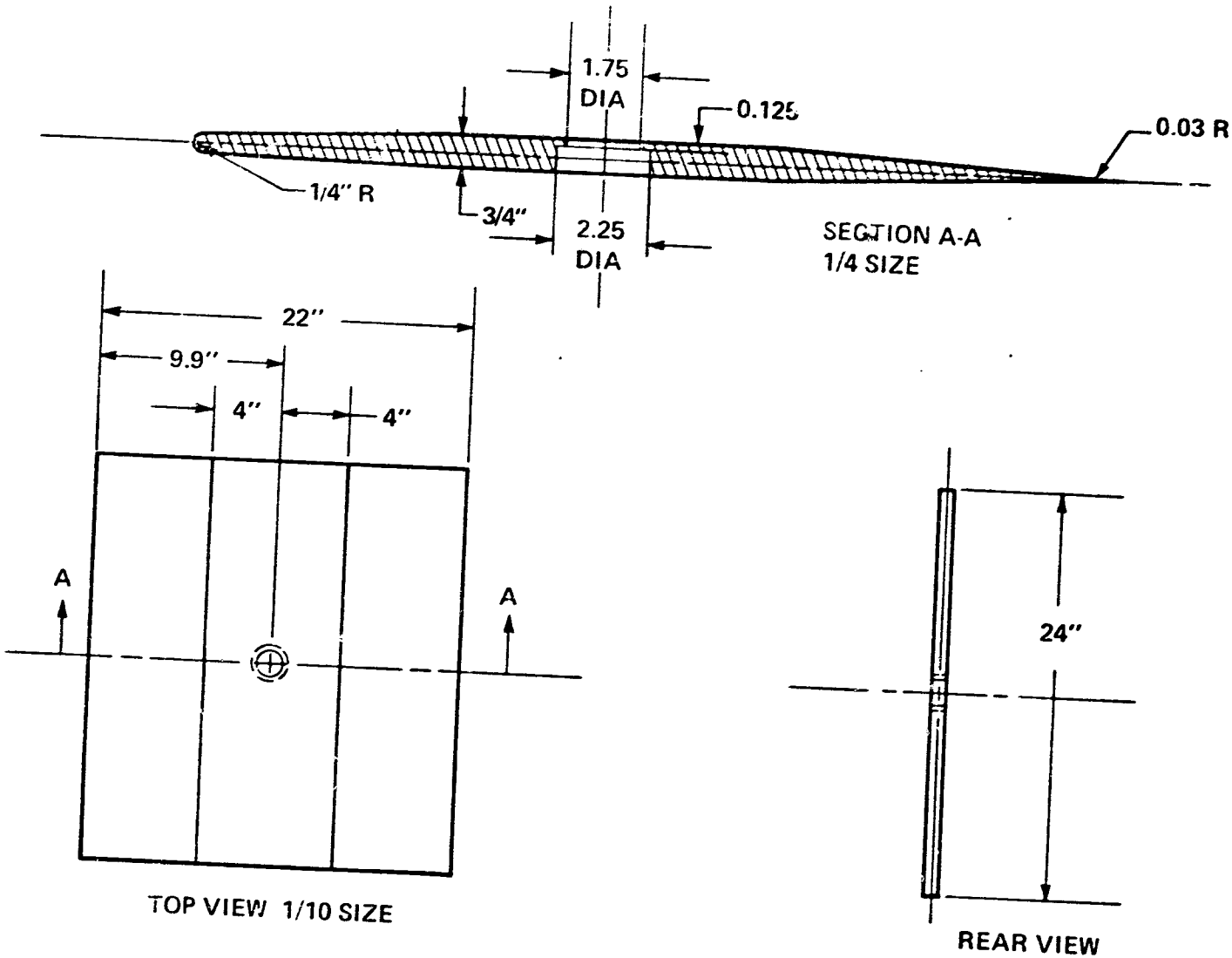

Figure 5 Airfoil Dimensions

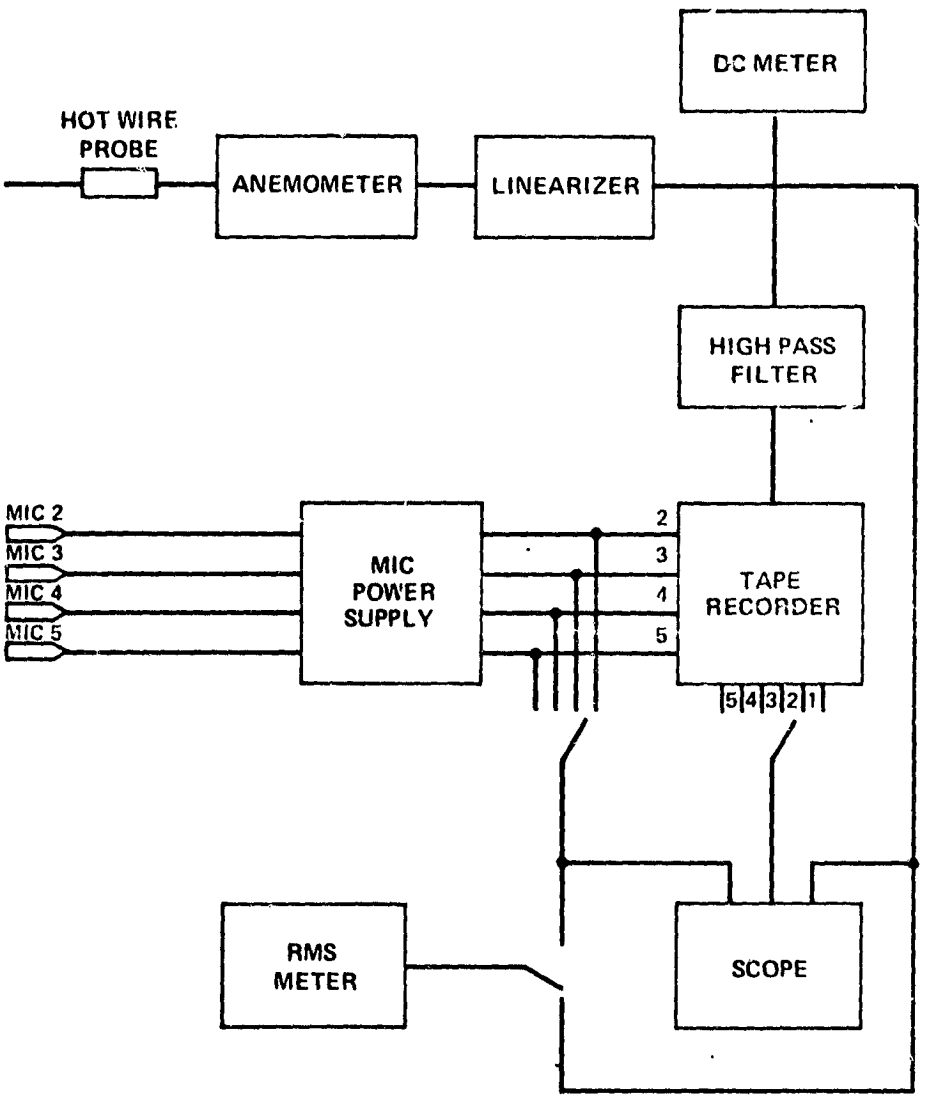

Figure 6a Schematic Diagram of Instrumentation; Data Acquisition

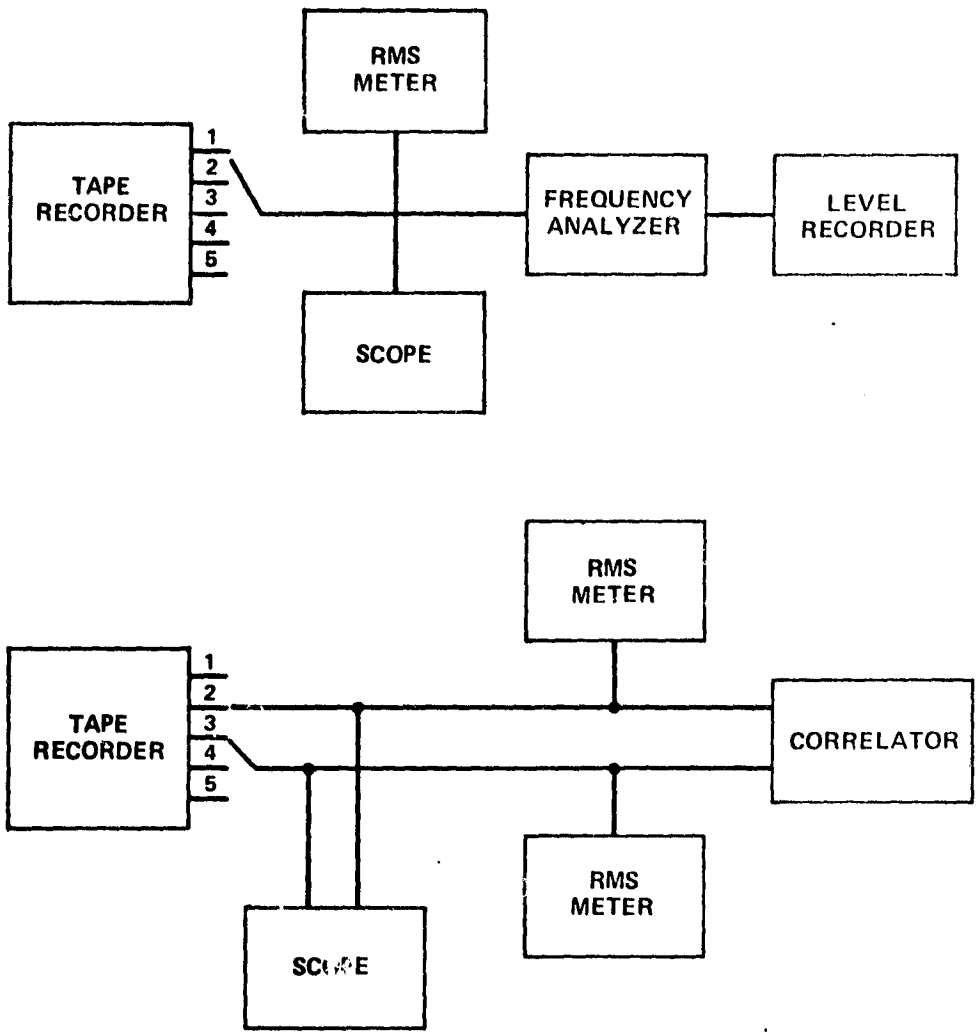

Figure 6b Schematic Diagram of Instrumentation; Data Processing

ORIGINAL PAGE IS
POOR QUALITY

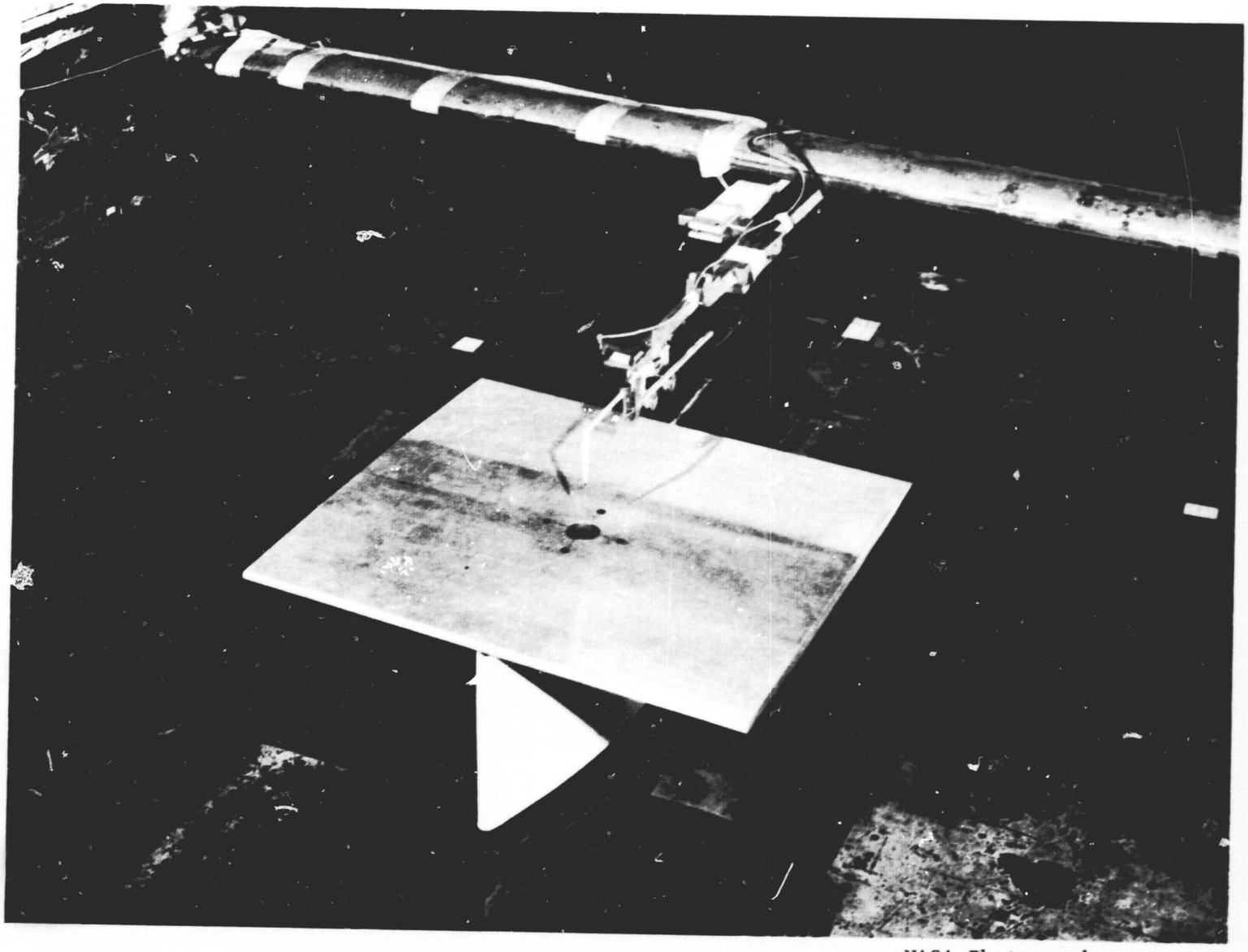

NASA Photograph

Figure 7 Airfoil,Probe, and Traversing Mechanisms

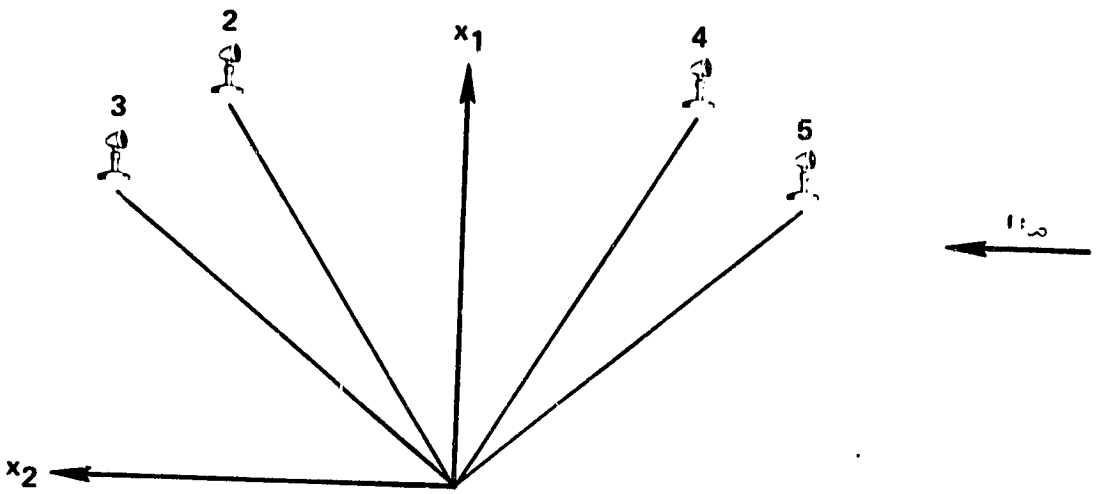

PLANE $x_1 - x_2$

MIC	x_1 (in)	x_2 (in)	x_3 (in)	|x| (in)	θ (deg)
2	52.1	32.2	0	61.25	31.7
3	38.8	47.1	0	61	50.5
4	52.1	-31	0	60.63	30.1
5	38.8	-45	0	60.25	49.9

Figure 8 Microphone Disposition Number 1

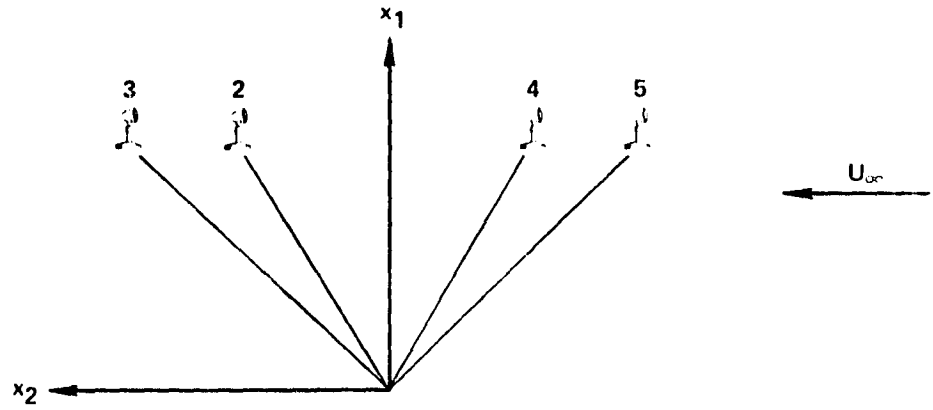

VIEW OF PLANE x_1x_2

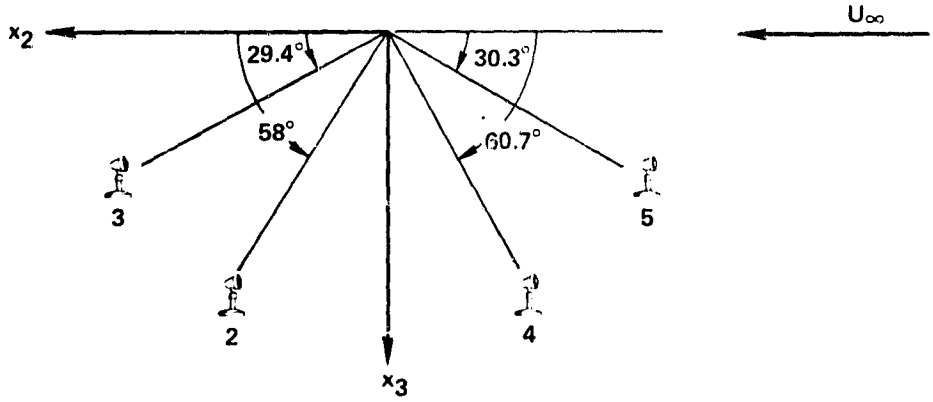

TOP VIEW PLANE x_2x_3

MIC	x_1 (in)	x_2 (in)	x_3 (in)	|x| (in)	θ (deg)
2	39	24.9	39.75	61	50.25
3	39	40.9	23	61	50.25
4	39	-22.3	39.75	60	49.5
5	39	-39.4	23	60	49.5

Figure 9 Microphone Disposition Number 2

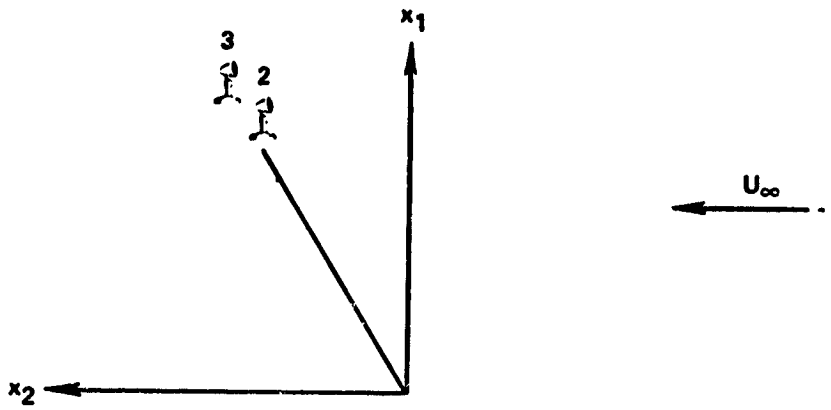

SIDE VIEW PLANE x_1x_2

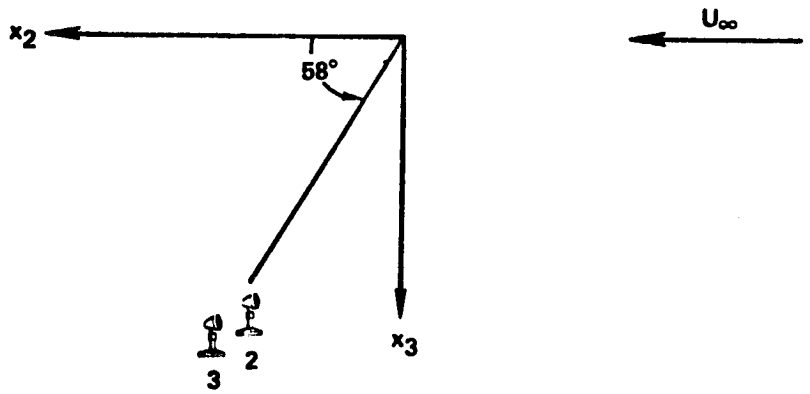

TOP VIEW PLANE x_2x_3

MIC	x_1 (in)	x_2 (in)	x_3 (in)	|x| (in)	θ (deg)
2	39	24.9	39.75	61	50 25
3	47.5	28.4	48.25	73.4	49.7

Figure 10 Microphone Disposition Number 3

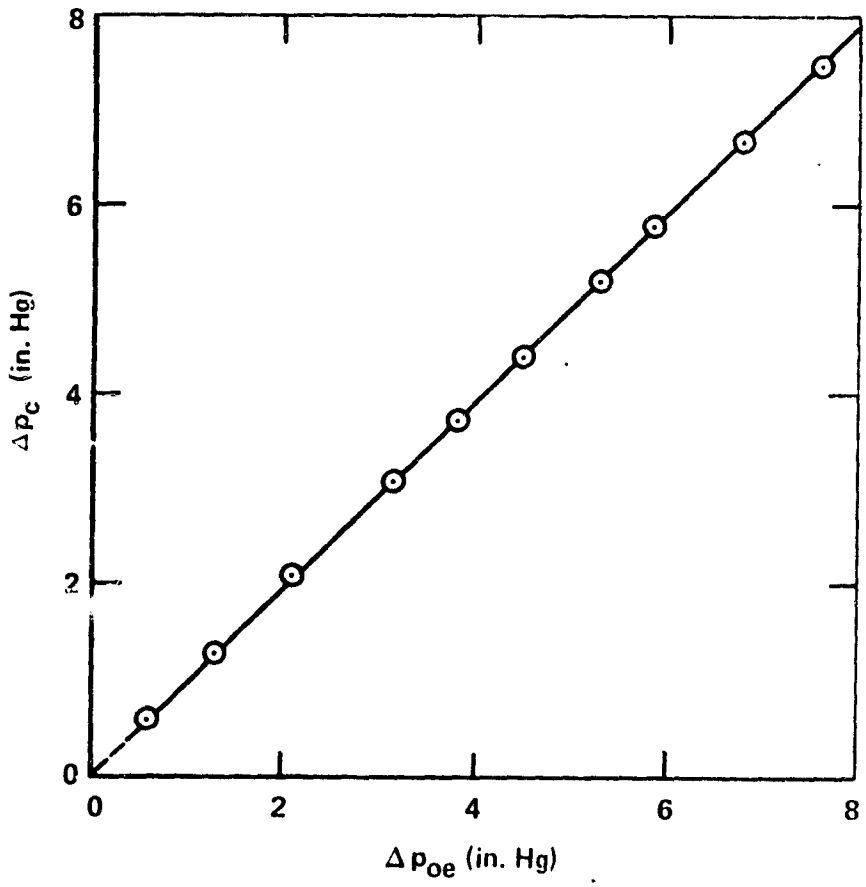

Figure 11 Plenum Pressure vs. Total Pressure at the Jet Exit

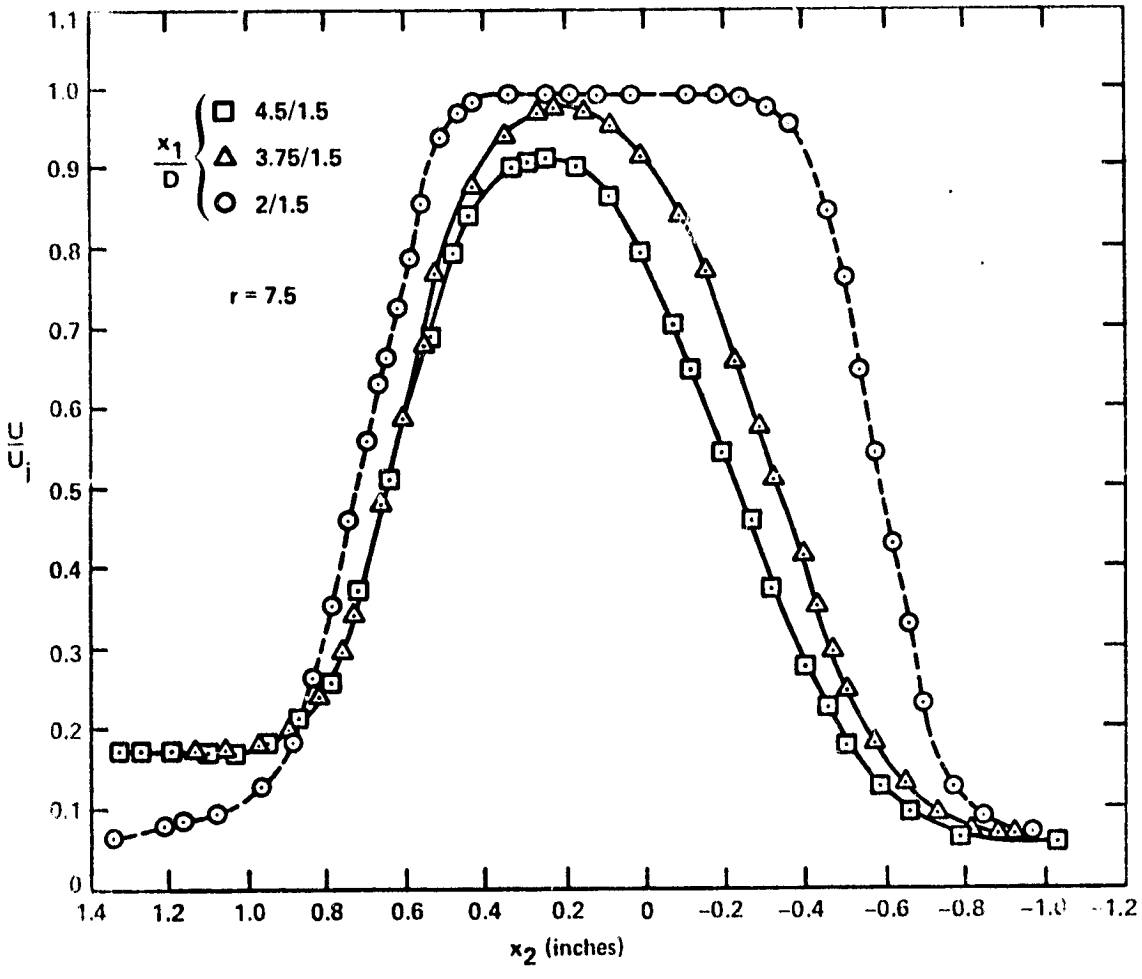

Figure 12 Typical Profiles of $\frac{U}{U_j}$

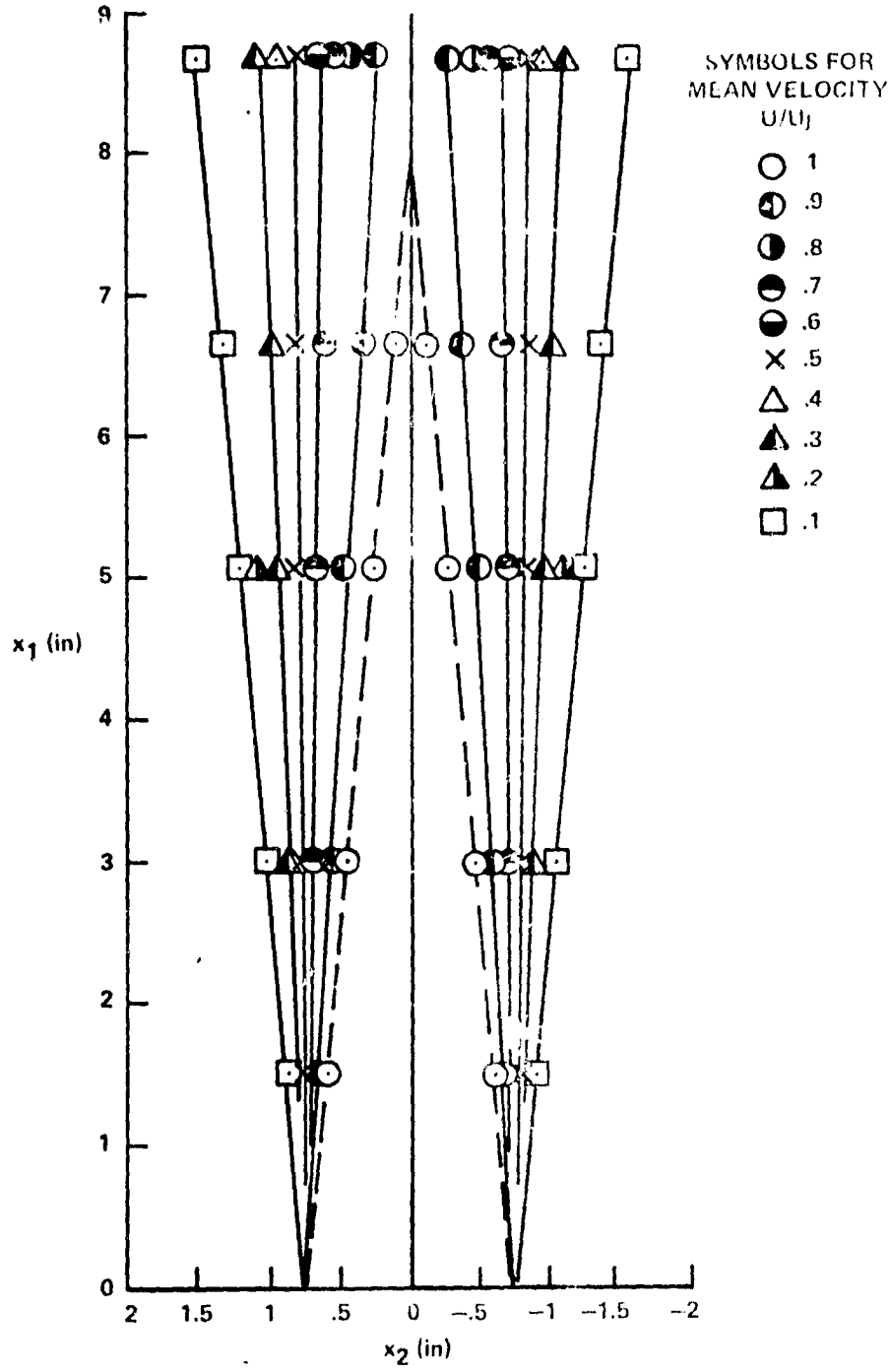

Figure 13a Magnitude of the Jet Mean Velocity in the Plane of Symmetry; r=∞ .

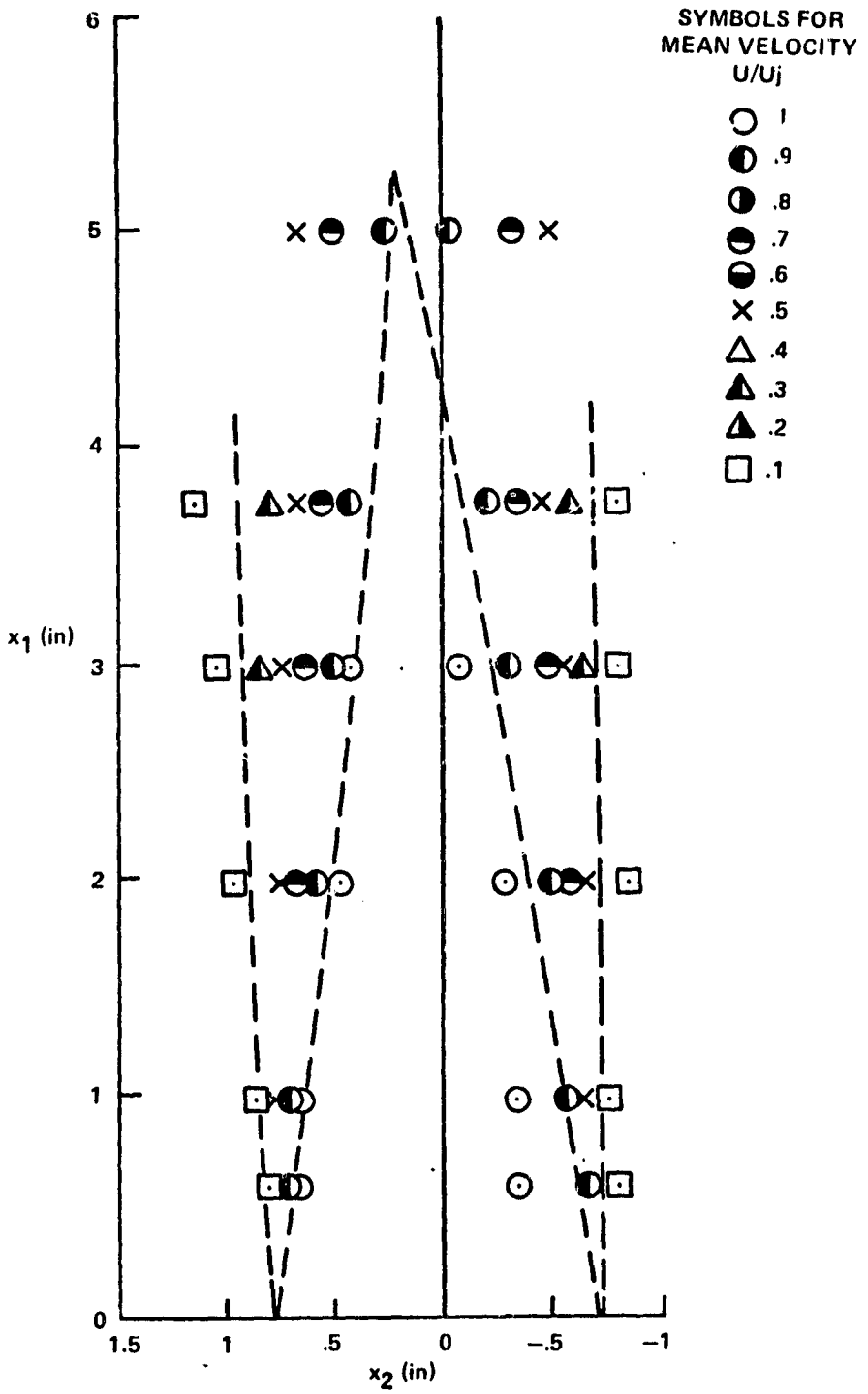

Figure 13b Magnitude of the Jet Mean Velocity in the Plane of Symmetry; r=9.4 .

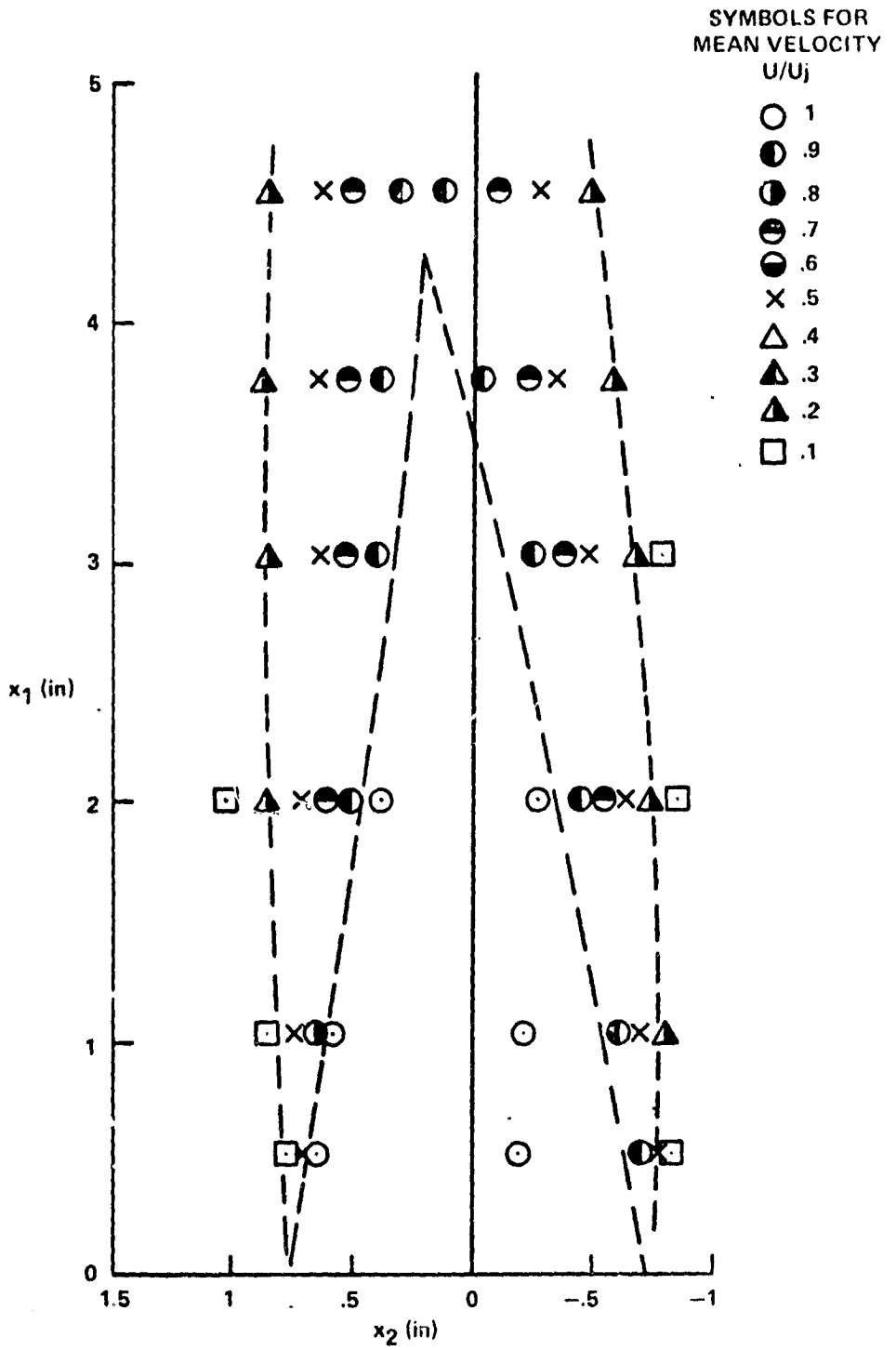

Figure 13c Magnitude of the Jet Mean Velocity in the Plane of Symmetry; r=7.5

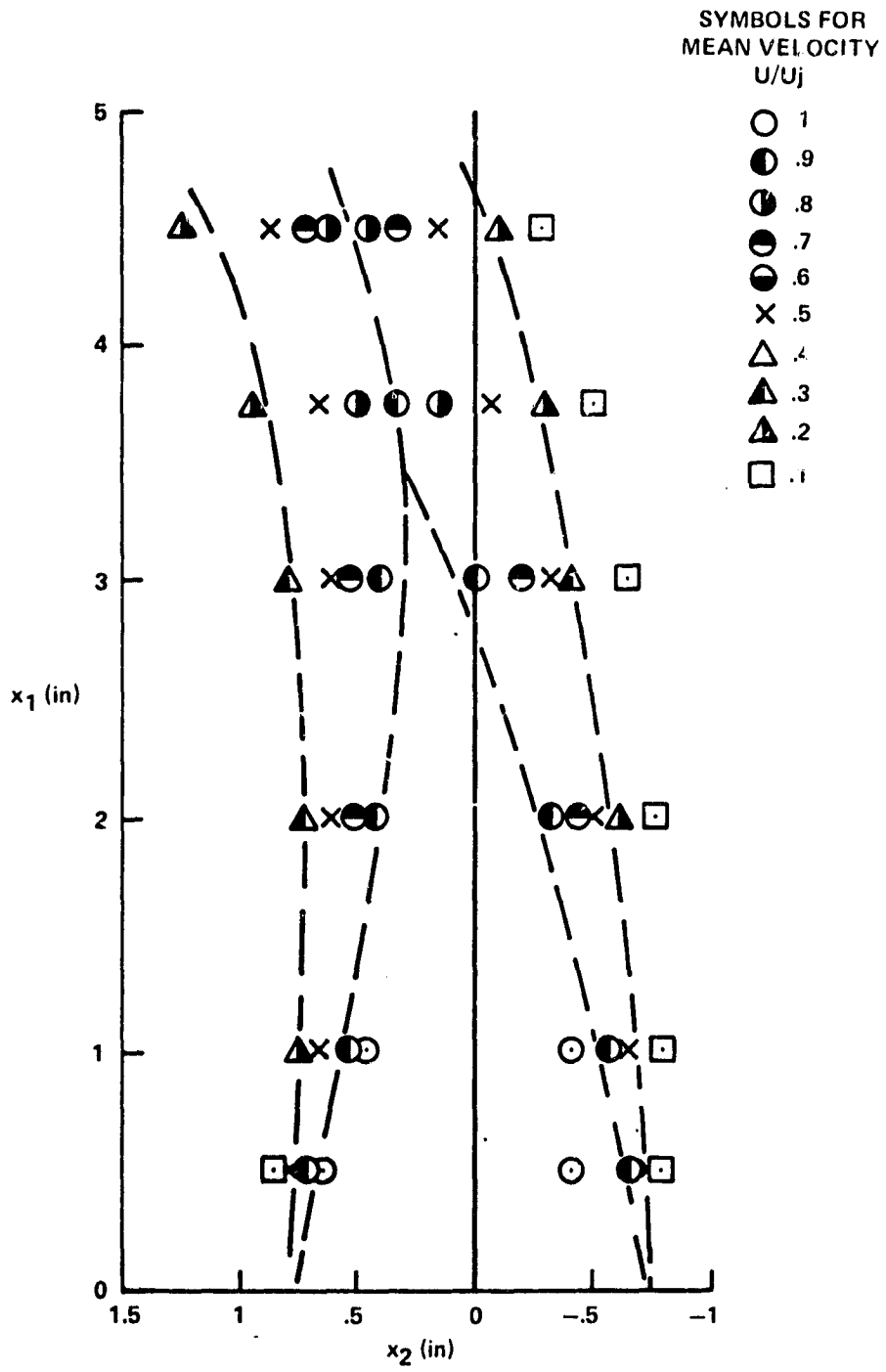

Figure 13d Magnitude of the Jet Mean Velocity in the Plane of Symmetry; r=5.6

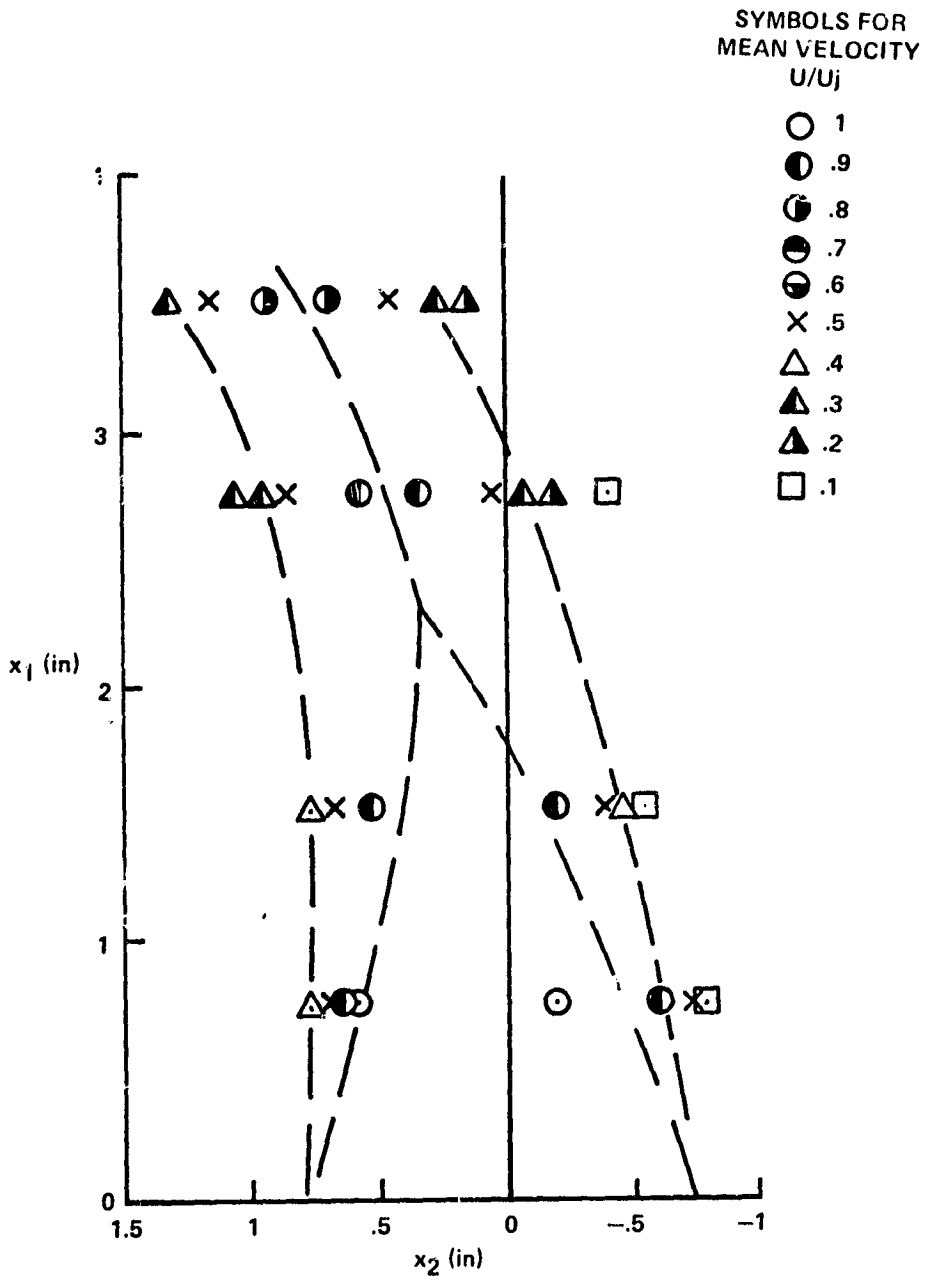

Figure 13e Magnitude of the Jet Mean Velocity in the Plane of Symmetry: r=3.7

c - 2

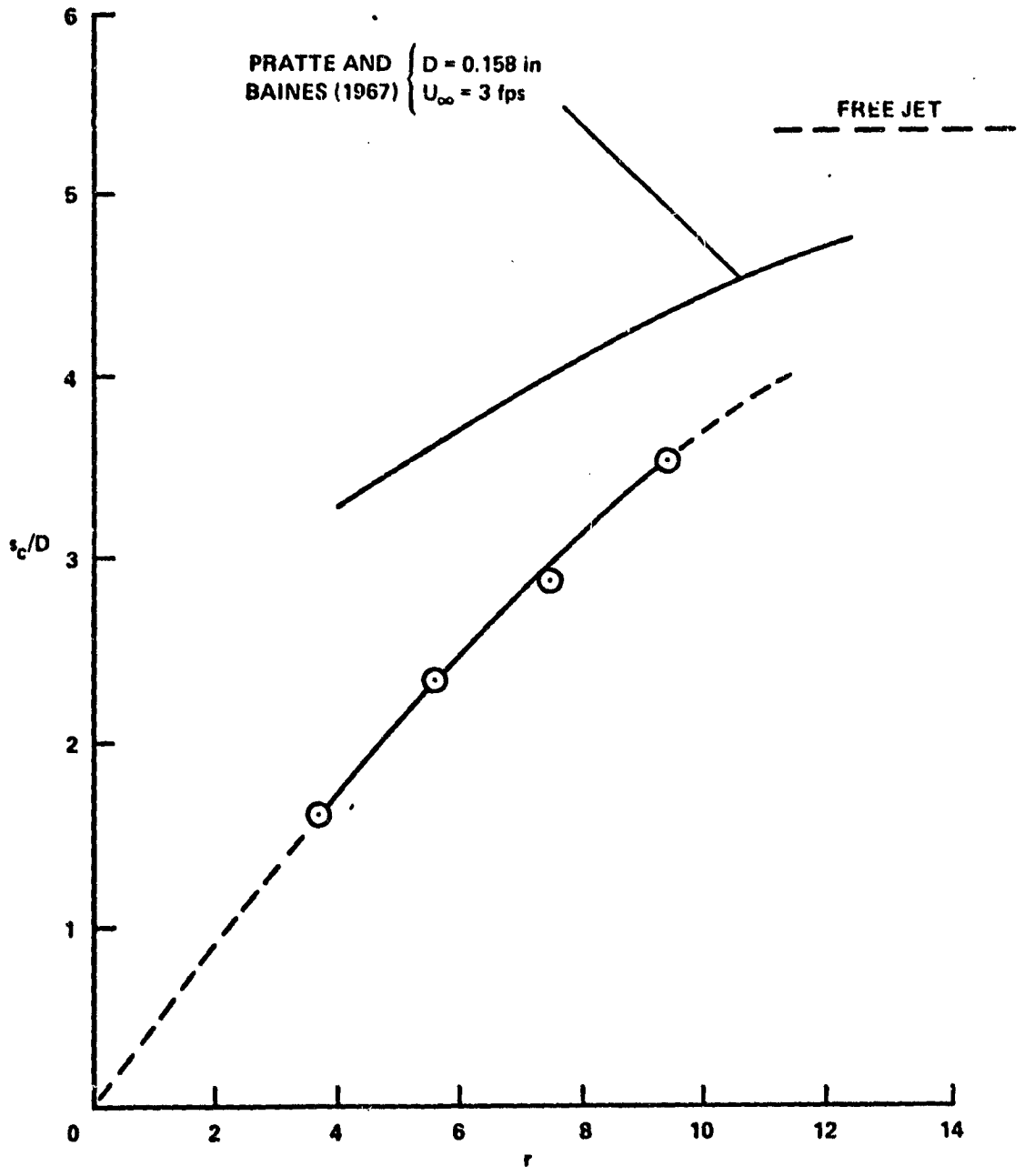

Figure 14 Length of the Potential Core as a Function of r.

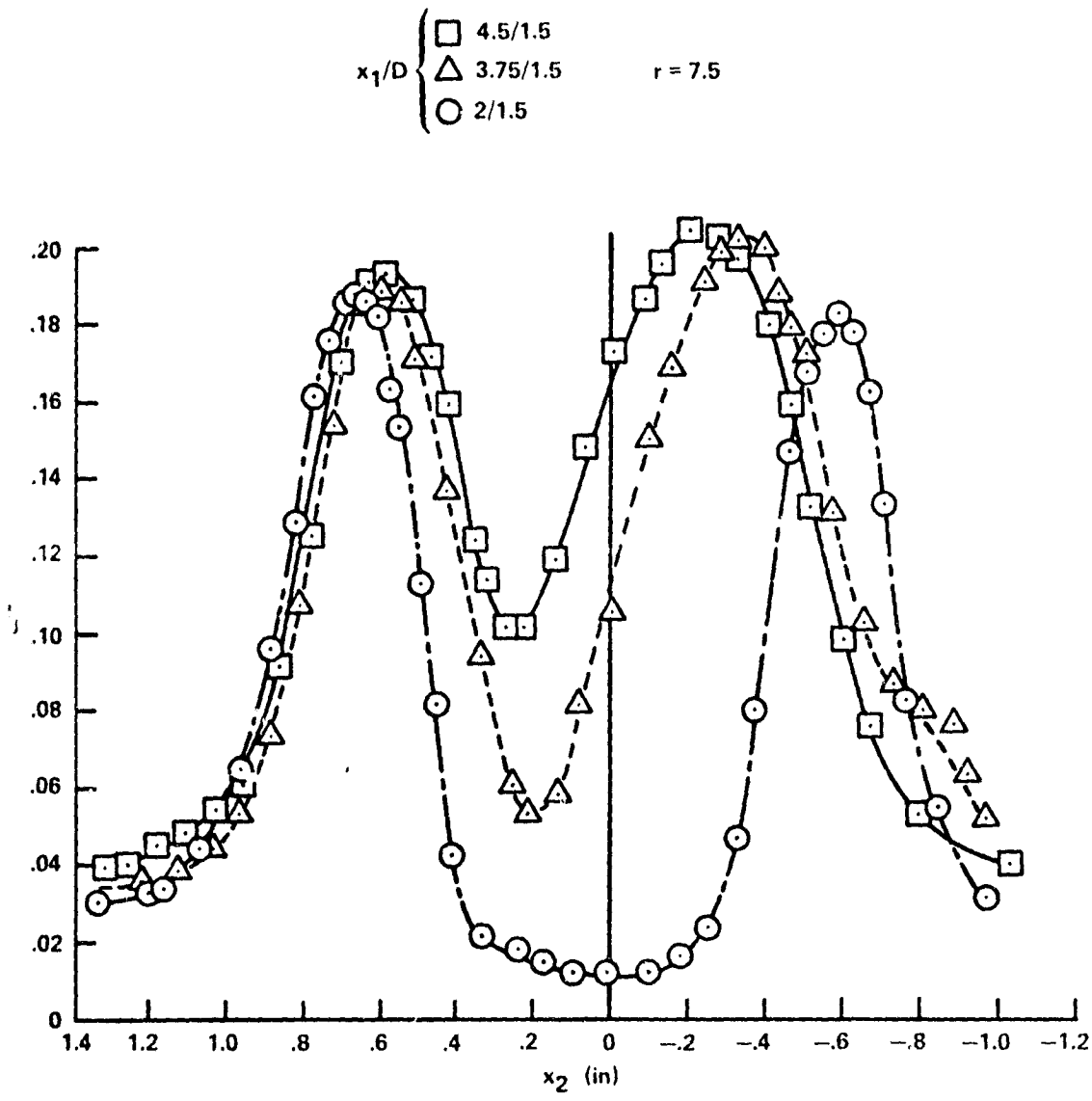

Figure 15 Typical Profiles of Turbulent Intensity

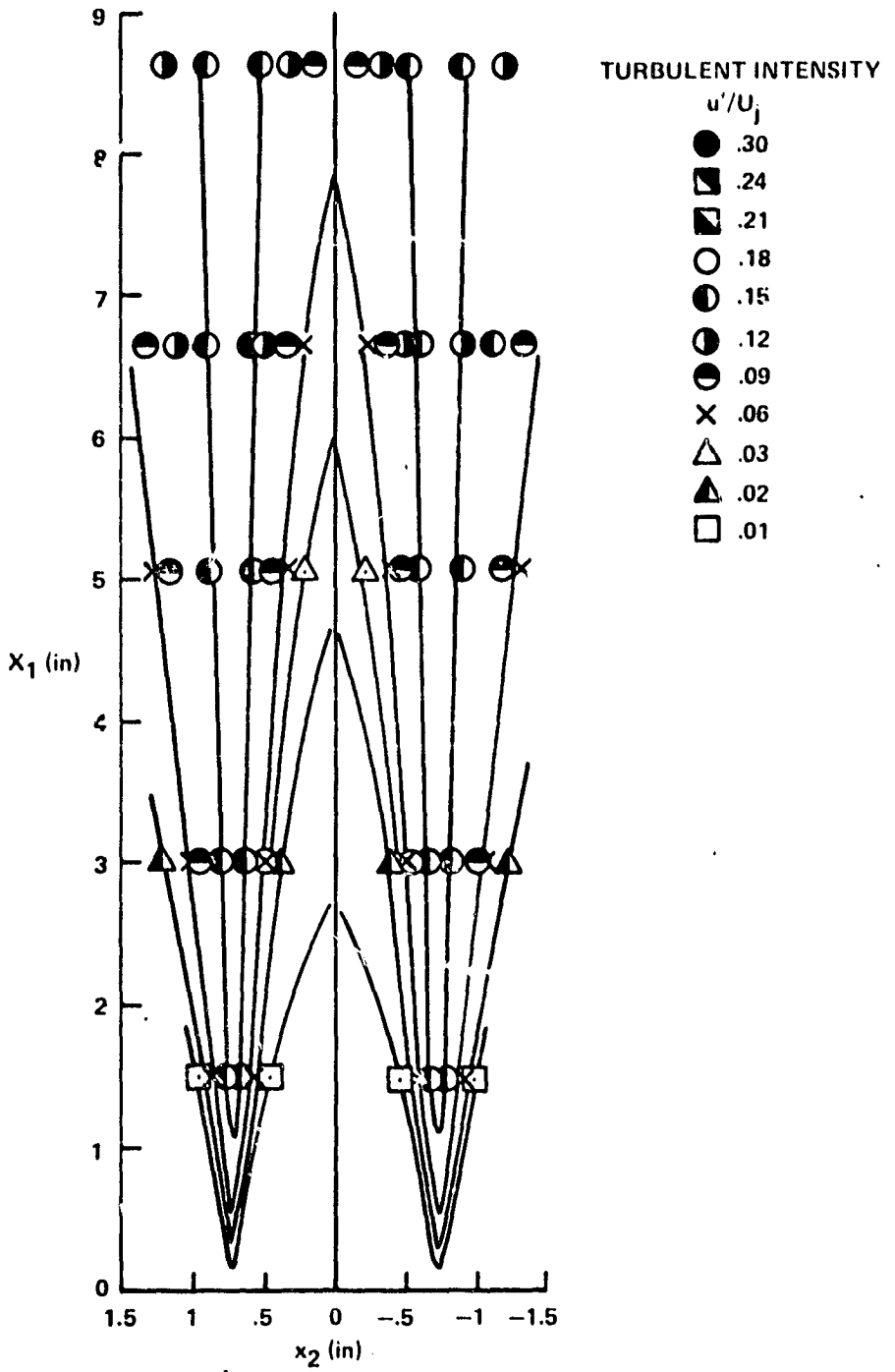

Figure 16a Distribution of Turbulent Intensity in the Plane of Symmetry; r=∞ .

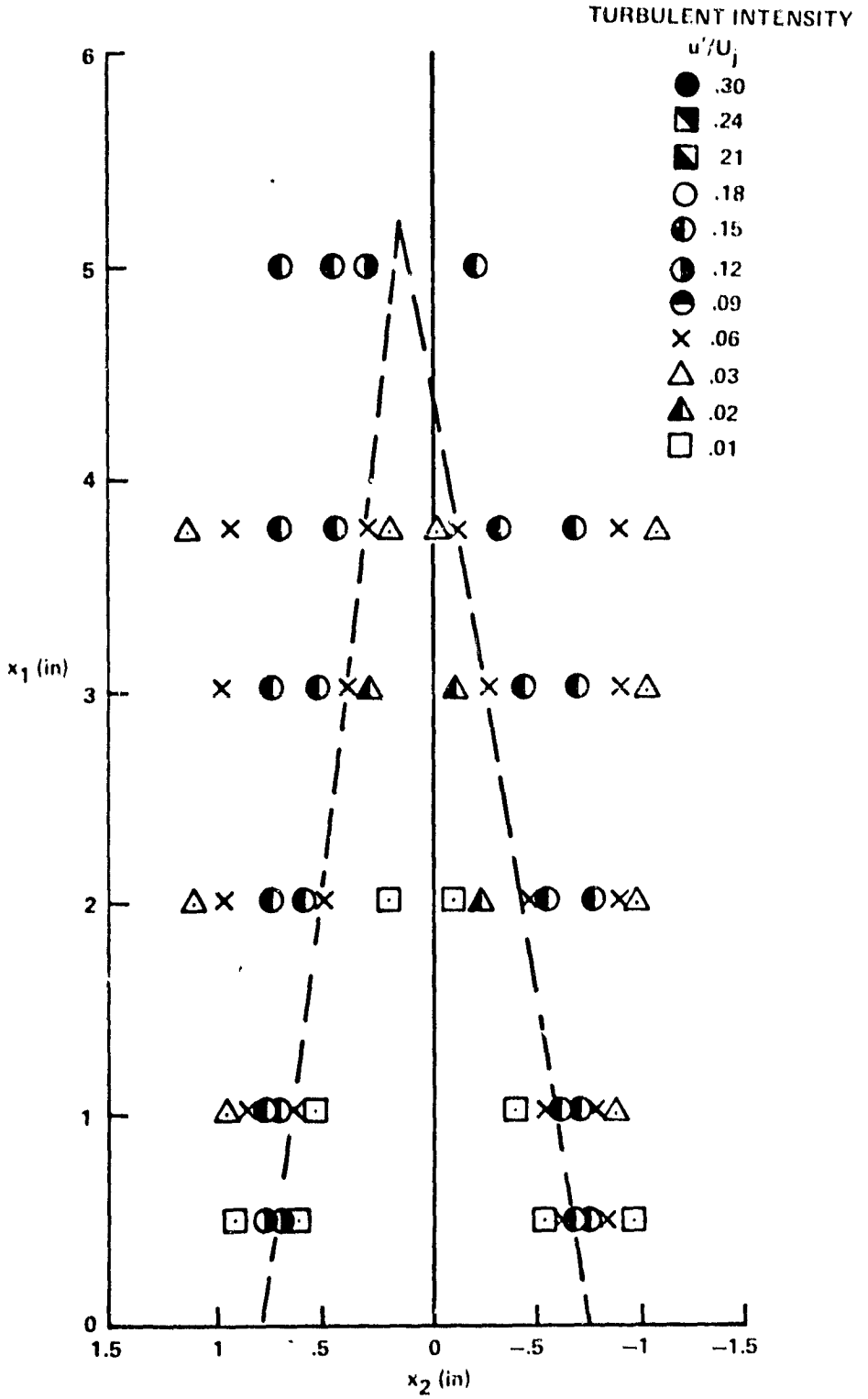

Figure 16b Distribution of Turbulent Intensity in the Plane of Symmetry; r=9.4

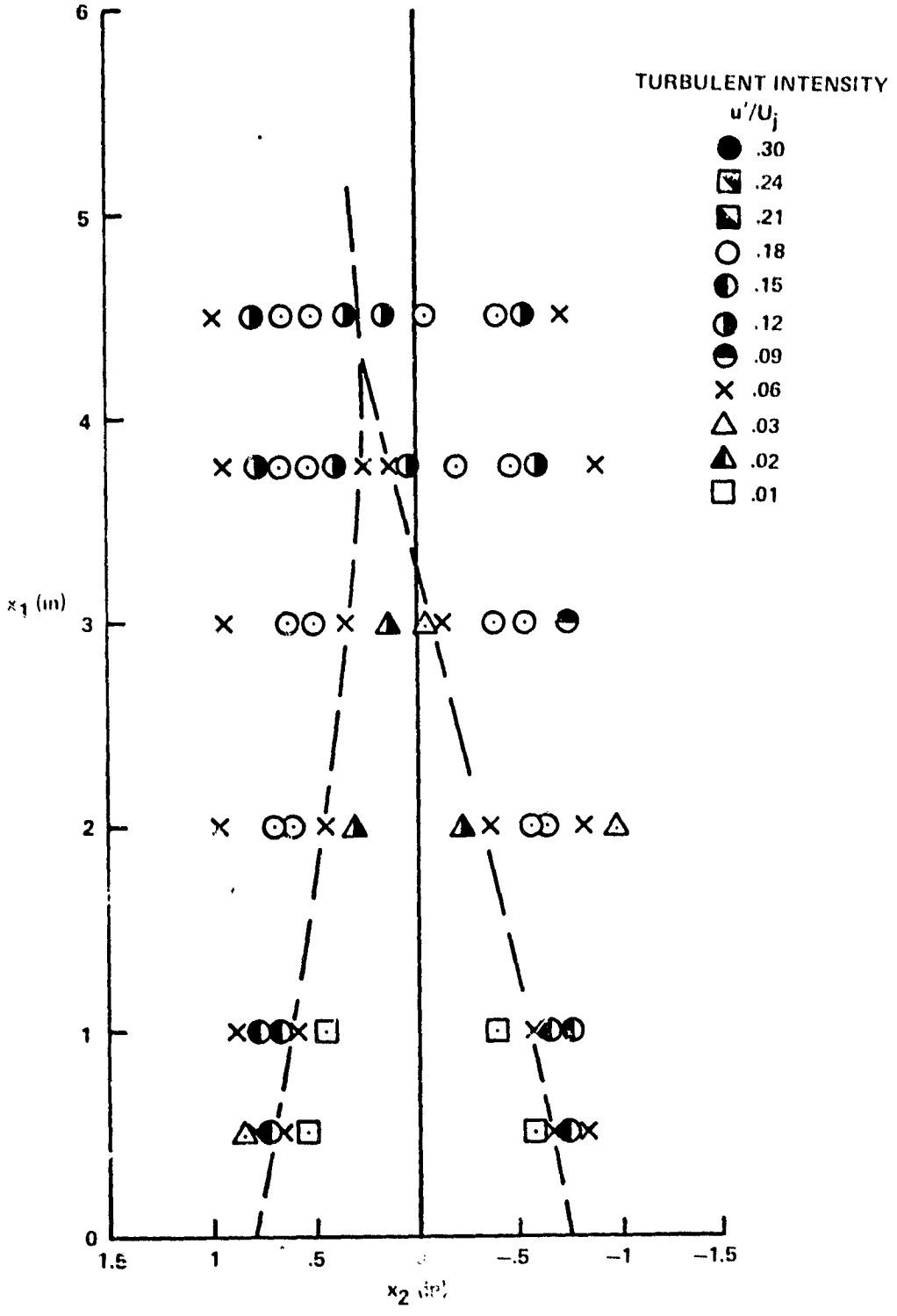

Figure 16c Distribution of Turbulent Intensity in the Plane of Symmetry; r=7.5

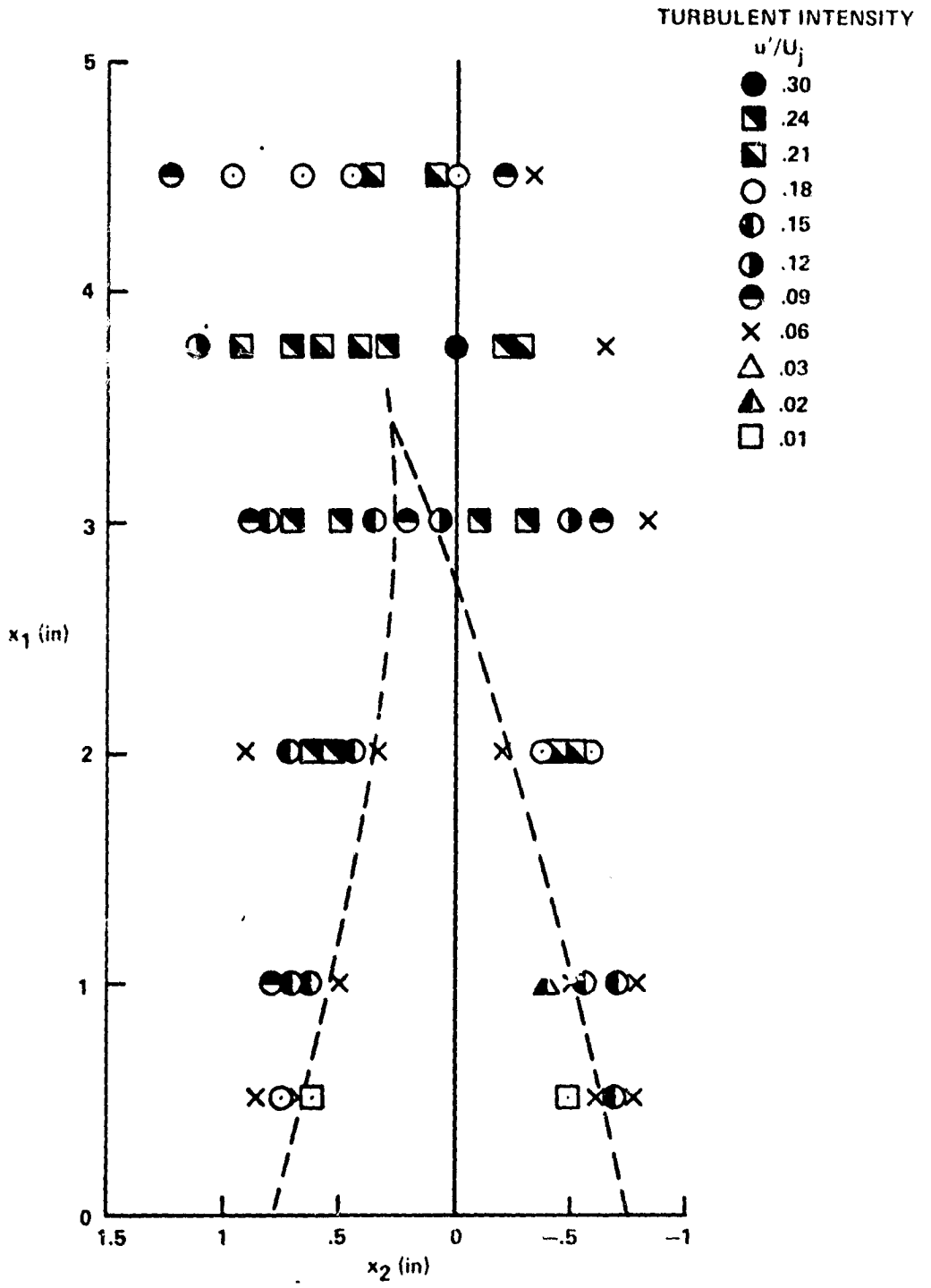

Figure 16d Distribution of Turbulent Intensity in the Plane of Symmetry; r=5.6

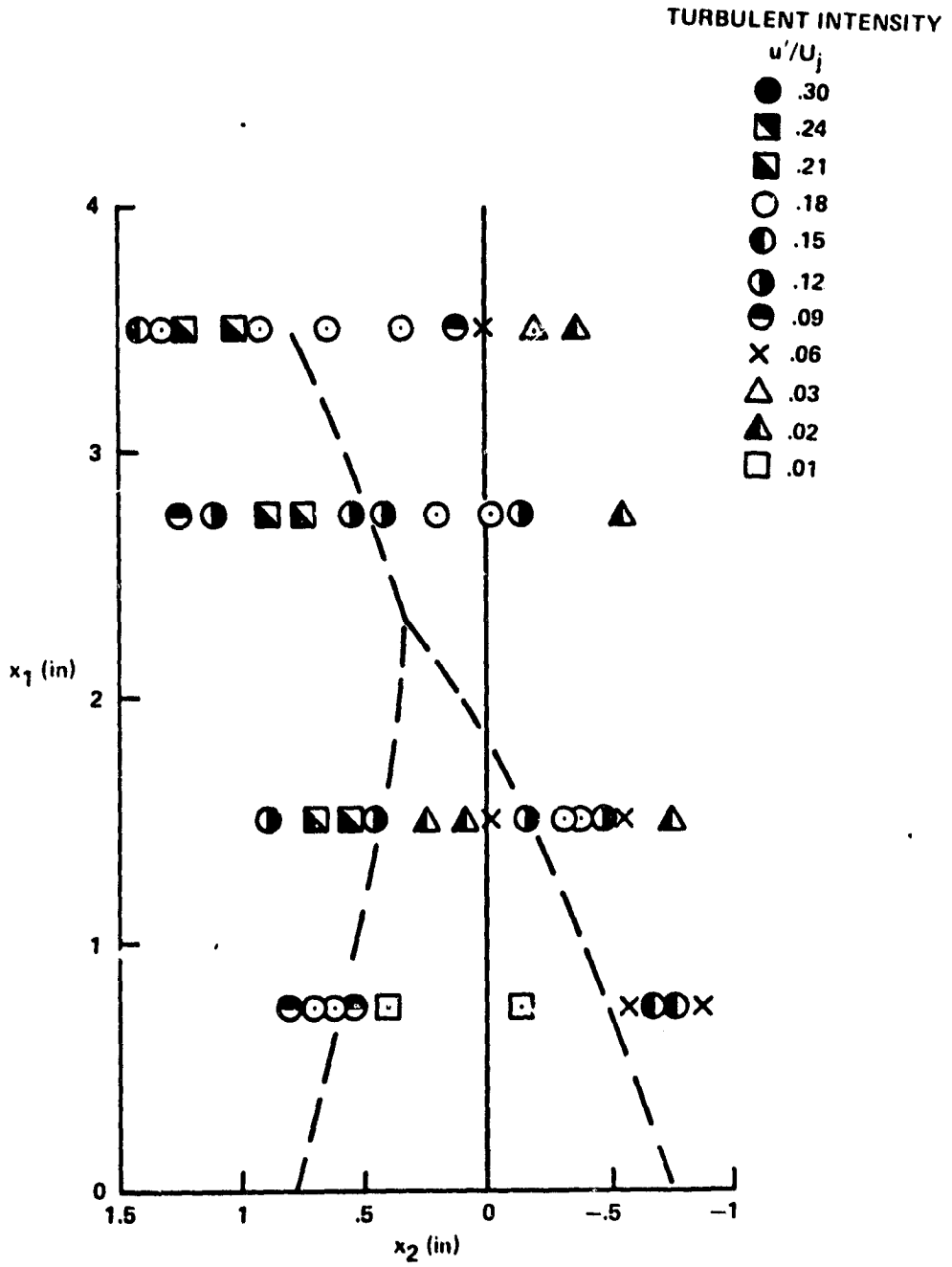

Figure 16e Distribution of Turbulent Intensity in the Plane of Symmetry; r=3.7

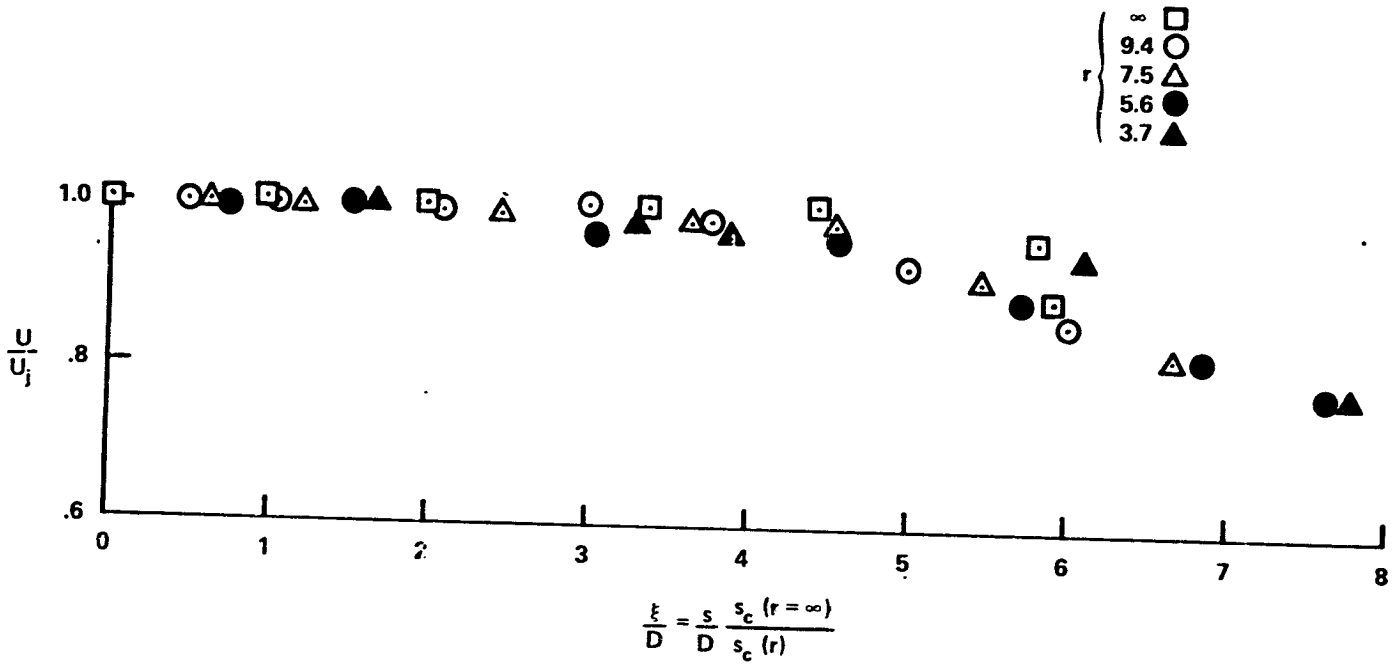

Figure 17 Magnitude of the Mean Velocity along the Jet Axis.

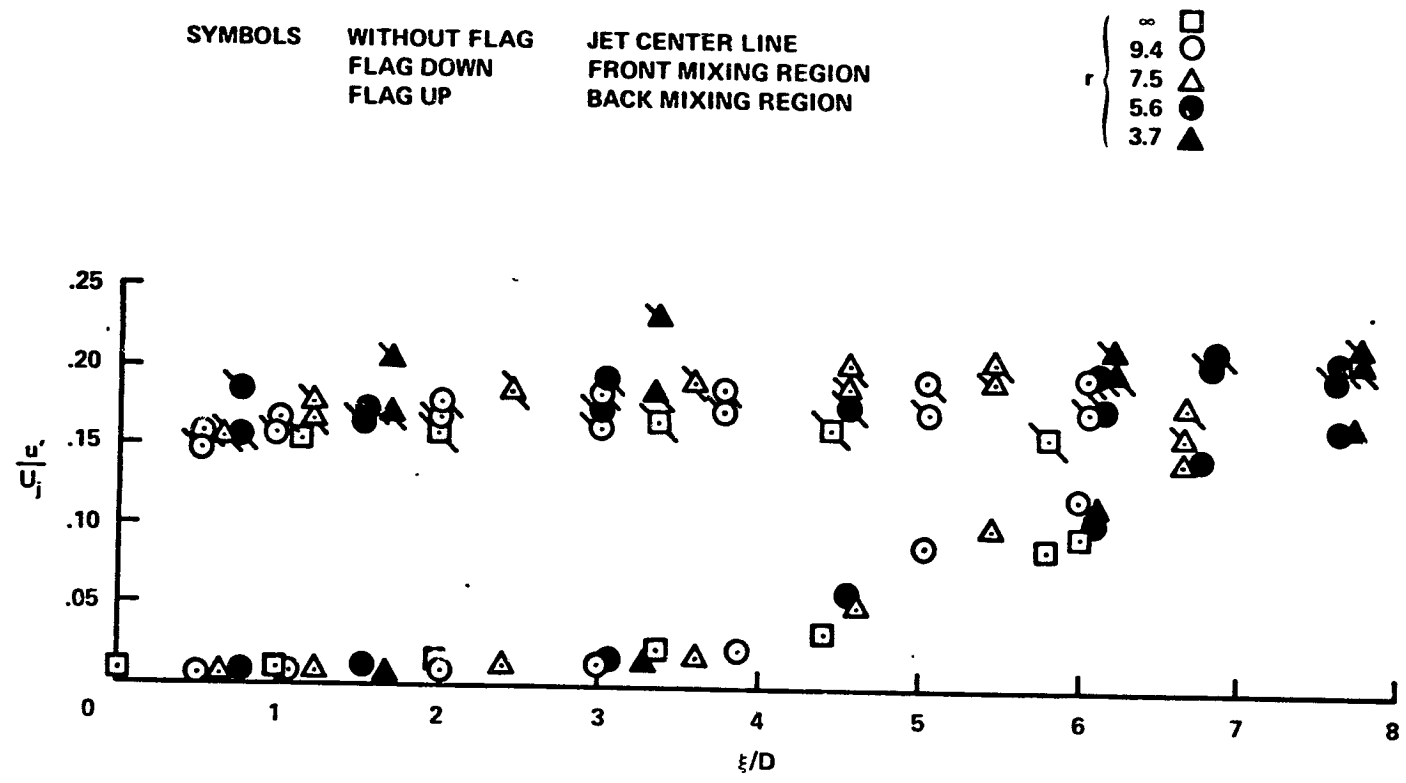

Figure 18 Axial Distribution of Turbulent Intensity

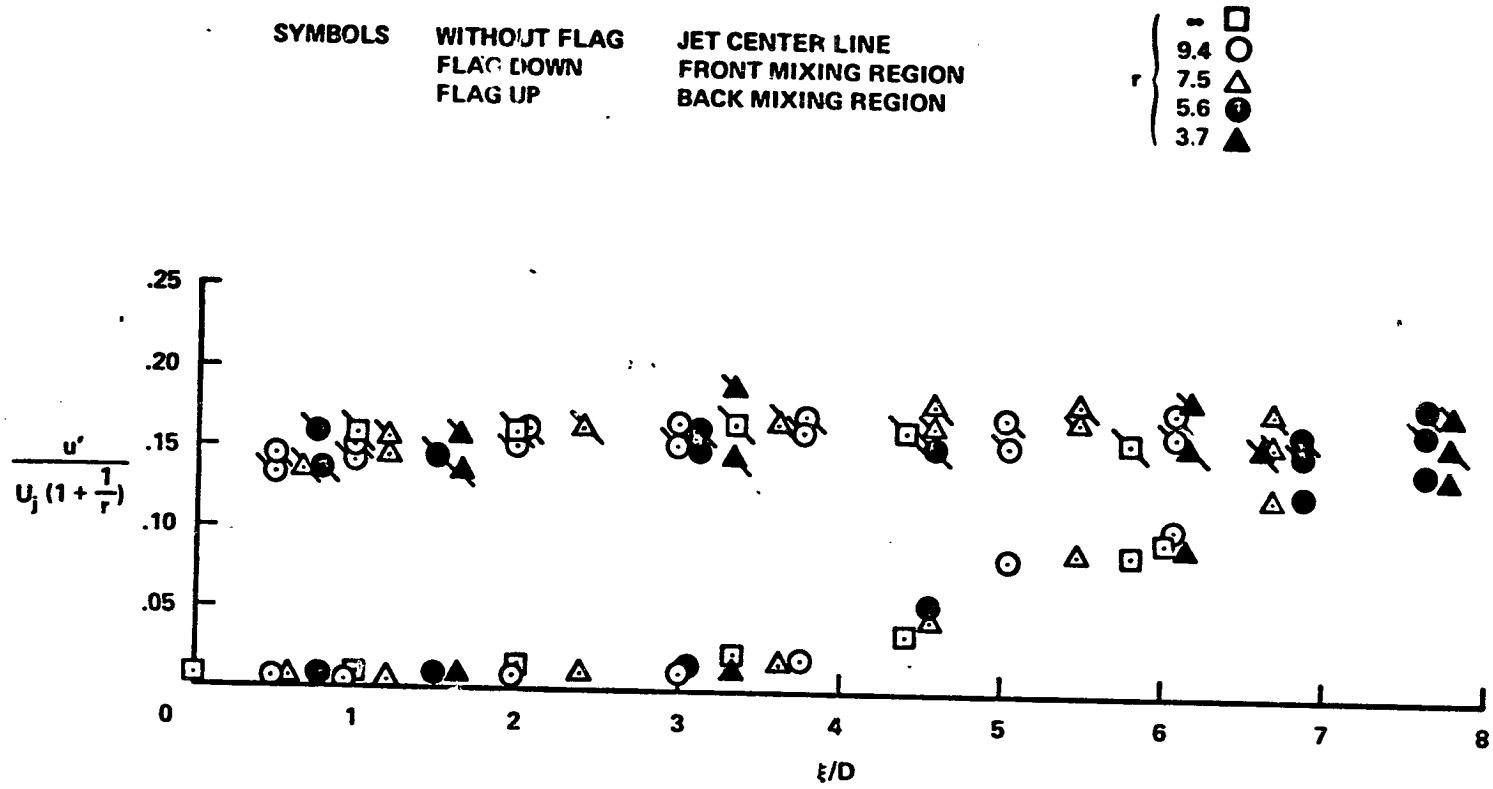

Figure 19 Axial Distribution of Normalized Turbulent Intensity

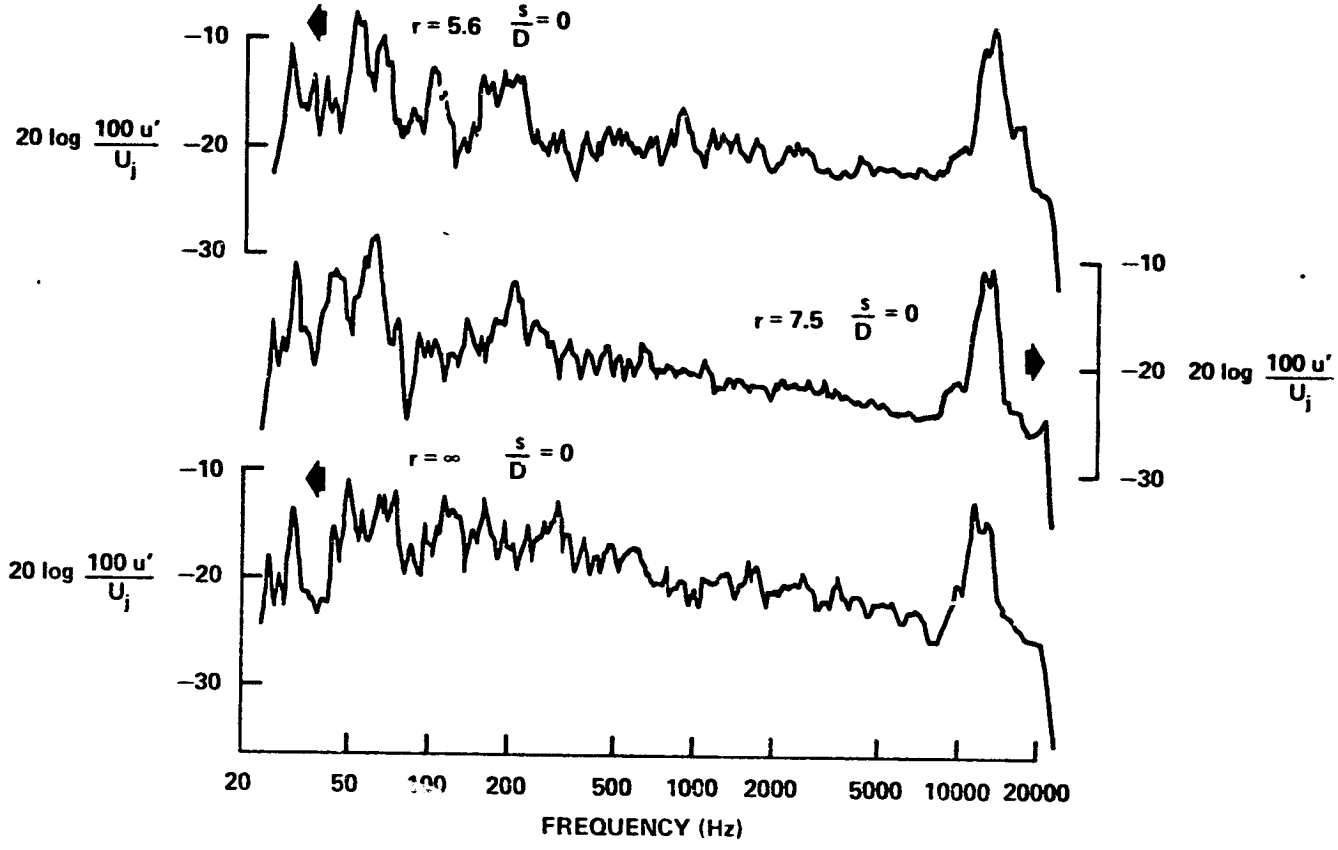

Figure 20 Turbulent Frequency Spectra at Jet Exit

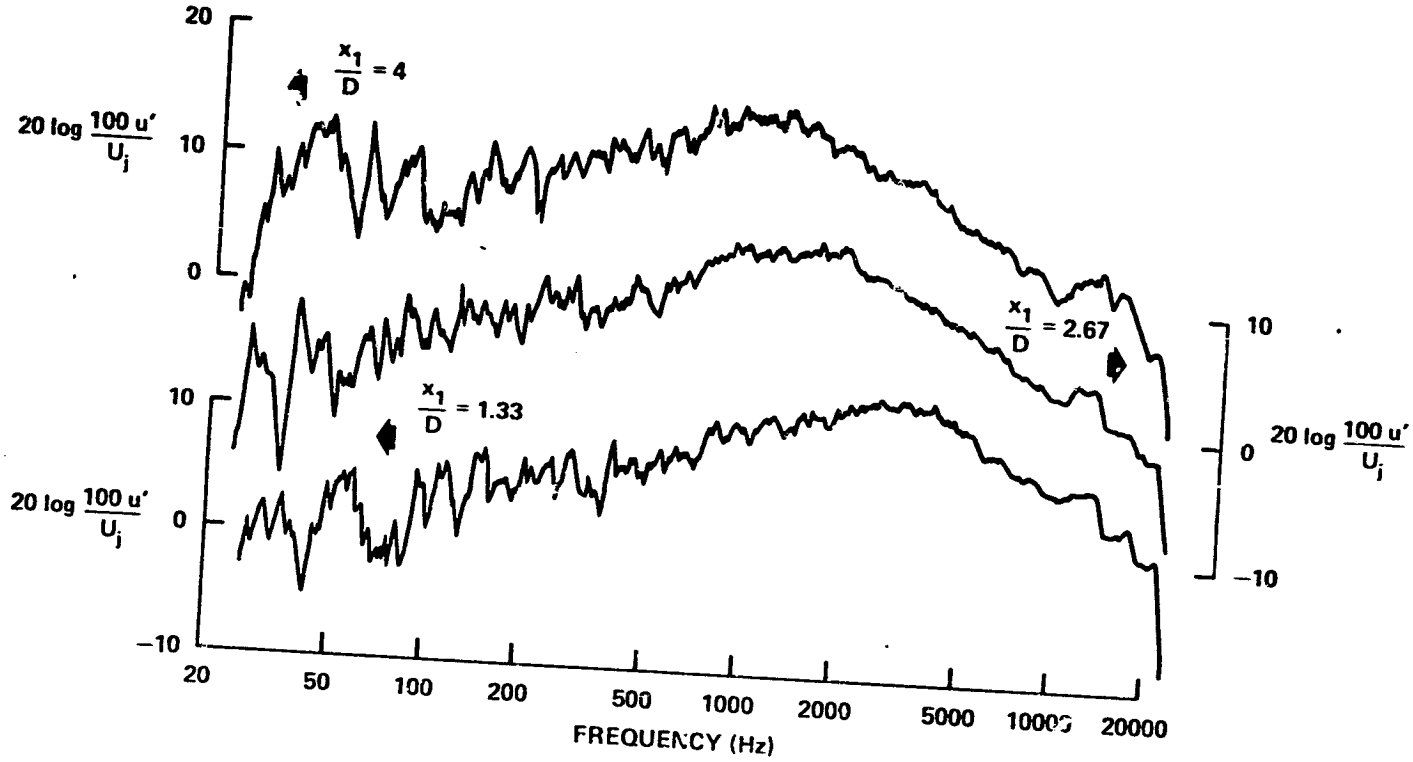

Figure 21 Turbulent Frequency Spectra in the Front Mixing Region; r=9.4

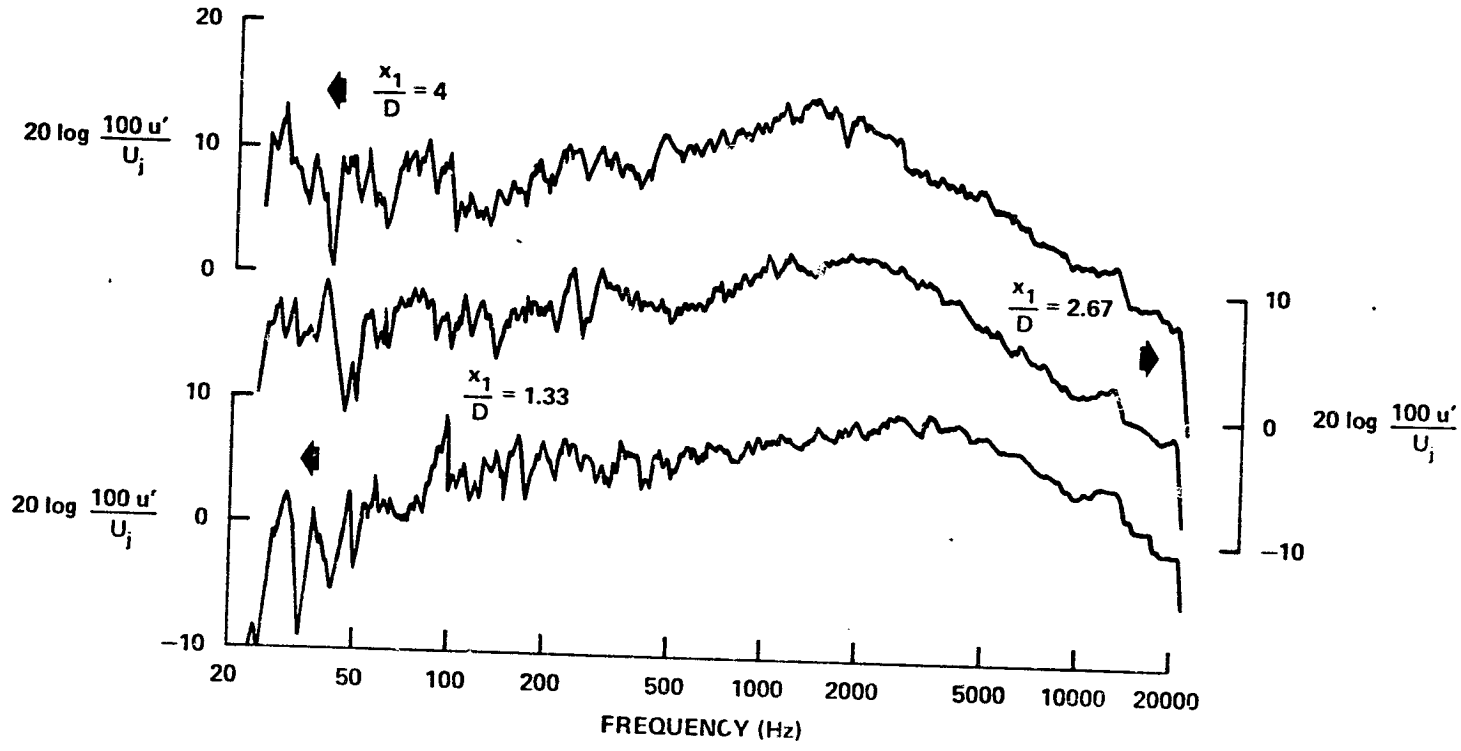

Figure 22 Turbulent Frequency Spectra in the Back Mixing Region: r=9.4

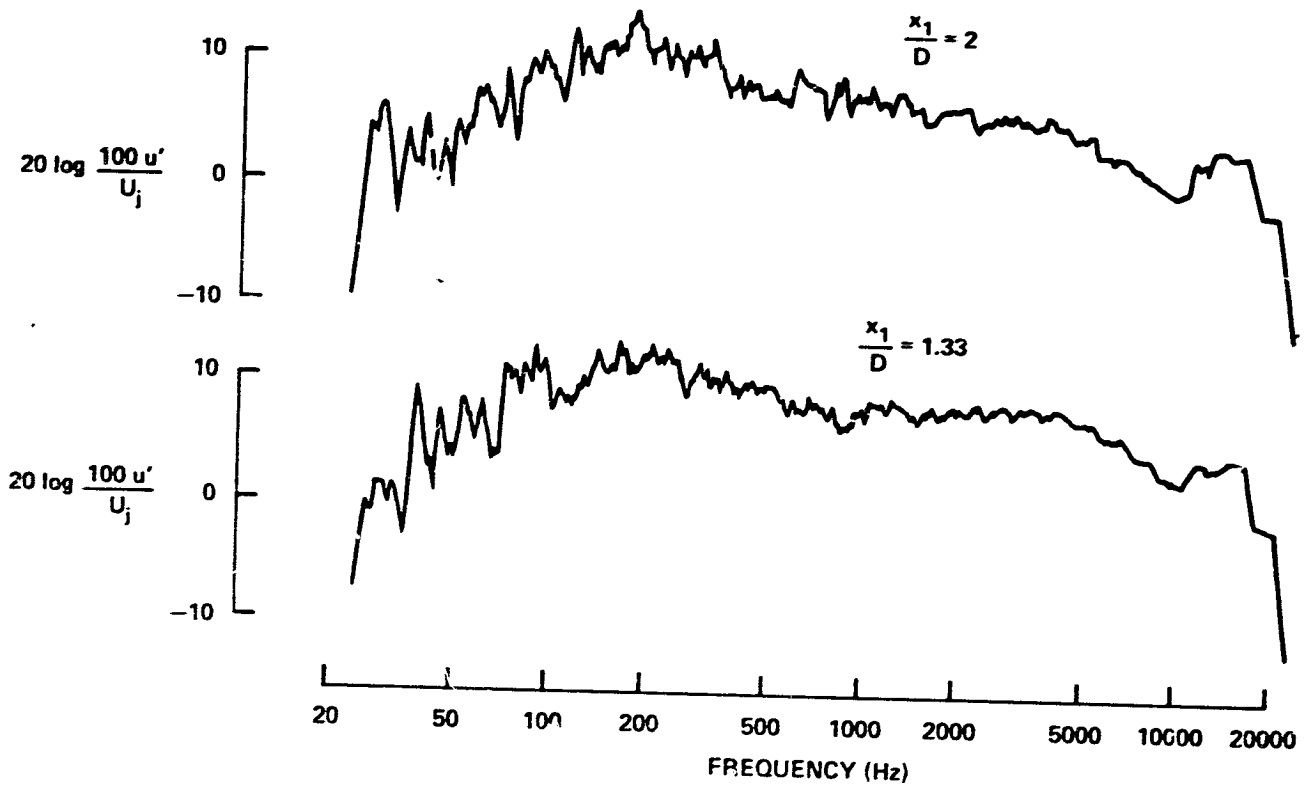

Figure 23 Turbulent Frequency Spectra in the Back Mixing Region; r=5.6

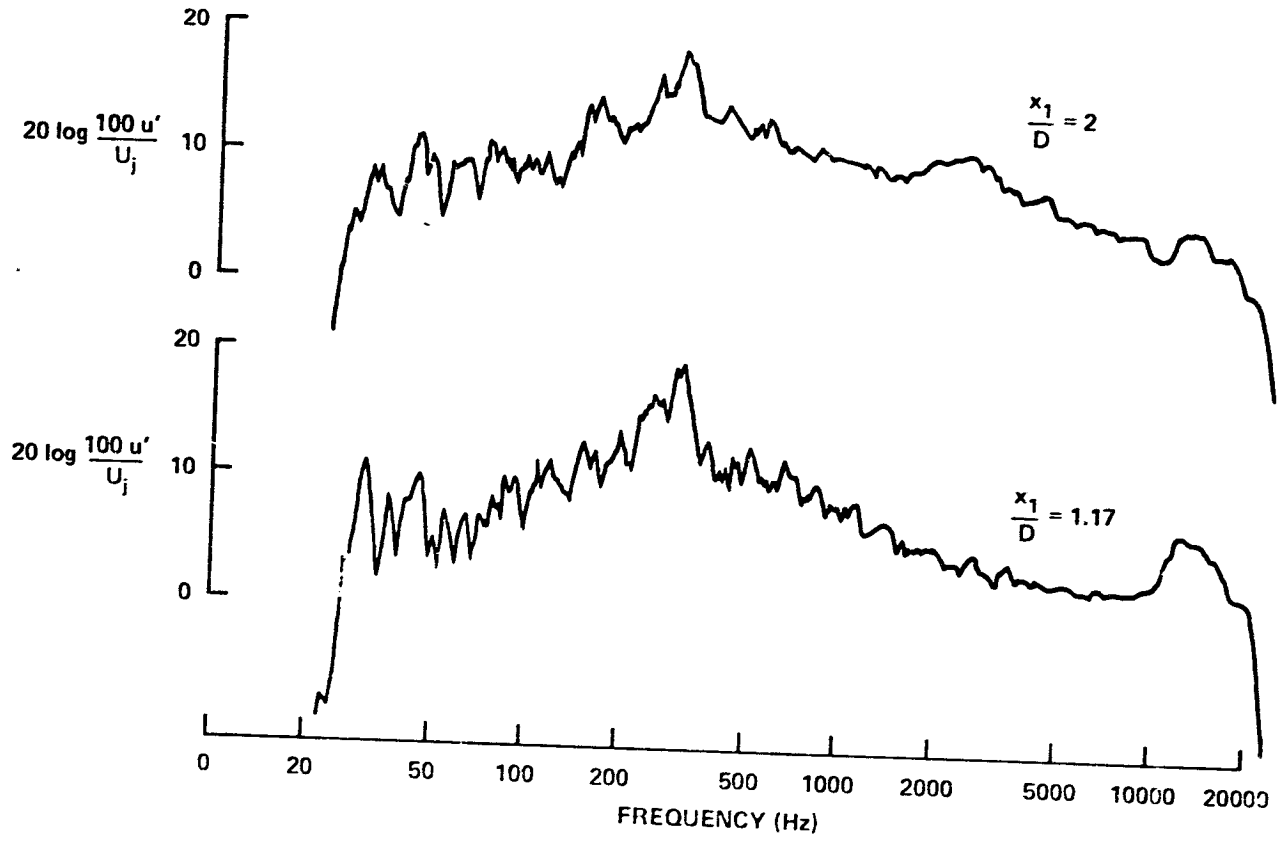

Figure 24 Turbulent Frequency Spectra in the Back Mixing Region; r=3.

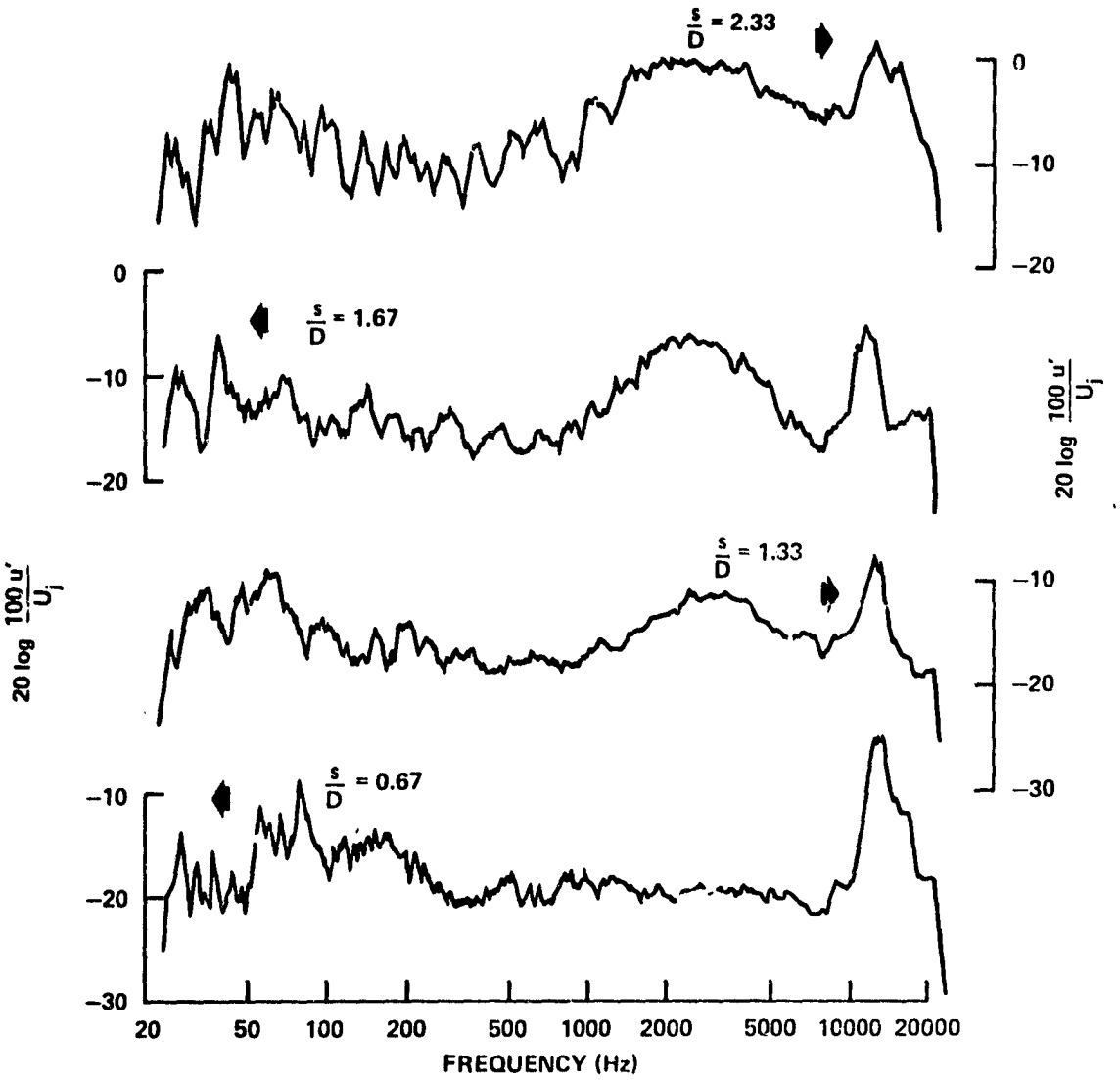

Figure 25 Turbulent Frequency Spectra in the Potential Core; r=7.5

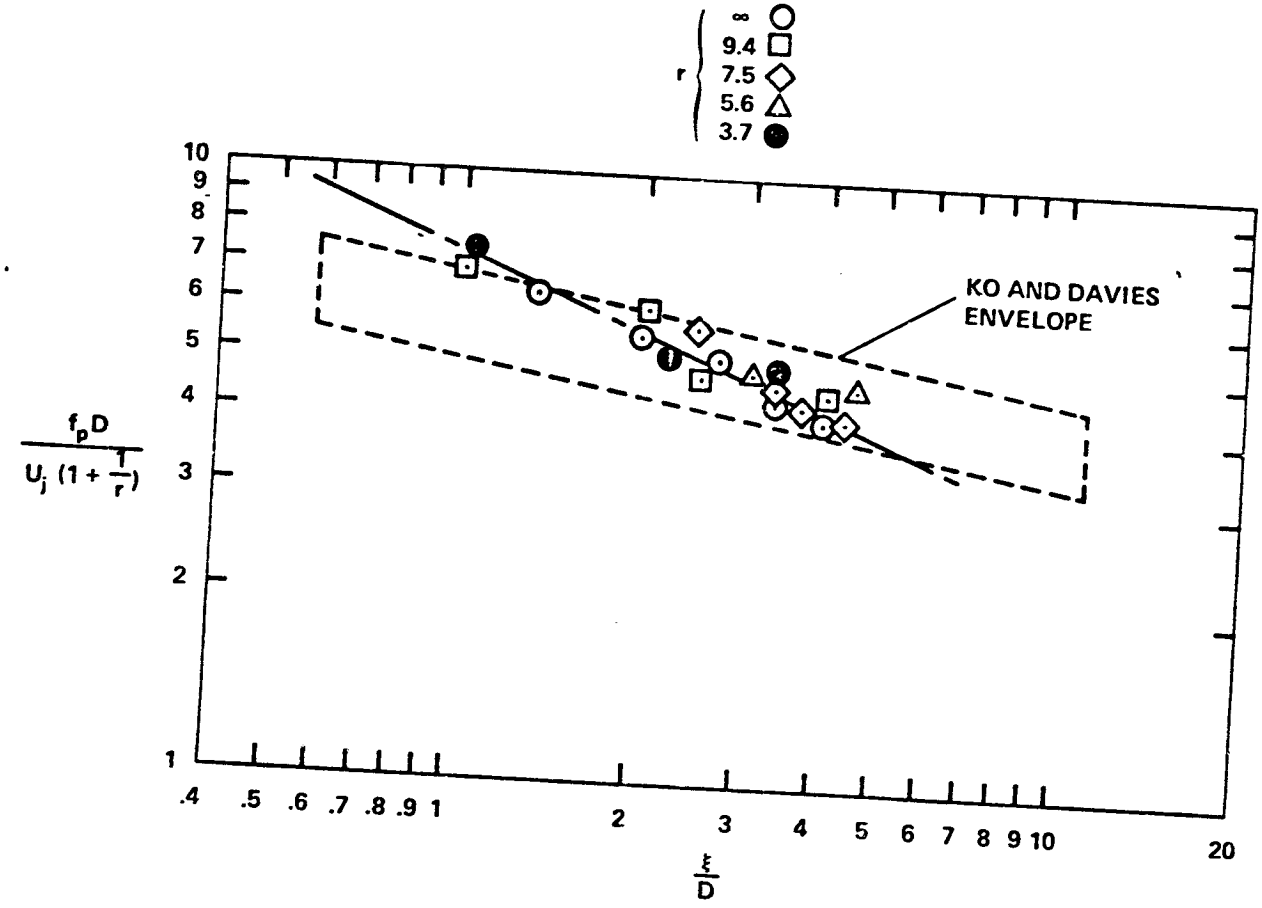

Figure 26 Axial Distribution of the Normalized Strouhal Number Inside the Potential Core

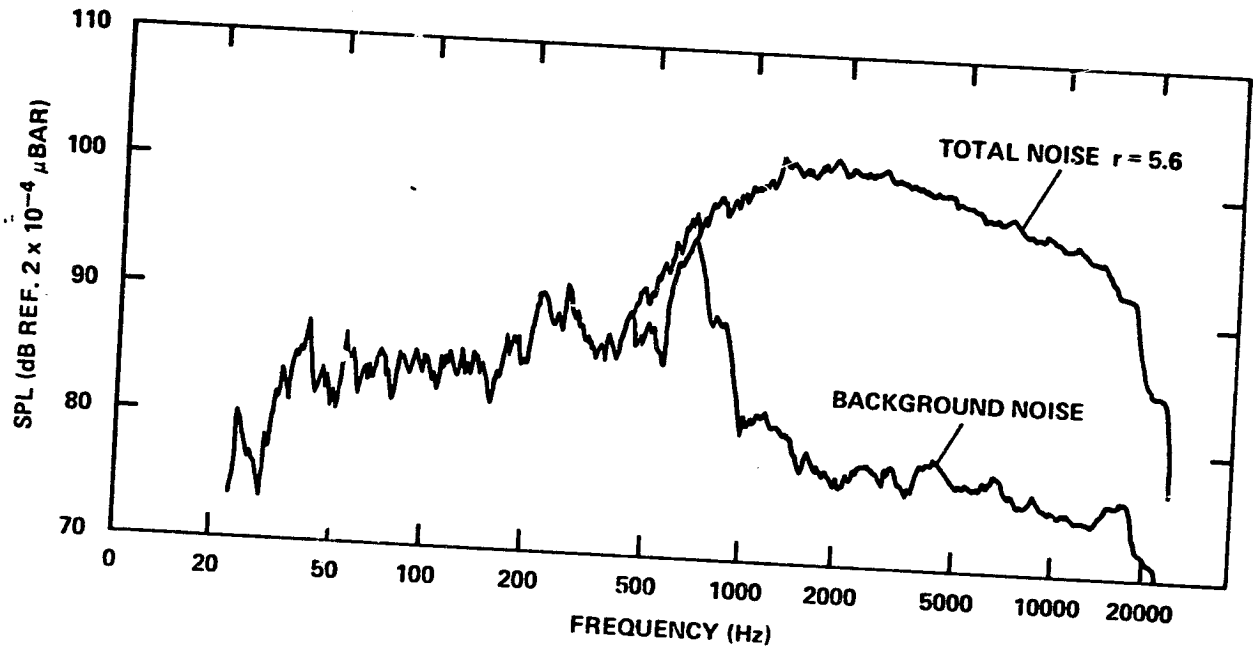

Figure 27 Frequency Spectra Measured by Microphone 3(1).

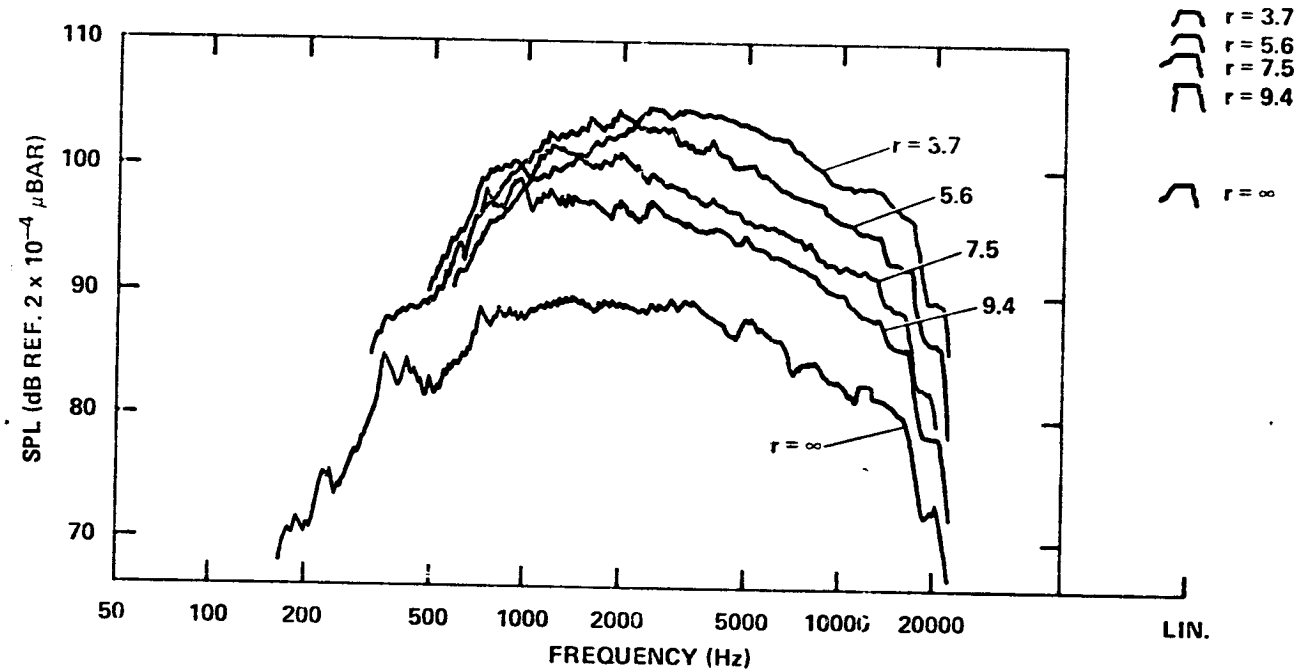

Figure 28 Frequency Spectra of Jet Noise Measured by Microphone 2(1)

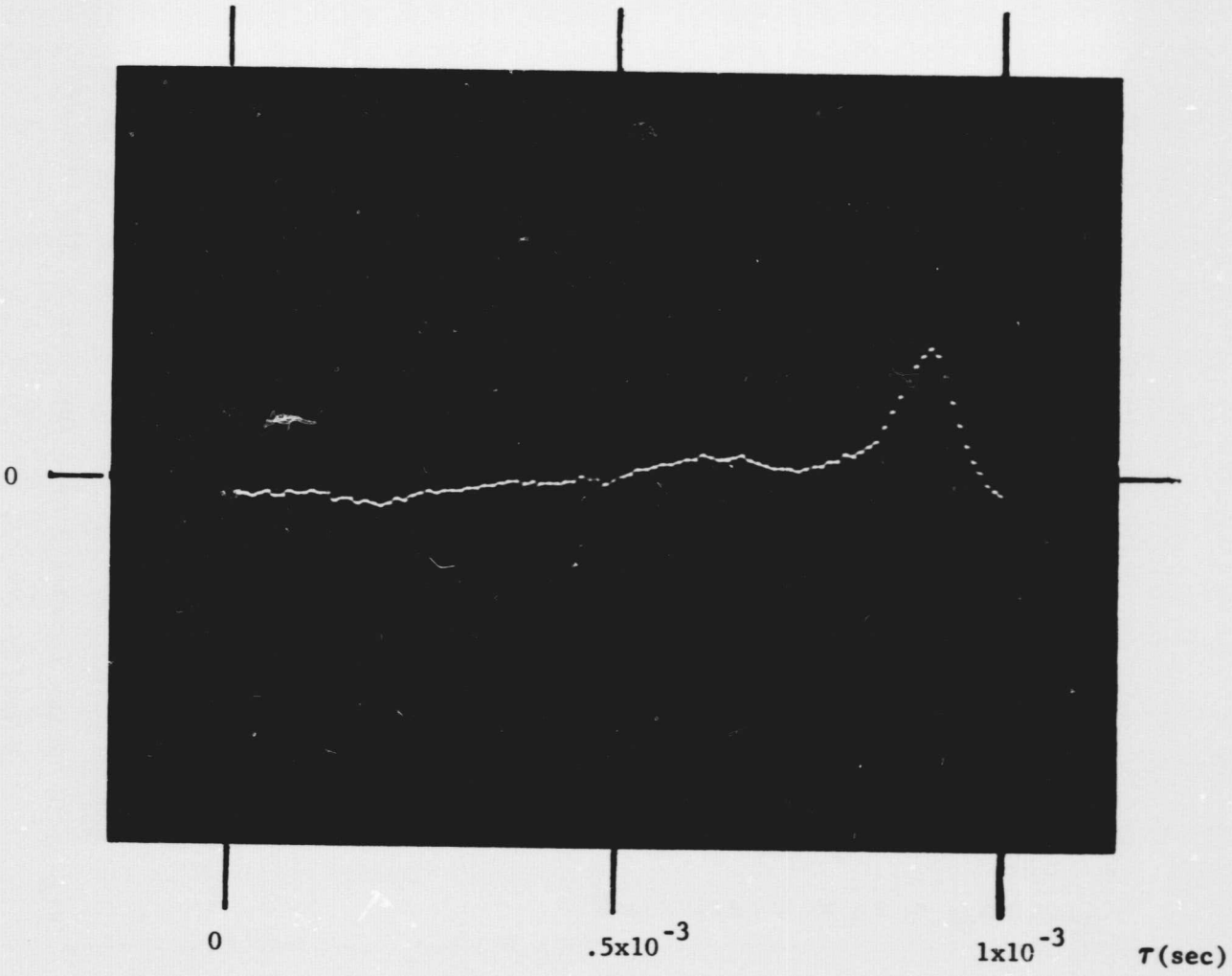

ORIGINAL PAGE IS OF POOR QUALITY

Figure 29 Two Microphone Cross-Correlation; $r=\infty$, $M_e=.58$

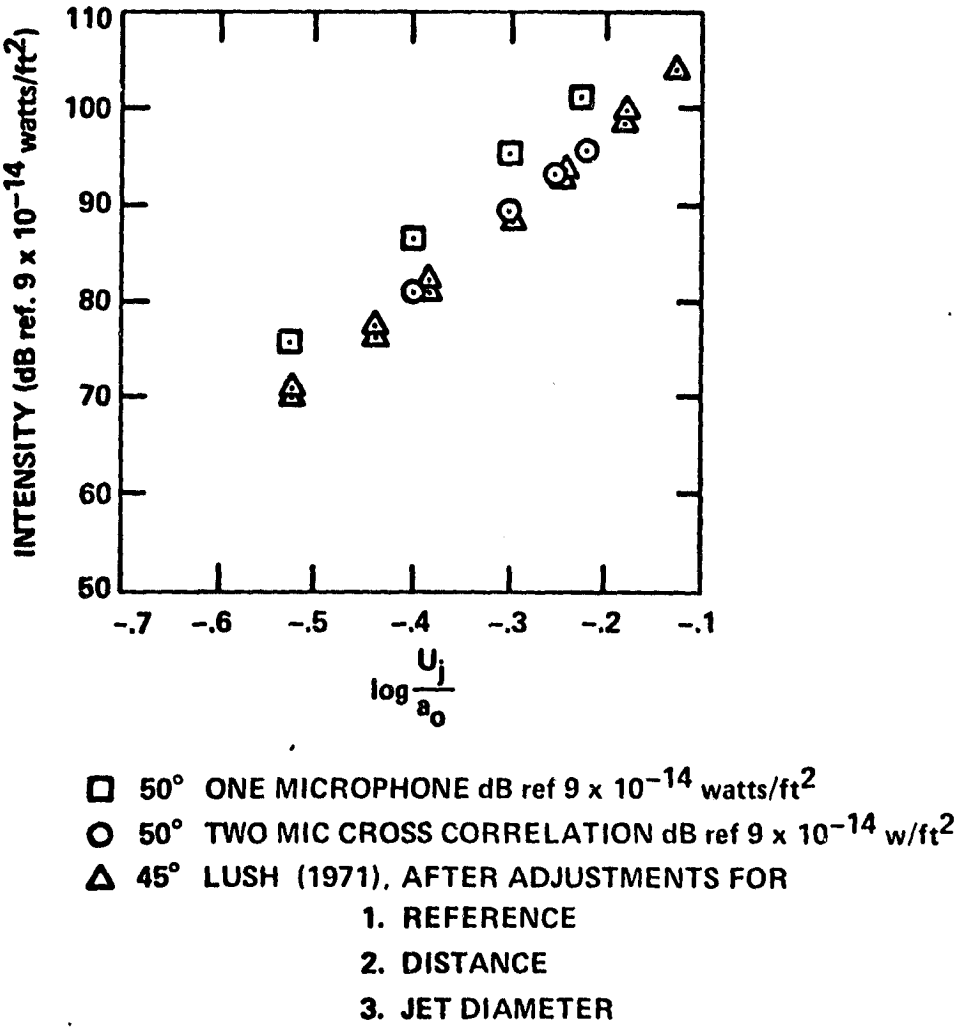

Figure 30 Noise Intensity as a Function of the Free Jet Velocity.

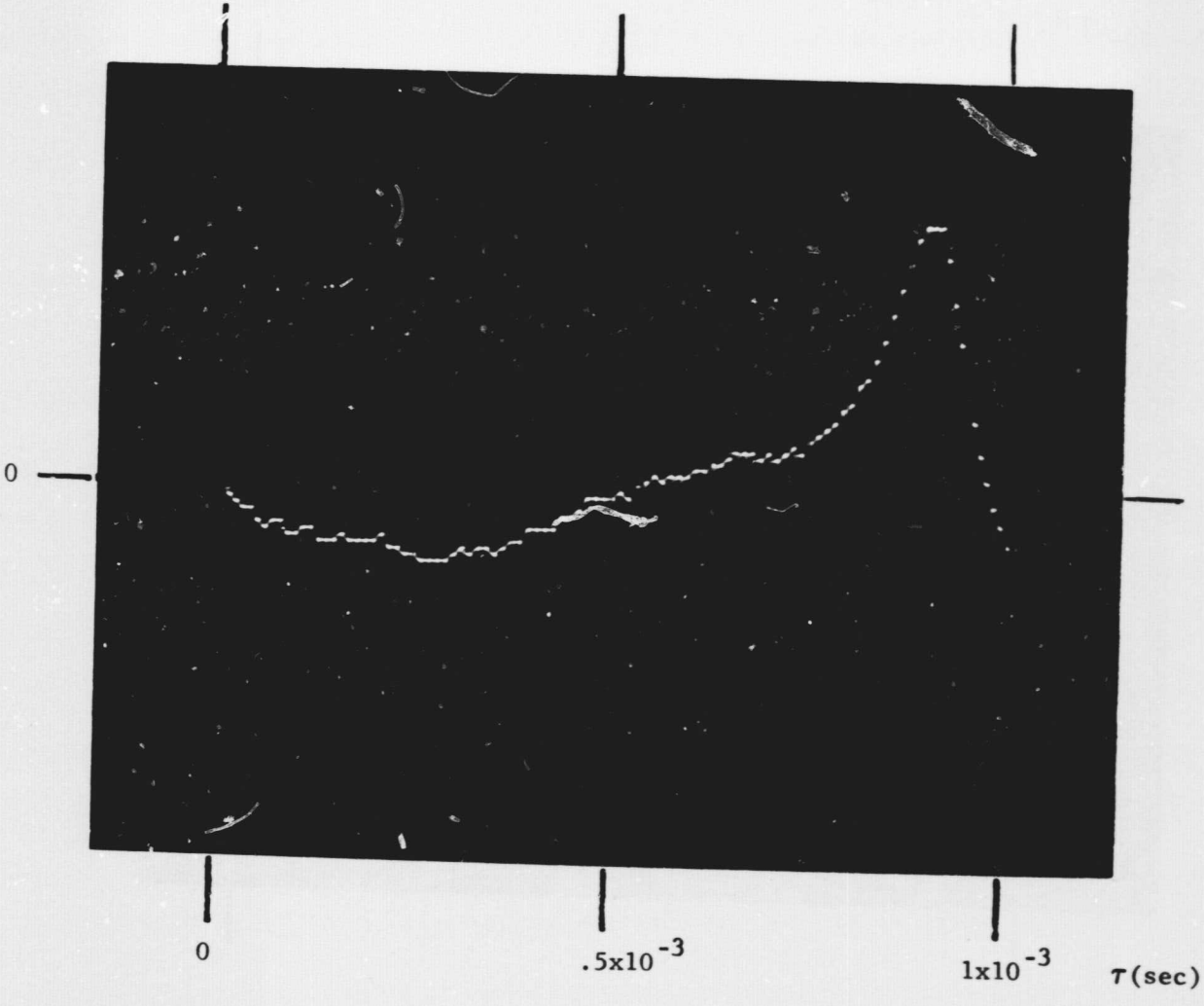

Figure 31 Two Microphone Cross-Correlation; r=9.4

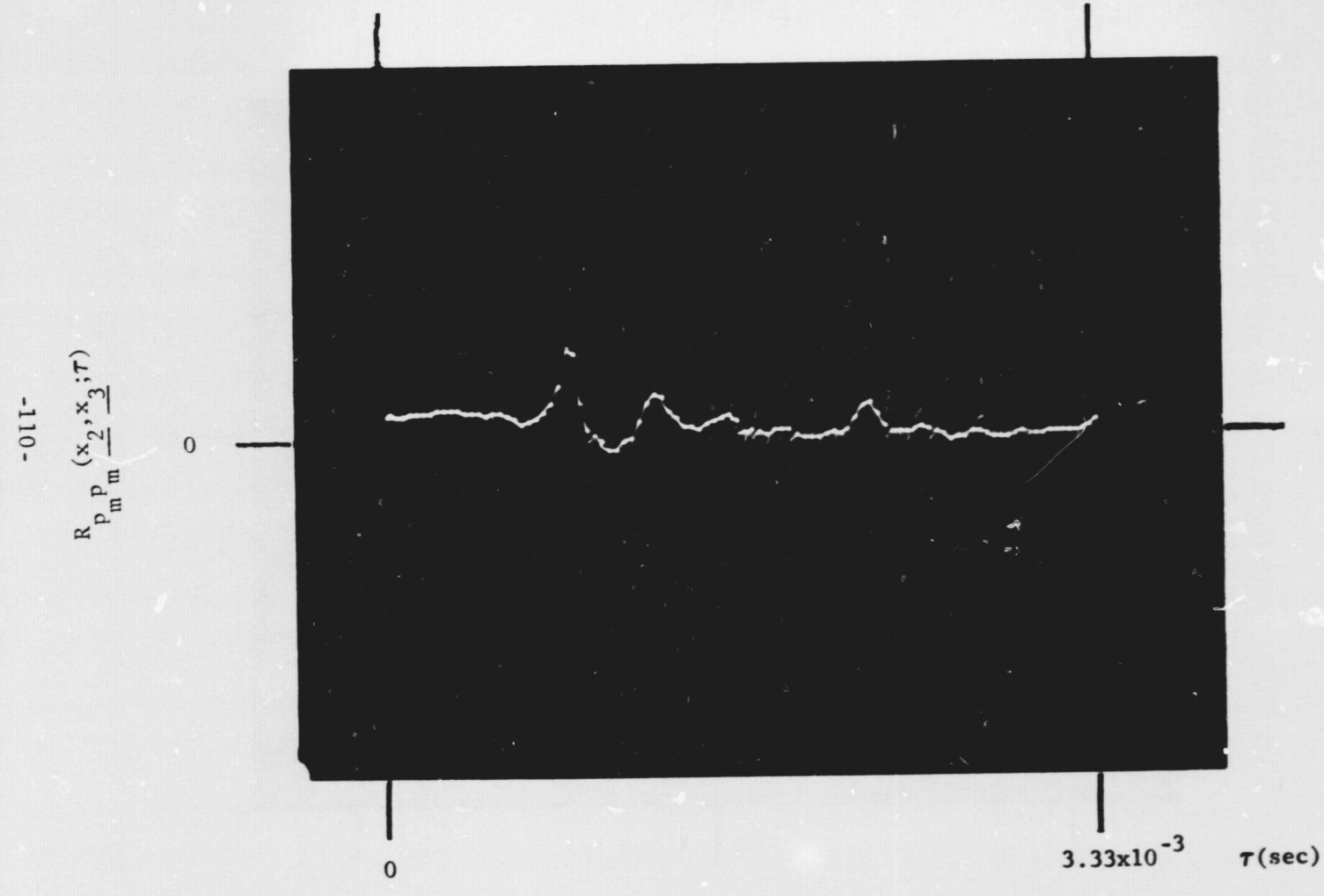

Figure 32 Two Microphone Cross-Correlation; r=3.7

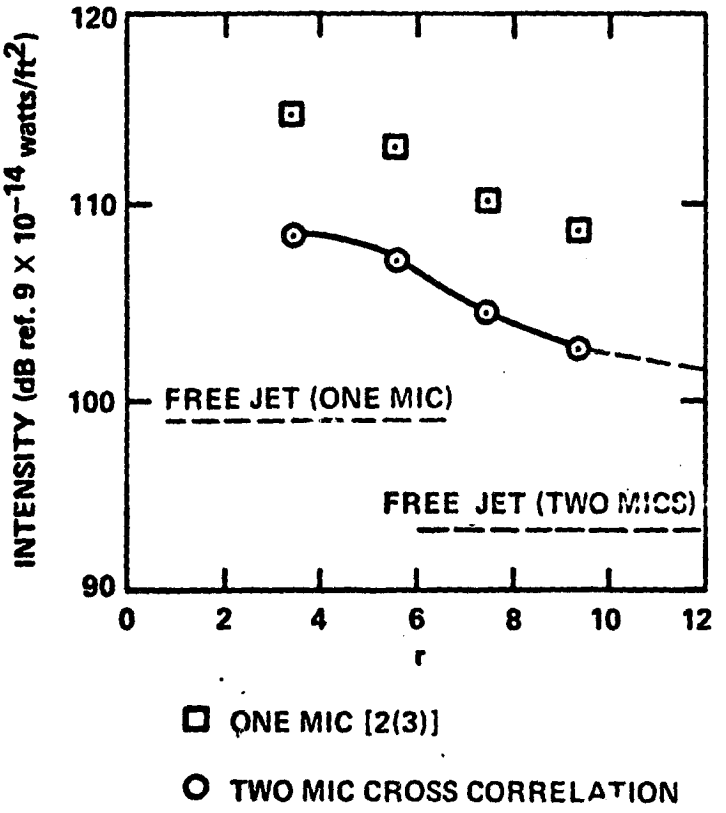

Figure 33 Noise Intensity as a Function of the Velocity Ratio r.

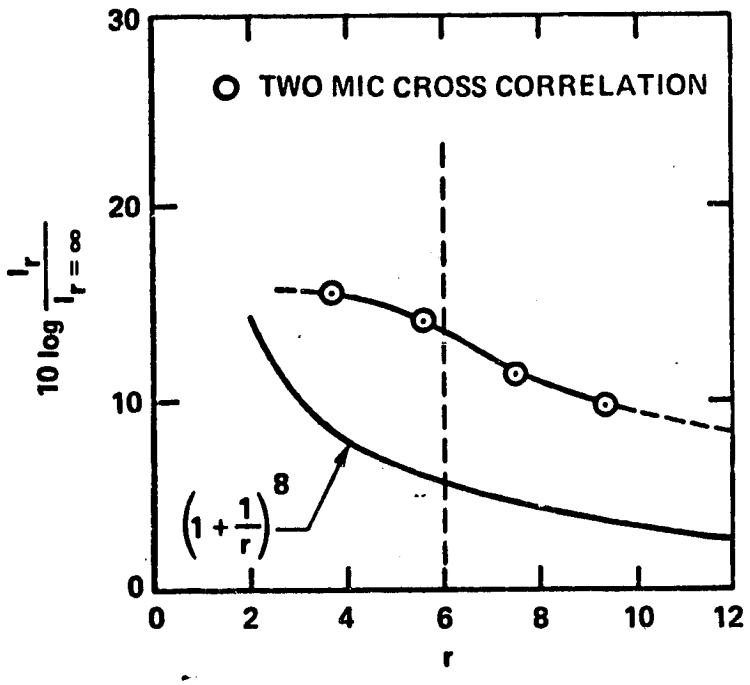

Figure 34 Relative Noise Intensity of the Crossflow Jet.

APPENDIX A

HOT WIRE ANEMOMETRY WITH COMPRESSIBILITY EFFECTS

The output voltage of a constant temperature hot wire anemometer (CTA) may be expressed [see Bradshaw, (1971)] in the following form:

$$V_{CTA}^2 = A + B(\rho U)^n \tag{A.1}$$

where V_{CTA} is the anemometer output voltage, ρ and U are respectively the density and velocity of the fluid at the point where the hot wire sensor is located, and A, B, and n are constants to be determined experimentally. The value of the exponent n is always close to 1/2. Equation A.1 shows that the anemometer output voltage is a nonlinear function of the mass flow ρU.

A linearizer is basically an electronic analog computer that linearizes the anemometer output voltage with the aid of specific transfer functions. In the particular case of the DISA 55D10 Linearizer the transfer function is given by:

$$V_{LIN} = K\left(V_{CTA}^2 - A\right)^{\frac{1}{n}} \tag{A.2}$$

where V_{LIN} is the Linearizer output voltage and K is a constant. Equation A.2 is applied to equation A.1 to give:

$$V_{LIN} = K_1 \rho U \tag{A.3}$$

where K_1 is another constant which can be adjusted with the gain control of the linearizer.

In the case of incompressible flows, where the density is a constant itself, V_{LIN} is proportional to the flow velocity only

and equation A.3 can be rewritten in the classical form:

$$V_{LIN} = K_2 U \tag{A.4}$$

Due to the simplicity of equation A.4, the constant temperature hot wire anemometer with linearizer has been one of the most valuable instruments for the measurement of mean and turbulent velocities in incompressible flows. When compressibility effects begin to be important, however, equation A.3 shows that the output voltage of the linearizer is a linear function of the mass flow ρU . In some flows it is possible to express the density as a function of the velocity and then obtain a direct relationship between the linearizer voltage and the flow velocity. A cold jet exhausting into a medium at rest is an example of such a flow.

Let a cold free jet be represented by its plenum chamber conditions and by the ambient conditions where p, ρ, and T represent pressure, density, and temperature respectively. The subscript 0 refers to the plenum chamber where the fluid velocity is approximately zero, ∞ represents the ambient conditions of the medium into which the jet is exhausting, and the subscript e represents the jet conditions at the jet exit. The jet velocity is changed by adjusting the plenum conditions since the ambient conditions are assumed to be fixed. It is further assumed that the plenum temperature T_0 is also constant and equal to the ambient temperature T_∞ , and also that the air is a perfect gas. Thus, the plenum pressure can be rewritten as

$$p_0 = C_1 \rho_0 \tag{A.5}$$

where

$$C_1 = RT_0 = RT_\infty \tag{A.6}$$

is a constant. It is also assumed that the fluid undergoes an isentropic transformation in going from the plenum chamber to the jet exit. Hence, the stagnation conditions at the exit are the same as those at the plenum chamber, allowing the following equation to be written

$$\frac{p_0}{p_e} = \left(\frac{\rho_0}{\rho_e}\right)^{\gamma} \tag{A.7}$$

where γ is the ratio of the specific heats at constant pressure and at constant volume of the air. A boundary condition of the flow is expressed by the equality between the jet static pressure p_e and the ambient pressure p_∞

$$p_e = p_\infty \tag{A.8}$$

In the ambient medium,

$$p_\infty = RT_\infty \rho_\infty = C_1 \rho_\infty \tag{A.9}$$

where C_1 is given by A.6. Equations A.5, A.7, A.8, and A.9 are combined to give

$$\rho_e = \rho_\infty \left(\frac{p_0}{p_e}\right)^{\frac{\gamma-1}{\gamma}} \tag{A.10}$$

This last equation can be rewritten in the following form (see Liepmann and Roshko):

$$\rho_e = \rho_\infty \left[1 + \frac{\gamma-1}{2} M_e^2\right] \tag{A.11}$$

where $M_e = \frac{U_j}{a_e}$ is the local Mach number of the flow, U_j is the jet velocity at the exit and a_e is the sound speed also at the jet exit.

For a hot wire located at the jet exit, the linearizer output voltage is given by (see eq. A.3):

$$V_{LIN} = K_1 \rho_e U_j$$

which combined with A.11 gives:

$$V_{LIN} = K_1 \rho_\infty U_j \left[1 + \frac{\gamma-1}{2} M_e^2\right] \tag{A.12}$$

It has been shown (see Liepmann and Roshko) that

$$\frac{a_0^2}{a_2^2} = \frac{T_0}{T_e} = \left[1 + \frac{\gamma-1}{2} M_e^2\right] \tag{A.13}$$

Here, a_0 is the speed of sound in the plenum chamber, or in the ambient medium in virtue of A.6. Equation A.13 may be rewritten in the following form:

$$\frac{a_0^2}{U_j^2} = M_e^2 \left[1 + \frac{\gamma-1}{2} M_e^2\right] \tag{A.14}$$

Then, obtaining the value of M_e^2 from A.14 and substituting it in A.12 gives

$$V_{LIN} = K_1 \rho_\infty U_j \left[1 + \frac{(\gamma-1)U_j^2}{2a_0^2 - (\gamma-1)U_j^2}\right] \tag{A.15}$$

Equation A.15 expresses the direct relationship of the linearizer output voltage with the flow velocity when a hot wire is placed at the exit of a jet under the conditions assumed. Observe the

nonlinearity of the linearizer voltage with the flow velocity due to the second term within the parenthesis. The magnitdue of this term can be obtained with the known values of p_e and ρ_0 (from equations A.10 and A.11), to determine the error involved when equation A.12 is used in the following approximate form:

$$V_{LIN} \simeq K_1 \rho_\infty U_j \tag{A.16}$$

Multiply and divide equation A.12 by $a_0 a_e$ and use equation A.13 to obtain:

$$V_{LIN} = K_1 \rho_\infty a_0 M_e \left[1 + \frac{\gamma-1}{2} M_e^2 \right]^{1/2} \tag{A.17}$$

which is another form to express the relationship of the linearizer output voltage. Here, V_{LIN} is shown as a function of the local Mach number at the jet exit. Equation A.17 may also be written in the following approximate form:

$$V_{LIN} \simeq K_1 \rho_\infty a_0 M_e \tag{A.18}$$

Though the error involved by using equation A.18 as an approximation of A.17 also depends on the jet Mach number, it is smaller than the error involved when equation A.16 is used as an approximation for A.12.

APPENDIX B

DIMENSIONAL ANALYSIS OF THE ACOUSTIC INTENSITY

Lighthill (1952) has shown by dimensional analysis that, for a free jet, the acoustic intensity at a point $\underline{x}$ in the radiation field is roughly proportional to

$$\rho_0 U^8 a_0^{-5} \frac{\ell^2}{|\underline{x}|^2} \tag{B.1}$$

where U and ℓ are respectively a characteristic velocity and a characteristic length of geometrically similar jet flows. In arriving at B.1 Lighthill made use of the non-changing peculiarity of the Strouhal number $f\ell/U$ to substitute a characteristic frequency of the flow, f, by the ratio U/ℓ. If we substitute U/ℓ for f in B.1, the intensity may be said to be roughly proportional to

$$\rho_0 f^4 U^4 a_0^{-5} \ell^6 |\underline{x}|^2 \tag{B.2}$$

Now, let us take the same jet, with a crossflow present, and let us apply some of the steps followed by Lighthill (1952), to derive a proportionality relationship for the acoustic intensity of the noise radiated from a crossflow jet. Before going on, we should strongly observe that, rigorously, this dimensional analysis could not be performed because a geometrical similarity does not exist in the flow of a jet under the influence of different crossflow velocities. However, just to obtain a rough analytical estimate for comparing the acoustic intensity of a crossflow jet with the

acoustic intensity of the same jet under free conditions, let us disregard this lack of geometrical similarity being aware of the resulting consequences.

The expression for the acoustic intensity at a point $\underline{x}$ in the radiation field, for the case of a jet in a cross stream, is given by equation 3.17. The amplitude of the cross-correlation $R_{v_x^2 v_x^2}$ in that equation will, at corresponding points of similar flows, be proportional to U_c^4, with U_c being a typical velocity of the crossflow jet. In the same equation, the fourth derivative with respect to time will be proportional to f_c^4 where f_c is a characteristic frequency of the crossflow jet. A characteristic linear dimension of the jet flow is ℓ_c. Similar arguments as those used by Lighthill (1952) may be used to conclude that the acoustic intensity of a jet in a crossflow is roughly proportional to

$$\rho_0 f_c^4 U_c^4 a_0^{-5} \ell_c^6 |\underline{x}|^2 \qquad \text{(B.3)}$$

This relation is perfectly valid for comparison of geometrically similar crossflow jets, that is, for comparison of different crossflow jets with the same velocity ratio r. For comparing the same jet with different values of r though, we have to disregard the non-existence of geometrical similarity. By doing so, the characteristic length ℓ_c can be taken equal to ℓ, the same characteristic length of the free jet, and the characteristic velocity U_c and frequency f_c, due to the experimental observations of this report,

can be substituted respectively by $U\left(1 + \frac{1}{r}\right)$ and $f\left(1 + \frac{1}{r}\right)$.

In this case, the acoustic intensity of the jet in a cross stream is roughly proportional to

$$\rho_0 f^4 \left(1 + \frac{1}{r}\right)^4 U^4 \left(1 + \frac{1}{r}\right)^4 a_0^{-5} \ell^6 |\underline{x}|^2 \qquad \text{(B.4)}$$

If we now divide relation B.4 by B.2 assuming that the proportionality factors of those two relations are the same, we arrive at the following expression:

$$\frac{I_r(\underline{x})}{I_{r=\infty}(\underline{x})} = \left(1 + \frac{1}{r}\right)^8 \qquad \text{(B.5)}$$

Equation B.5 shows in a rough approximation, the amount of increase in the acoustic intensity of a crossflow jet as compared to the acoustic intensity of the same jet under free conditions.

REFERENCES

Abramovich, G.N., "The Theory of Turbulent Jets", MIT Press, Massachusetts Institute of Technology, Cambridge, Mass., (1963).

Bendat, J.S., and Piersol, A.G., "Random Data: Analysis and Measurements Procedures", Wiley-Interscience, New York, NY, (1971).

Bradshaw, P., "An Introduction to Turbulence and its Measurement", Pergamon Press, New York, NY (1971).

Chassaing, P., George, J., Claria, A., and Sananes, F., "Physical Characteristics of Subsonic Jets in a Cross Stream", J. Fluid Mech. Vol. 62, pt. 1, 41-64, (1974).

Cole III, J.E., "The Influence of a Crossflow on Jet Noise", NASA CR 2169, (1972).

Cole III, J.E., "Noise Characteristics of a Turbulent Crosswind Jet", AIAA Journal, Vol. 12, 198-202, (Feb. 1974).

Davies, P.O.A.L., Fisher, M.J., and Barratt, M.J., "The Characteristics of the Turbulence in the Mixing Region of a Round Jet", J. Fluid Mech. Vol. 15, 337-367, (1963).

Davies, P.O.A.L., Ko, N.W.M., and Bose, B., "The Local Pressure Field of Turbulent Jets", ARC-CP 989, (1968).

Ffowcs Williams, J.E., "The Noise from Turbulence Convected at High Speed", Phil. Trans. Roy. Soc. London A 255, 469-503, (1963).

Fisher, M.J., Lush, P.A., and Bourne, M.H., "Jet Noise", J. Sound Vib., Vol. 28 (3), 563-585, (1973).

Hu, Galen, Flügge-Lotz, I., and Karamcheti, K., "An Analysis of a Two-Dimensional Propulsion Wing", Report on the Theoretical Aspects of NASA Contract NAS 2-4657, Submitted by Aeromarine Research Corporation, (1971).

Hickey, D.H., Soderman, P.T., and Kelly, M.W., "Noise Measurements in Wind Tunnels", NASA SP-207, 399-408, (1969).

Jordinson, R., "Flow in a Jet Directed Normal to the Wind", R and M 3074, British Aero. Res. Council, (October 1956).

Keffer, J.F., "The Physical Nature of the Subsonic Jet in a Cross Stream", NASA SP 218, 19-36, (1969).

Keffer, J.F., and Baines, W.D., "The Round Turbulent Jet in a Cross Wind", J. Fluid Mech., Vol. 15, pt. 4, 481-496, (1963).

Kirk, J.V., Hall, L.P., and Hodder, B.K., "Aerodynamics of Lift Fan Aircraft", NASA TM X-62, 086, (Sept. 1971).

Ko, N.W.M., and Davies, P.O.A.L., "The Near Field Within the Potential Cone of Subsonic Cold Jets", J. Fluid Mech., Vol. 50, pt. 1, 49-78, (1971).

Lassiter, L. W., and Hubbard, H.H., "Experimental Studies of Noise from Subsonic Jets in Still Air", NACA Tec. Note 2757, (1952).

Laurence, J.C., "Intensity, Scale, and Spectra of Turbulence in the Mixing Region of a Free Subsonic Jet", NACA Report 1292, 891-917, (1956).

Liepmann, H.W., and Roshko, A., "Elements of Gasdynamics", John Wiley and Sons, Inc., New York, NY, (1967).

Lighthill, M.J., "On Sound Generated Aerodynamically. I-General Theory", Proc. Roy. Soc. A 211, 564-587, (1952).

Lighthill, M.J., "On Sound Generated Aerodynamically. II-Turbulence as a Source of Sound", Proc. Roy. Soc. A 222, 1-32, (1954).

Lilley, G.M., "On the Noise from Air Jets", ARC 20, 376-N40-FM 2724, (1958).

Lush, P.A., "Measurements of Subsonic Jet Noise and Comparison with Theory", J. Fluid Mech., Vol. 46, pt. 3, 477-500, (1971).

McMahon, H.M., Hester, D.D., and Palfery, J.G., "Vortex Shedding from a Turbulent Jet in a Cross-Wind", J. Fluid Mech., Vol. 48, pt. 1, 73-80, (1971).

Mikolowski, W.T., "An Experimental Investigation of a Jet Issuing from a Wing in a Crossflow", Ph. D. Thesis, Georgia Institute of Technology, (May 1972).

Morkovin, M.V., "Fluctuations and Hot-Wire Anemometry in Compressible Flows", North Atlantic Treaty Organization, AGARDograph 24, (Nov. 1956).

Mosher, D.K., "An Experimental Investigation of a Turbulent Jet in a Crossflow", Ph. D. Thesis, Georgia Institute of Technology, (Dec. 1970).

Peterson, A.P.G., and Gross Jr., E.E., "Handbook of Noise Measurement", General Radio Company, Concord, Mass., (1972).

Powell, A., "On the Generation of Noise by Turbulent Jets", Amer. Soc. Mech. Engr., ASME Paper 59-AV-53, (1959).

Pratte, B.D., and Baines, W.D., "Profiles of the Round Turbulent Jet in a Cross Flow", J. of the Hydraulics Division, Proceedings of the ASCE, Vol. 92, No. HY6, 53-64, (Nov. 1967).

Proudman, I., "The Generation of Noise by Isotropic Turbulence", Proc. Roy. Soc., A 214, 119-132, (1952).

Ribner, H.S., "The Generation of Sound by Turbulent Jets", Advances in Applied Mechanics, Vol. 8, 103-182, Academic Press, (1964).

Siddon, T.E., "Some Observations on Source Detection Methods with Application to Jet Noise", the Second Interagency Symposium on University Research in Transportation Noise, North Carolina State University, (June 1974).

Stimpert, D.L., and Fogg, R.G., "Effects of Crossflow Velocity on the Gereration of Lift Fan Jet Noise in VTOL Aircraft", NASA CR-114571, (Feb. 1973).

Widell, K.E., "Stresses and Deformations in Hot-Wire Probes", DISA Inf. Bulletin No. 2, 14-17, (July 1965).

Wooler, P.T., "Development of an Analytical Model for the Flow of a Jet into a Subsonic Crosswind", NASA SP-218, 101-118, (1969).

Wooten, D.C., Wooldridge, C.E., and Amaro, A.J., "The Structure of Jet Turbulence Producing Noise", Final Report, National Aeronautics and Space Administration, Contract No. NASW-1938, (June 1952).